NAVAL POSTGRADUATE SCHOOL
Monterey, California

THESIS

An Observational Study of the Local and Remote Response of the Equatorial Pacific to Westerly Wind Events during the 1991-92 El Niño

by

Grant Alexander Cooper, IV

December 1992

Thesis Advisor: James T. Murphree

Approved for public release; distribution is unlimited

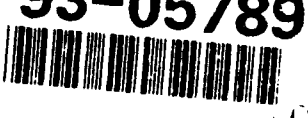

DISCLAIMER NOTICE

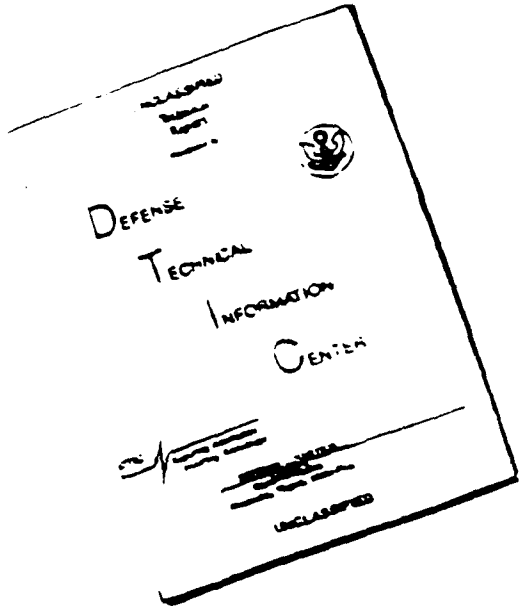

THIS DOCUMENT IS BEST QUALITY AVAILABLE. THE COPY FURNISHED TO DTIC CONTAINED A SIGNIFICANT NUMBER OF PAGES WHICH DO NOT REPRODUCE LEGIBLY.

REPORT DOCUMENTATION PAGE

Form Approved
OMB No. 0704-0188

1a REPORT SECURITY CLASSIFICATION: Unclassified	1b RESTRICTIVE MARKINGS:
2a SECURITY CLASSIFICATION AUTHORITY:	3 DISTRIBUTION/AVAILABILITY OF REPORT: Approved for public release; distribution is unlimited
2b DECLASSIFICATION/DOWNGRADING SCHEDULE:	
4 PERFORMING ORGANIZATION REPORT NUMBER(S):	5 MONITORING ORGANIZATION REPORT NUMBER(S):
6a NAME OF PERFORMING ORGANIZATION: Naval Postgraduate School; 6b OFFICE SYMBOL (If applicable): 35	7a NAME OF MONITORING ORGANIZATION: Naval Postgraduate School
6c ADDRESS (City, State, and ZIP Code): Monterey, CA 93943-5000	7b ADDRESS (City, State, and ZIP Code): Monterey, CA 93943-5000
8a NAME OF FUNDING/SPONSORING ORGANIZATION: ; 8b OFFICE SYMBOL (If applicable):	9 PROCUREMENT INSTRUMENT IDENTIFICATION NUMBER:
8c ADDRESS (City, State, and ZIP Code):	10 SOURCE OF FUNDING NUMBERS: PROGRAM ELEMENT NO; PROJECT NO; TASK NO; WORK UNIT ACCESSION NO

11 TITLE (Include Security Classification) AN OBSERVATIONAL STUDY OF THE LOCAL AND REMOTE RESPONSE OF THE EQUATORIAL PACIFIC TO WESTERLY WIND EVENTS DURING THE 1991-92 EL NINO

12 PERSONAL AUTHOR(S): Cooper, Grant, A.

13a TYPE OF REPORT	13b TIME COVERED	14 DATE OF REPORT (Year Month Day)	15 PAGE COUNT
Master's Thesis	FROM ____ TO ____	December 1992	110

16 SUPPLEMENTARY NOTATION: The views expressed in this thesis are those of the author and do not reflect the official policy or position of the Department of Defense or the U.S. Government

17 COSATI CODES			18 SUBJECT TERMS (Continue on reverse if necessary and identify by block number)
FIELD	GROUP	SUB GROUP	El Nino, Westerly Wind Bursts, Equatorial Air-Sea Interaction, Ocean Kelvin Waves

19 ABSTRACT (Continue on reverse if necessary and identify by block number)

The upper equatorial Pacific Ocean response to anomalous westerly wind forcing during the 1991-92 El Nino was examined using observational oceanographic and atmospheric data from equatorial moorings and the Navy's operational analyses. A strong 30-60 day signal was observed in the zonal winds and is mainly a result of westerly wind events. The local response to anomalous westerly winds differed between the western and eastern equatorial Pacific. In the western Pacific, westerly wind events tended to produce rapid decreases in sea surface temperature (SST) (up to 1°C). These decreases were followed serveral days later by SST increases due to horizontal warm water advection and downwelling. In the central and eastern equatorial Pacific, westerly wind events were expressed mainly as weakenings of the easterlies. (Continued on next page)

20 DISTRIBUTION/AVAILABILITY OF ABSTRACT	21 ABSTRACT SECURITY CLASSIFICATION
☒ UNCLASSIFIED/UNLIMITED ☐ SAME AS RPT ☐ DTIC USERS	Unclassified
22a NAME OF RESPONSIBLE INDIVIDUAL: J.T. Murphree	22b TELEPHONE (Include Area Code): (408) 646-2723; 22c OFFICE SYMBOL: MR/ME

Block 19 (Continued).

These weakenings caused decreases in equatorial upwelling and SST increases. Westerly wind events in the western Pacific were also associated with large thermocline temperature fluctuations (on the order of 10°C) in the central and eastern equatorial Pacific. These fluctuations propagated eastward at phase speeds consistent with first baroclinic equatorial Kelvin wave dynamics (i.e., 2.0-3.0 ms^{-1}). The ocean temperature fluctuations indicate basin wide wavelengths (about 15 x 10^3 km), with periods of 30-60 days.

Approved for public release; distribution is unlimited

An Observational Study of the Local and Remote Response of the Equatorial Pacific to Westerly Wind Events during the 1991-92 El Niño

by

Grant Alexander Cooper, IV
Lieutenant, United States Navy
B.S., San Diego State University, 1984

Submitted in partial fulfillment of the requirements for the degree of

MASTER OF SCIENCE IN METEOROLOGY AND PHYSICAL OCEANOGRAPHY

from the

NAVAL POSTGRADUATE SCHOOL
December 1992

Author: Grant Alexander Cooper, IV

Approved by: James Thomas Murphree
James T. Murphree, Thesis Advisor

Peter C. Chu
Peter C. Chu, Second Reader

Robert L. Haney
Robert L. Haney, Chairman, Department of Meteorology

ABSTRACT

The upper equatorial Pacific Ocean response to anomalous westerly wind forcing during the 1991-92 El Niño was examined using observed oceanographic and atmospheric data from equatorial moorings and the Navy's operational atmospheric analyses. A strong 30-60 day signal was observed in the zonal winds and is mainly a result of westerly wind events. The local response to anomalous westerly winds differed between the western and eastern equatorial Pacific. In the western Pacific, westerly wind events tended to produce rapid decreases in sea surface temperature (SST) (up to $1^{\circ}C$). These decreases were followed several days later by SST increases due to horizontal warm water advection and downwelling. In the central and eastern equatorial Pacific, westerly wind events were expressed mainly as weakenings of the easterlies. These weakenings caused decreases in equatorial upwelling and SST increases. Westerly wind events in the western Pacific were also associated with large thermocline temperature fluctuations (on the order of $10^{\circ}C$) in the central and eastern equatorial Pacific. These fluctuations propagated eastward at phase speeds consistent with first baroclinic equatorial Kelvin wave dynamics (i.e., 2.0 - 3.5 ms^{-1}). The ocean temperature fluctuations indicate basin wide wavelengths (about 15 x 10^3 km), with periods of 30-60 days.

TABLE OF CONTENTS

I. INTRODUCTION

The role of air-sea interactions within the western equatorial Pacific is a critical element in understanding the El Niño / Southern Oscillation (ENSO) cycle. Unfortunately, there is relatively little observational data, so the effects of atmospheric forcing on the tropical ocean are poorly understood. From basic air-sea relationships and recent observational studies (Lukas, 1988 and 1989; Lukas and Lindstrom, 1991), variations in atmospheric forcing in the western equatorial Pacific can be assumed to cause significant ocean responses. These responses include local and remote variations in sea surface temperature (SST), mixed layer depth, and heat, moisture, and momentum fluxes.

This observationally based study examines the equatorial ocean's response to variations in atmospheric forcing during the 1991-92 El Niño. The focus is on wind stress forcing from westerly wind events in the western and central Pacific and the responses to this forcing throughout the equatorial Pacific.

The association of western equatorial Pacific westerly wind events with the El Niño / Southern Oscillation (ENSO) phenomenon have been studied by Chu (1988), Lau et. al. (1989), Murakami and Sumathipala (1989), Giese and Harrison (1991), and Harrison and Giese (1991). These westerly wind

events appear to generate eastward propagating oceanic equatorial Kelvin waves. The eastern Pacific Ocean response to the downwelling phase of the Kelvin wave is expressed as warmer sea surface temperatures, deeper mixed layer depths, and a rise in sea level along the South American coast [Wyrtki, 1975; McCreary, 1976; Philander, 1981; Lukas et. al., 1984; Harrison and Schopf, 1984; Cane and Zebiak, 1985]. This expected response was observed in the eastern Pacific basin during the 1991-92 El Niño (Kousky, 1991a).

Lukas and Lindstrom (1991) analyzed conductivity-temperature-depth (CTD) profiles from the Western Equatorial Pacific Ocean Circulation Study (WEPOCS). During WEPOCS, phase II, conducted in January - February 1986, they found very little evidence of vertical heat flux out of the base of the mixed layer. They proposed that, except during strong westerly wind events, entrainment cooling may not be an important component of the heat budget of the western Pacific warm pool. During a westerly wind event, they observed that the mixed layer depth doubled and SST cooled by more than 1^{0}C. Without the westerly wind bursts, the mixed layer tended to warm. They further suggested "...ENSO phenomena may exist solely because there is an inadequate removal of heat from the upper layer of the western tropical Pacific Ocean by the mean ocean circulation."

McPhaden and Hayes (1991) examined a period of frequent westerly winds at 165^{0}E during the height of the 1986-87 El

Niño. They proposed that evaporative cooling related to wind speed variations, not entrainment, accounts for the observed SST and upper ocean heat content variability. They found no significant trend in SST cooling during several 5-10 ms^{-1} westerly wind bursts. From their data set, McPhaden and Hayes found no evidence of westerly burst involvement in ENSO related SST cooling.

During a westerly wind event in May 1982 in the western Pacific, Chu and Frederick (1990) observed that the mean SST dropped by $1^{\circ}C$. They attributed this drop in temperature to evaporative cooling and entrainment. Small sensible heat fluxes were observed, but the transfer of latent heat increased significantly from pre- to post-burst. This latent heat transfer added a relatively large amount of moisture to the atmosphere, which enhanced local convection.

Within the western equatorial Pacific, tropical cyclones are one of the likely generators of westerly wind bursts (Keen, 1982; Ramage, 1985; Nitta, 1989). Several strong westerly bursts associated with tropical cyclones (Yuri, Wilda, Val, Wasa, Axel, and Betsy) were identified during the fall and winter of 1991-92. These cyclones generated strong equatorial westerly winds in the western Pacific, which presumably affected the upper ocean, both locally and remotely.

The local results are a cooling of SSTs, deepening of the mixed layer, and large air-sea exchanges of heat, moisture,

and momentum. The strong winds would be expected to decrease the sea surface temperatures by evaporative cooling in proportion to the wind speed (McPhaden and Hayes, 1991). Increased mixing and entrainment of cooler water is also expected, but in proportion to the cube of the wind speed (McPhaden and Hayes, 1991). The entrainment rate and its effect upon SSTs are expected to depend strongly upon the static stability and initial mixed layer thickness. (Webster and Lukas, 1992).

Persistent westerlies blowing across the equatorial Pacific warm pool would also tend to advect warm water eastward and cause equatorward convergence, due to Coriolis effects. These processes should, in turn, increase the temperature and depth of the mixed layer. This mixed layer deepening would tend to generate equatorially trapped Kelvin waves. Thus, strong westerly wind events should also force equatorially trapped internal Kelvin waves (Gill and Rasmusson, 1983), which would propagate from the western Pacific forcing region into the eastern Pacific. McPhaden and Hayes (1991) proposed that Kelvin wave forcing is proportional to the square of the wind speed.

In this study, I examine both the local and remote ocean responses to westerly wind events. In particular, I explore the following questions:

(1) What are the local responses to strong westerly wind forcing? In particular, what is the local SST and mixed layer response?

(2) What are the remote responses to the wind forcing? In particular, is there a Kelvin wave response?

This study will attempt to address these issues by examining observational atmosphere and ocean data from the Tropical Oceans Global Atmosphere (TOGA) program during the 1991-92 ENSO. The TOGA program was established to examine the relationships between short-term climate variations and ENSO. This moored buoy array was established to provide the spatial and temporal scales needed to resolve the large scale ocean response to variations in atmospheric forcing (McPhaden and Hayes, 1991).

Chapter II describes the observational background, data sources, methods, and data averaging procedures. Results are presented in Chapter III and conclusions in Chapter IV.

II. ANALYSIS PROCEDURES

A. OBSERVATIONAL BACKGROUND

During the 1991-92 El Niño / Southern Oscillation (ENSO) event, SST's in the central and eastern equatorial Pacific increased from late 1991 until January 1992, when the event entered the mature phase (Kousky, 1992a). In addition to SST increases, this event manifested itself as wind, mixed layer, thermocline, and sea level anomalies throughout the tropical Pacific.

Figure 1 shows that during the six month study period, from October 1991 through March 1992, positive SST anomalies propagated eastward and weak negative anomalies formed in the western equatorial Pacific. The monthly mean SST anomalies in the central and eastern Pacific were greater than 1^0C and anomalies greater than 2^0C occurred from December through March (Figs. 1 c-f). A maximum temperature anomaly of 5^0C was observed along the Peruvian coast in March (Kousky, 1992c).

Kousky (1991a) speculated that a relaxation of the western Pacific easterly winds in September 1991 may have initiated an oceanic Kelvin wave which reached the South American coast at the end of October. The downwelling phase of this ocean Kelvin wave was identified from a thermocline depth increase in the eastern Pacific and a decrease in the central and western Pacific (Kousky, 1991a). Figure 2 shows

equatorial depth-longitude sections of ocean temperatures for October and March. The 20°C isotherm represents the approximate thermocline depth. In October, the thermocline is below 150 m from 120°E to approximately 120°W, but shoals rapidly further east. By March, the thermocline east of 120°E has deepened to approximately 100 m and the western and central Pacific thermocline has shoaled to less than 150 m. The thermocline along the South American coast deepened to approximately 100 m in March, which is 30 m deeper than the 1986-87 El Niño (Kousky, 1992c).

The SST anomalies correspond very well to the sea level anomalies shown in Figure 3. These sea level anomalies indicate an eastward propagation of higher sea levels, which caused sea levels to rise in the eastern Pacific and decrease in the western Pacific. In December, two separate negative sea level anomalies formed west of the date line at approximately $\pm 10^{\circ}$ latitude and became most pronounced in January. The central and eastern equatorial Pacific was dominated from October through March by a single ridge of higher sea levels. The propagation of sea level increases along the western American coast in March were identified by Kousky (1992c) as evidence for coastally trapped Kelvin waves.

Figure 4 shows that in the fall, the monthly mean 850 mb winds in the equatorial western Pacific switched from easterlies to weak westerlies which strengthed during the early winter. By February, the westerlies had diminished and

again become easterly. The central and eastern Pacific mean winds remained easterly during the fall and winter months.

As shown in Figure 4 b,d,f,g,h, and j, during this El Niño, equatorial westerly winds at 850 mb extended east of the date line from October 1991 through March 1992. At times, these westerlies exceeded 10 ms^{-1}, probably due to the influence of tropical cyclones. Relaxations of the easterly winds at 850 mb in the central and eastern equatorial Pacific produced westerly wind anomalies in this region for the entire six month period. Thus, throughout this period, and all along the equator at 850 mb, the winds were either eastward or less westward than normal. This relaxation of normal easterlies may produce westerly wind anomalies, even if the observed winds are still easterly.

B. DATA

To investigate the observational data from the 1991-92 El Niño, I have examined daily-averaged in-situ atmosphere and ocean data from the equatorial Pacific. Measurements of zonal and meridional surface wind components, sea surface temperatures, and ocean temperatures at fixed depths were obtained from the TOGA-TAO (Tropical Ocean -Global Atmosphere - Thermal Array for the Ocean) ATLAS (Autonomous Temperature Line Acquisition System) moored buoys. The ATLAS buoy spacing of 15^{0} of longitude and 0^{0}, $\pm 2^{0}$, $\pm 5^{0}$, and $\pm 8^{0}$ of latitude from the equator, are based on coherence scales of the tropical

Pacific wind field (Harrison and Luther, 1990). Additional measurements of surface wind components, sea surface temperature, and ocean current components were obtained from EPOCS (Equatorial Pacific Ocean Climate Studies) moored buoys.

This study examines TOGA-TAO ATLAS buoys at longitudes 110°W, 124°W, 140°W, 155°W, 169°W, 170°W, 165°E, and 156°E. Only longitudes 124°W, 155°W, 169°W and 170°W have ATLAS buoys located directly on the equator. Additional equatorial information ((u,v) winds, SST, and (u,v) ocean currents) is provided by three EPOCS buoys located on the equator at 110°W, 140°W, and 165°E. To focus on equatorial conditions and remain well within the equatorial waveguide, the latitudinal distribution of this study is from 2°N to 2°S. The buoy locations for this data are shown in Figure 5.

Data were transmitted by the buoys in near real-time via Service ARGOS. Linda Mangum of the National Oceanic and Atmospheric Administration's (NOAA) Pacific Marine Environmental Laboratory (PMEL) Seattle, WA provided the buoy data for this study.

Surface winds are measured at four meters above the sea surface. Sea surface temperatures are measured at one meter below the surface. Ocean currents are measured at ten meters depth at 165°E and 110°W and at three meters depth at 140°W.

For a general synoptic overview, I have examined the Navy Operational Global Atmospheric Prediction System (NOGAPS) analyzed surface wind fields. (See Hogan and Rosmond, 1991;

and Goerss, 1991 for NOGAPS descriptions). This product helped in identifying the tropical cyclones associated with the observed westerly winds events. These winds also show the zonal and meridional extent of the westerly wind events.

C. GENERAL METHODS

The primary analysis tools that I have used in this observational study are time series methods. The buoy data time series and cross-correlations of the zonal winds, or wind stresses, with ocean temperature are presented in Chapter III. The calculations used to produce the cross-correlations are in accordance with Box and Jenkins (1976).

All the TOGA and EPOCS data has been linearly detrended prior to performing the cross-correlations. Westerly wind events are either actual westerly winds, or relaxations of easterly winds. These events are represented by a positive zonal wind component, either in the actual wind data and/or in the linearly detrended wind time series. Zonal wind stress time series, a function of the total wind magnitude multiplied by the zonal wind, are also calculated and analyzed. Sea surface temperature and ocean current time series are used to analyze both the local and remote responses to wind forcing. The temporal and spatial variations of the 150, 140, and 100 m ocean temperatures are used to identify the propagation of equatorially trapped ocean waves.

Relationships between SST and wind forcing were examined by cross-correlating the local zonal winds and SST for each buoy location. As discussed in Chapter I, changes in SST due to evaporative cooling are proportional to the wind speed. For this study, only the zonal wind component was used, because I wanted to focus on the effects of westerly wind forcing on SST.

To determine the remote response of the equatorial ocean to westerly wind forcing, I have calculated the cross-correlations of the zonal wind stress and near-thermocline temperatures. This procedure helps to quantify the relationships, if any, between these fields. The zonal wind stress at 0^0 165^0E (from averaged ATLAS 2^0N, 2^0S and EPOCS 0^0N buoy winds) is used to represent the source of western equatorial wind forcing. The following relationship was used to calculate the zonal wind stress:

$$\tau_x = \rho_a C_D u \sqrt{u^2+v^2} \qquad (1)$$

τ_x is the zonal component of the wind stress, ρ_a is the air density (1.2 kg m^{-3}) , C_D is the drag coefficient (1.2 x 10^{-3}), and u and v are the zonal and meridional wind components. This location in the western Pacific was chosen since it was strongly influenced by westerly wind bursts for much of the six month period. In addition, EPOCS wind data was available for this location.

Additional cross-correlations were done using winds and temperatures that have been passed through 30 - 60 day, and 5 - 20 day bandpass filters. This was done to separate the intraseasonal oscillations (Madden and Julian, 1972) from the higher frequency westerly wind bursts. Filtering was performed by applying a fast Fourier transform (FFT) to the data, then eliminating frequency components outside the 30 - 60 day, or 5 - 20 day, window.

D. AVERAGING PROCEDURES

Equatorial data was not available for certain fields and times within the six month study period. Table 1 lists the ATLAS and EPOCS buoy data that was available, and indicates the fields and times for which data was not available. At locations on the equator without ATLAS buoy data, and thus without subsurface temperature information, I have calculated substitute data by averaging ATLAS data from 2°N and 2°S. The good cross-correlations at zero lag of the 150 m buoy temperatures at 2°N and 2°S (Fig. 6) indicate that this averaging produces reasonable substitute data. Figure 7 shows the analysis of Santos, et. al. (1992) of equatorial and averaged zonal winds and SSTs along 165°E. The comparison of data distributions between the 2°N and 2°S and averaged 2°N/2°S indicates that the averaging of winds, or SSTs, from 2°N and 2°S provides reasonable substitute equatorial data.

For many of the equatorial buoys, the data records are not continuous in time. Thus, it was necessary to average data from buoys at 2°N and 2°S along the same line of longitude in order to have continuous equatorial time series throughout the six month study period and at all the analyzed longitudes.

When available, EPOCS buoy wind data are averaged with 2°N and 2°S ATLAS winds to compensate for any missing data. This smooths the wind data and averages the wind forcing over a larger latitudinal range. Since the EPOCS buoys are located on the equator, the EPOCS winds are weighted more in this procedure than the ATLAS buoy winds. EPOCS winds are weighted 75% and ATLAS winds 25%. The ATLAS buoys at 0° 169°W and 0° 170°W were spliced together to form one continuous 183 day record. The location of this spliced time series is designated in this study as 0° 170°W.

III. DATA ANALYSIS

A. EQUATORIAL WIND FIELDS

Between 01 October 1991 and 31 March 1992, numerous zonally extensive westerly wind bursts were observed in the western equatorial Pacific. Several of these wind events occurred in association with tropical cyclones; in particular, typhoons Wilda, Yuri, Val, Wasa, Axel, and Betsy. The low level equatorial westerly winds of these cyclones greatly enhanced the eastward wind stress acting on the ocean surface.

NOGAPS surface wind analysis and observed buoy wind data indicate two distinct equatorial surface wind regimes which existed during the study period. The surface winds shown in Figure 8 are representative of the westerly winds between 145°E and 165°E due to tropical cyclones, the generally strong and persistent easterly winds east of about 160°W, and the transition area between about 180°E and 160°W.

The zonal wind frequency histograms (Fig. 9) also confirm the difference in wind regimes. At the two buoys west of the date line, westerly winds are the most frequent. The transition region near 170°W is clearly composed of both westerly and easterly winds. East of the transition region, the winds are predominately easterly. Note that the most frequent equatorial westerly winds at 156°E and 165°E were only

about 1 ms^{-1}. Strong westerly events only constitute a very small percentage of the total zonal wind occurrences.

Figure 10 shows the equatorial zonal wind speed time series from 156°E to 110°W. As discussed above, there are two distinct equatorial wind regimes. The buoys at 156°E to 165°E clearly represent the westerly regime, while those at, and east of 155°W represent the easterly regime. The 170°W time series represents a transition region, since the data displays both westerly and easterly wind components.

During this study, the dominate features within the western equatorial Pacific were the westerly winds and the occurrence of several strong westerly wind bursts. These periods of intensified westerlies were caused by tropical cyclones. Strong westerly winds from the cyclones were superimposed upon the weak mean westerly flow, which greatly increased the eastward wind forcing.

At 0° 156°E (Fig. 10a) the two significant westerly events are from 30 October to 26 November and then from 25 December to 25 January. These events coincide with tropical cyclones Wilda and Yuri and the cross-equatorial cyclone pair, Axel and Betsy.

In the EPOCS data set at 0° 165°E (Fig. 10b), the prominent event is due to tropical cyclones Wilda and Yuri. This event produced a maximum westerly wind speed on 17 November of 11.7 ms^{-1}. A complete equatorial 183 day time

series at 165°E was constructed by averaging ATLAS and EPOCS data along 165°E at 2°N, 0°, and 2°S.

This weighted average time series at 0° 165°E is shown in Figure 10c and shows four distinct westerly wind events. The first westerly event, from 30 October to 24 November, has a maximum of 7.7 ms^{-1} due to Wilda and Yuri. This averaged wind speed has been reduced from the EPOCS value, since there were easterly winds at 2°N. The second westerly event is from 26 November to 20 December. This 6.2 ms^{-1} maximum corresponds to southern hemisphere cyclones Val and Wasa. The third, and largest event is from 23 December to 12 January. Its wind speed maximum on 8 January of 11.9 ms^{-1} is due to cross-equatorial cyclones Axel and Betsy. The fourth event occurs from 15 January until 26 January and has a maximum of 7.3 ms^{-1} due to tropical storm Kelvin.

Figure 10d shows the winds in the transition region at 170°W. The westerlies are still present and in some cases as intense as those in the western Pacific, but oscillate between the westerlies and easterlies with a strong 40 - 60 day period. The westerly wind event from 18 -23 November is probably due to the influence of cyclones Wilda and Yuri. Cyclones Val and Wasa's influence may be seen from 29 November to 13 December. Westerlies are also observed from the middle to the end of January, and then again at the end of March.

The easterly wind regime begins with the 0° 155°W time series (Fig. 10e). Note though that there are periods of

easterly wind relaxations and sometimes actual westerly winds. Except for the small wind reversal in the first week of December, the winds are easterly until mid-January. Then a significant westerly event occurs from 18 - 31 January, with a maximum westerly wind speed component of 9.3 ms^{-1}. This strong event may correspond to the westerly winds seen at somewhat earlier times at 170°W, 165°E and 156°E.

Persistent easterly winds occurred on the equator at 140°W, 124°W, and 110°W (Figs. 10f-h). However, in each of the three time series, the easterly winds relax and at times turn westerly. This relaxation of the normal easterlies represents an increase in the westerly wind component and is thus a westerly wind event. At 140°W the equatorial easterlies slacken and turn westerly from 23 - 28 January. The buoy data at 124°W shows a wind reversal on 23 - 25 November, but data is missing from the end of January until the end of March 1992. At 110°W the easterlies reverse from 28 - 29 January.

Figure 11 shows the linearly detrended time series plots of the zonal winds. The 165°E EPOCS wind series is not included, because of the lack of continuous data. After detrending the winds, the westerly winds in the western Pacific have been reduced in strength (Figs. 11a and b). In the transition region, the 170°W time series (Fig. 11c) is similar, due to the almost equal occurrence of westerlies and easterlies. Figures 11 d,e,f, and g highlight the reduced easterlies in the eastern Pacific at the end of January and

beginning of February 1992. The linearly detrended data emphasizes the importance of easterly wind relaxation as a form of westerly wind event.

Figure 12 shows the periodograms for six sets of wind data. The zonal winds at 124°W were not included, due to the data gaps. With two exceptions, the 60 day period is the dominant signal in the zonal winds. At 165°E the strongest period is 182 days and at 110°W it is 90 days. In Figure 12a the broad 20 - 90 day peak at 156°E has the strongest signal at 60 and 45 days, with other peaks at 182 and from 15 to 6.5 days. Figure 12b shows that the equatorial zonal winds at 165°E have distinct 182, 60, 22, and 12 day components. The winds at 170°W (Fig. 12c) had a strong 60 day signal, as was seen in the zonal wind time series (Fig. 10d). This 60 day signal was the strongest observed for any of the buoy locations. There are additional distinct peaks at 170°W at 182, 26, and 18 days. At 0°155°W (Fig. 12d) a 36 - 90 day signal is dominant, with other clear peaks at 13.5, 9, and 8 days. The zonal wind periodogram for 0°140°W (Fig. 12e) also shows a broad intraseasonal (36 - 90 day) signal and others at 13.5, 9, 6.5, and 5 days. Figure 12f shows that the strongest signal in the zonal winds at 0°110°W is also an intraseasonal one, with maximum strength at 60 and 90 days. Other distinct peaks are at 36, 20, 15, 13, and 10 days with lesser signals from 9 to 4 days.

B. SEA SURFACE TEMPERATURES

Figure 13 shows the time series plots of SST for the seven equatorial longitudes. As was seen with the zonal winds (Fig. 10), the sea surface temperatures can also be separated into two regimes. The negative linear trend of the SSTs at 156°E, 165°E and 170°W (Figs. 13a-c) defines the first regime. Equatorial SSTs decreased about -0.1 °C per month at 156°E, -0.2 °C per month at 165°E, and -0.1 °C per month at 170°W. The second SST regime occurred from 155°W to 110°W where there was a positive linear trend (Figs. 13d-g). At 155°W, the SST increased about 0.2 °C per month. For 140°W, 124°W, and 110°W, SST increased 0.2 °C per month, 0.6 °C per month, and 0.8 °C per month, respectively.

Throughout the six month study period, SST anomalies associated with the 1991-92 El Niño were positive east of the dateline and negative to the west (Fig. 1). Thus, the linear SST trends seen in Figure 13 are consistent with the broad scale El Niño anomalies. The temperature increase at 0°155°W (Fig. 13d) during December and January corresponds to the location and times of the large SST anomalies seen in Figure 1e and d.

Figure 14 shows the periodograms for the SST time series. The periodogram for 0°124°W is not included, since there is a lack of continuous data. Aside from the semi-annual (182 day) period, the major periods in the SST data were 90, 60, and 45 days.

The SSTs at 0°156°E (Fig. 14a) showed the strongest high frequency signal. The primary period is 90 days with other contributions at 60, 45, 26, 18, 15, 10, and 9 days. The SSTs at 0°165°E have their primary period (Fig. 14b) at 60 and 45 days, with three additional periods of 23, 15, and 12 days. Figures 14c and d show that the dominant period at 0°170°W and 0°155°W is the 182 day semi-annual cycle. Secondary peaks occur at 30 and 60 days. A strong 60 day period is shown in Figure 14e for SSTs at 0°140°W. The other distinct peaks are at 26 and 18 days. Figure 14f shows that the major peaks in SST at 0°110°W are at 90 and 36 days.

The time scales of the SST variations are also revealed in the linearly detrended temperature series (Fig. 15). These series emphasize strong intraseasonal variability of the SSTs throughout the basin. These detrended SSTs will be discussed further in Section D of this Chapter when the relationship of SST to local wind forcing is examined.

C. OCEAN TEMPERATURES AT 150, 140 AND 100 METERS

To determine the influence of remote westerly wind forcing on the equatorial Pacific thermocline, I have analyzed equatorial subsurface temperatures at 150 m (at 156°E, 165°E, and 170°W), 140 m (at 155°W, 140°W, 124°W, and 110°W) and 100 m (at 110°W). These combinations of depths were chosen in order to examine the subsurface temperatures that display large amplitude variations and which represent the near-

thermocline depths discussed in Chapter II. As will be shown, the subsurface temperatures indicate that several oceanic Kelvin waves may have propagated from 170°W to 110°W.

During the six month study period, the western and eastern equatorial Pacific subsurface temperature structures differed dramatically (Fig. 16). The ocean temperatures in the western Pacific (Figs. 16a and b) varied slowly and generally decreased from mid-November 1991 through the end of March 1992. In the central and eastern Pacific, the ocean temperatures (Figs. 16c-g) displayed large temperature fluctuations at near-thermocline depths.

Figure 17 displays the meridionally averaged 150 m temperatures at 156°E, with and without the linear trend. These temperatures are the averages of the 2°N and 2°S temperatures at 156°E. In the raw data time series (Fig. 17a) the temperatures are nearly constant at approximately 23°C from October through mid-November. They then decrease gradually to approximately 18°C by early February. Temperatures then increase to approximately 20°C by the end of March. The linear trend for the entire six month record shows that the temperature decreases about 0.9°C per month. However, this linear trend may not be the best approximation of the long-term variation since the series is clearly not linear over the six month period. The linearly detrended series (Fig. 17b) shows that the 150 m temperatures increase by approximately 2°C from October through early November.

Another temperature increase of approximately 4 °C occurs from the first week in February until the end of March. The latter temperature increase follows a period of strong westerly winds in January (Fig. 10a).

Figure 18a shows that the same general pattern in 150 m temperatures exists at 165°E. The linear trend is -0.8°C per month, and there is a decrease in temperatures beginning in mid-November. This temperature decease is more pronounced than at 156°E. The 150 m temperatures are approximately 23°C until 16 November, then decrease to approximately 18°C - 20°C by 31 November. This decrease may correspond to the 11.7 ms^{-1} westerly wind burst observed in EPOCS data on 17 November (Fig. 10b). The detrended data (Fig. 18b) indicates a temperature increase in October and then a sharp 3.5°C temperature decrease in mid-November. The detrended 150 m temperatures at 156°E and 165°E also show a clear difference in early December when the temperatures at 165°E began to slowly increase while at 156°E the temperature was still decreasing.

The warming indicated in the linearly detrended 150 m temperatures during October and early November corresponds to the relaxation of easterly winds and the onset of an eastward 10 m current (Fig. 19a). The eastward currents (South Equatorial Current reversal) and 150 m temperature increases may correspond to downwelling due to Ekman convergence and the initiation of the downwelling phase of a Kelvin wave.

Figure 20a shows the 150 m temperatures for 0° 170°W. This time series shows much more intraseasonal variability than at 156°E or 165°E. Distinct temperature maxima of 29.0°C and 29.1°C are evident on 24 November and 19 January, respectively. A possible maximum of 27.4°C occurred near the beginning of the record on 17 November. Note that the January maxima represents a 12°C rise and fall in the 150 m temperatures. The three maxima are separated by about 40 - 60 days. The maxima may be associated with downwelling and may indicate the passage of the downwelling phases of equatorial Kelvin waves. The linear trend for this series represents an overall cooling of about -1.3°C per month. This cooling is mainly due to persistent cool temperatures during February and March.

ATLAS buoys at, and east of, 155°W measure temperatures at 140 m instead of 150 m. The 140 m temperatures series at 155°W (Fig. 20b) has three maxima of 26.7°C on 17 October, 29.3°C on 08 December, and 29.5°C on 30 January. The periods between the maxima are about 40 - 60 days, as at 170°W. The magnitude of the temperature variations are also similar. The linear trend is -1.2°C per month, again due to the persistent cool temperatures in February and March.

The averaged 140 m temperature series for 0° 140°W (Fig. 20c) is missing data from 17 October through 26 November. Two temperature maxima are seen, with a possible third temperature maximum of 25.9°C on 14 October. The second maximum of 26.8°C

on 15 December and the third maximum of 27.6°C on 01 February are better represented. After the third warming event, the temperatures decreased approximately 15°C. The warming events again show a 40 - 60 day period. As observed from the previous data, a general cooling of -1.4°C per month occurs over the six month period.

A comparison of the zonal winds (Fig. 10f), the zonal currents (Fig. 19b), and the 140 m temperatures (Fig. 20c) at 140°W shows that the periods of cool 140 m temperatures in early January and at the end of February and first part of March were periods of westward winds and currents. The periods of warm 140 m temperatures in the latter part of January and early February were times of eastward winds and currents. These current and temperature relationships suggest that eastward currents are associated with warmer 140 m temperatures, a thicker mixed layer, and a depressed thermocline. Westward currents and cooler 140 m temperatures are associated with the opposite. These relationships are consistent with those expected from the passage of a Kelvin wave. On the other hand, the wind - current relationships suggest that the current reversals may have been associated mainly with the local westerly wind events in late January and early February.

Further east at 124°W the 140 m temperature series (Fig. 20d) is missing data from 01 October through 03 December. Two maxima of 24.5°C and 26.0°C occur on about 20 December and 10

February. These maxima were 52 days apart and probably correspond to the second and third maxima in the 140 m temperature series at 140°W. The linear temperature trend of the available data indicates a cooling of -1.7°C per month.

Figure 20e shows the meridionally averaged 140 m temperature time series at 110°W. At this depth, the large variations at 170°W - 124°W did not occur. Except for a 2°C temperature increase on 28 October, the 140 m temperature variations were small until 16 December. The temperature then increased to a second maximum of 15.8°C on 03 January (67 days between peaks). The third maximum of 17.2°C occurs 40 days later on 12 February and is the largest temperature variation (only 3°C) observed at this depth. The linear temperature trend is 0.1°C per month.

The temperature variations at 110°W are possibly smaller than further to the west, because the thermocline is well above 140 m (Fig. 2). The 3°C temperature variation in February may represent an especially large amplitude Kelvin wave. Another, and no entirely separate, explanation is that the thermocline at 110°W was deeper during February. Figure 16g indicates that the thermocline may have been about 30 m deeper in February than in January. Kousky (1992b) also suggests that the eastern Pacific thermocline was deeper during February.

To examine the vertical extent of the large 150 and 140 m temperature variations (Figs. 16c-g and Fig. 20), I also

analyzed the 100 m temperatures. Figures 21a and 22a show meridionally averaged temperatures at 100 m for 156°E and 165°E. They display the same general temperature pattern as the 150 m temperatures (Figs. 17a and 18a). At 156°E, the cooling trend is about -0.6°C per month, but at 165°E it increases to -0.9°C per month. Figure 21b is the linearly detrended series for 156°E, which shows, after a 2°C temperature increase in October, a temperature decrease until mid-February. The 100 m temperatures then increased approximately 4°C through the end of March. Figure 22b shows the linearly detrended 100 m temperature at 165°E. The temperature increased approximately 3°C until mid-November, then decreased until mid-January. Then, over the next two and half months, it increased by approximately 6°C. For both locations, the detrended temperature increase in October and November occurred at the same time as a reversal in the South Equatorial Current (SEC) and the development of a strong eastward current at 10 m at 165°E (Fig. 19a). Thus, these wind, 100 m temperature, and 10 m current relationships are similar to those seen in the analyses of the 140 m temperatures at 140°W. These relationships are, again, consistent with those expected from the passage of a Kelvin wave.

The 100 m temperature series from 0° 170°W to 0° 140°W (Figs. 23a-c) show very little variability until late February when the 100 m temperatures suddenly decreased. This sudden

temperature decrease may be associated with the strong upwelling observed in the 150 and 140 m temperatures (Fig. 20). Prior to the cooling in February and March, the 100 m temperatures were similar to the SSTs (Fig. 13), which indicates that the mixed layer extended to or below this depth. This is consistent with the equatorial cross-section shown in Figure 2.

In Figure 23d, the 100 m temperatures at 124°W are shown to differ from those to the west. The series shows more variability than at 170°W - 140°W, and is similar to the 140 m temperature series (Fig. 20d). However, the 100 m temperature variations are larger than 140 m. Figure 23e shows three separate 100 m temperature maxima at 0° 110°W. This is in contrast to the 140 m temperatures (Fig. 20e), which display little variability. The first temperature maximum of 22.1°C occurs on 09 November. The second is 23.3°C and occurs on 02 January. On 26 February there is a third temperature maximum of 25.9°C. These warm temperature maxima have a period of approximately 55 days, which is consistent with the intraseasonal periods found basin-wide in 150 - 140 m temperatures. The linear trend of the 100 m temperatures at 110°W is 0.3°C per month.

In summary, the 100 m and 140 m temperature variations at 110°W are qualitatively similar and are approximately in phase. However, the 100 m temperature variations are two to four times larger.

Periodograms for the 150 - 140 m temperatures between 165°E and 155°W, and the 100 m temperatures at 110°W are shown in Figure 24. Analyses for 140°W and 124°W are not included because of lack of continuous data. At 156°E (Fig. 24a) and 165°E (Fig. 24b), the dominant period is 182 days, but there is also an intraseasonal (60-90 day) signal. Figure 24c shows that the dominant period for the 150 m temperatures at 0°170°W is 60 days, but there are other peaks at 182, 45, and 30 days. The 140 m temperatures at 155°W have primary periods (Fig. 24d) at 182, and 45-60 days. At 110°W (Fig. 24e) the 100 m temperatures have a broad period of 45-90 days and a secondary period of 182 days.

D. LOCAL SST RESPONSE TO ZONAL WINDS

As discussed in Chapter I, evaporative heat loss from the oceans surface is proportional to the wind speed (McPhaden and Hayes, 1991). This relationship is useful in determining the effects of local winds on sea surface temperatures. Additionally, cooling due to the mixing of cooler, deeper water with warmer surface waters is proportional to the cube of the wind speed. This entrainment cooling will vary with several factors, in particular, the depth of the mixed layer (Webster and Lukas, 1992).

In addition to causing cooling through evaporation or entrainment, westerly wind events may also cause warming through their impacts on surface currents. Westerly wind

events may cause eastward surface currents, with Ekman convergence toward the equator producing an equatorward intensification of the flow (Cane, 1980; Gill and Rasmusson, 1983). This equatorward convergence will tend to produce equatorial downwelling. The eastward current will also tend to advect warm surface waters from the western Pacific warm pool, thereby, increasing local SSTs. Acceleration of the eastward surface currents was observed in the EPOCS zonal current data (Fig. 19). The $0^{0}165^{0}E$ eastward current (Fig. 19a) reached speeds in excess of 1 ms^{-1}. Flow speeds greater than 1 ms^{-1} have been observed in previous studies (Webster and Lukas, 1992). The 10 m current at $165^{0}E$ is also well correlated with the local winds, as shown in Figure 25a.

Both the cooling and warming effects of the wind at $165^{0}E$ are suggested in Figure 26 from Santos et. *al*. (1992). This Figure shows two general relationships: (1) At wind magnitudes less than about 7 ms^{-1}, SSTs decrease as winds increase; and (2) for winds greater than 7 ms^{-1}, the SSTs tend to increase. The SST decrease with increased wind may be explained by increased entrainment and evaporation. The SST increase with increased wind suggests that the warming processes discussed above may operate most effectively during strong wind events. At $165^{0}E$ these strong winds occur only during westerly wind events that persist for several days or more (see Fig. 10c). Of course, strong persistent winds are necessary for reversing the South Equatorial Current to

produce eastward flow and equatorial downwelling. Thus, it appears that there may have been two local wind-SST regimes in the west Pacific during the study period. The first was a weak wind-cooling regime associated with evaporation and entrainment. The second was a strong wind-warming regime associated with warm water advection and downwelling.

Figure 19b shows a westward to eastward current reversal at $0^{0}140^{0}W$ in late January. This occurs during a relaxation and reversal in the easterly winds (Fig. 10f). The winds and currents are fairly well correlated (Fig. 25b) when the zonal winds lead the currents by about five days. Such eastward currents may have been important in advecting warmer waters from the central Pacific during the 1991-92 El Niño.

The western Pacific wind regime includes longitudes $156^{0}E$ and $165^{0}E$ which were dominated by strong westerly winds during the study period (Fig. 10). Examples of significant air-sea interaction due to these strong westerly winds are suggested by the two sharp decreases in SST at $156^{0}E$ and $165^{0}E$ (Figs. 15a and b). The decrease in SST coincides with the westerly wind events of November and January (Fig. 10a-c). The temperatures decreased approximately $1^{0}C$, which is consistent with previous studies by Chu and Frederick (1990) and Lukas and Lindstrom (1991).

Figure 27 shows the cross-correlations of non-filtered zonal winds and SST. The winds at $156^{0}E$ are negatively correlated with the SSTs, when the winds lead SSTs by about

zero to 18 days (Fig. 27a). This means that an increase (decrease) in the westerly wind is associated with a local SST cooling (warming) that may develop very rapidly and persist for a week or more. The weak positive correlations when the winds lead the SSTs by about 25 - 45 days suggests that there may have been a delayed warming response to westerly wind events. Positive correlations occur when the SST leads the wind by 5 - 30 days. These suggest that SST increases precede the development of tropical cyclones and their associated westerly winds by about one week to one month.

The estimated cross-correlations between the zonal winds and SSTs at 165°E (Fig. 27b) are similar to those at 156°E. When the winds lead SSTs, they are negatively correlated for lags of about zero to 40 days. These correlations are stronger than at 156°E and occur over a longer lag range. This suggests that the cooling effects are greater at 165°E. At both equatorial locations, the local SSTs quickly decreased in response to the onset of the westerly winds. The wind-SST correlations are weakly positive when the winds lead by about 40 days which, as at 156°E, might indicate some temperature advection effect from sustained westerlies. When the SSTs lead winds, there are positive correlation peaks at lags of about 30 days, which is also similar to what was seen at 156°E (Fig. 27a).

Figure 27c shows the estimated cross-correlations of winds and SSTs at 0° 170°W. This equatorial longitude is in

the transitional wind regime with an almost equal distribution of easterlies and westerlies (Fig. 10d). The wind and SST correlations show a basically symmetric pattern with little or no correlation near zero lag. Notice the dramatic change in the overall correlation pattern from those for 156°E and 165°E. When the winds lead the SSTs, the data are positively correlated for lags from about zero to 45 days. This suggests that the SSTs increase with an increase in the westerlies. At short time lags when the SSTs lead the winds, an increase in SST may cause a corresponding increase in the westerlies.

The buoy at 155°W is in the western part of the equatorial easterly wind regime (see Chapter II, Section A). Thus, at this longitude, and all longitudes further east, increases in the westerly wind generally corresponded to just a decrease in the easterly winds. Thus, a positive variation in the wind corresponds to a decrease in wind speed; and, therefore, a decrease in evaporation and entrainment. Note that this is the opposite of the situation in the westerly regime (156°E and 165°E) where the mean wind is weak and a positive wind variation generally corresponds to an increase in the wind speed; and, therefore, an increase in evaporation and entrainment. The wind-SST correlations for this location (Fig. 27d) show that when the winds lead the SSTs, the correlations are slightly negative at zero lag, but positive at lags of about 10 - 25 days, and negative at lags of about 30 - 60 days. Stronger correlations exist when the SSTs lead

the zonal winds. For negative lags of about zero to 15 days, the correlations suggest that an increase in SST may actually decrease the westerlies. The two fields are positively correlated when the SST leads by 20 - 55 days, which suggests that SST increases lead to increases in the westerlies.

The estimated cross-correlations for 140°W (Fig. 27e) are roughly similar to those at 155°W. They show essentially no correlation between the zonal winds and SSTs at zero lag. At this longitude, easterly winds are dominant, which might explain the relatively strong positive correlations when the winds lead the SST by about 2 - 30 days. Since 140°W is in the easterly wind regime, an increase in the wind indicates a weakening of the easterly wind. From Figure 27e, this weakening corresponds to an SST warming within the next few weeks. This may be explained by a reduction of the evaporation, entrainment, and upwelling associated with strong easterly winds.

Figure 27f shows the cross-correlations of zonal winds and SSTs at 110°W. For positive lags (wind leads SST), the correlations are qualitatively similar to those for 155°W and 140°W. When the zonal winds lead the SSTs, the correlations are positive for lags from zero to approximately 30 days. Correlations are negative for lags of 40 - 70 days. When the SSTs lead the winds, the data are negatively correlated at lags of 15 - 40 days.

There are distinct patterns in the correlations between the various wind and SST time series which correspond to the observed wind regimes. The correlation patterns for 156°E and 165°E are similar, which may be because both locations are in the westerly wind regime. In the easterly wind regime, the correlations for 155°W, 140°W, and 110°W are also similar. Correlation patterns in the transitional wind regime (170°W) are similar to those in the easterly wind for positive lags, and similar to those in the westerly regime for negative lags.

In the western equatorial Pacific, an increase in the westerlies results in almost immediate SST cooling and, at some time in the future, SST warming. Conversely, in and east of the zonal wind transition region, an increase in the westerlies (i.e., a decrease in the easterlies) produces warming followed by cooling a month or more later. In the easterly wind regime, the SSTs become warmer at short time lags after the winds become less easterly and more westerly. The observed easterly wind relaxations and westerly wind anomalies (Fig. 11) probably correspond to a reduction in evaporation, mixing, and equatorial upwelling of colder water. Thus, an increase in westerly winds within the eastern Pacific would tend to increase the local SSTs. Thus, the different correlation patterns seen at positive lags (Fig. 27) may be explained by the different background wind fields.

To determine the periods of the variations which contribute to these correlations, I have filtered the zonal

winds and SSTs to obtain the 30 - 60, and 5 - 20 day components. Figure 28 shows the cross-correlations for the 30 - 60 day filtered data and Figure 29 shows the 5 - 20 filtered data correlations. These filtered correlations suggest that the intraseasonal (30 - 60 day) oscillations are dominated by the overall wind and SST relationships (Fig. 27), but the 5 - 20 day oscillations do make a significant contribution at certain lags.

In summary, the factors affecting the local SSTs are: (1) the strength and direction of the wind variations; (2) evaporative and entrainment cooling; (3) downwelling due to Ekman convergence; and (4) warm water advection from wind induced surface currents. This very complicated issue deserves further in-depth analyses, which, unfortunately, are beyond the scope of this study.

D. REMOTE RESPONSE TO WESTERN PACIFIC WIND STRESS

The Atlantic Oceanographic and Meteorological Laboratory (AOML, 1992) reported on 06 March 1992 that "...in February a very large (20 - 40 cm) sea level pulse reached the Galapagos...at Kelvin wave speeds." This sea level rise was attributed to December's severe westerly winds in the central Pacific. The ATLAS buoy temperature (Fig. 20 and Figs. 23), and EPOCS zonal current (Fig. 19) data suggest the presence of an oceanic equatorial Kelvin wave, which might correspond to this observed sea level pulse.

Table 2 summarizes the 150, 140, and 100 m temperature maxima discussed in Section C. The third temperature maximum has the largest amplitude. This third pulse was possibly initiated by the westerly wind events described in Chapter II, Section A.

Assuming that this third pulse represented the downwelling phase of a Kelvin wave, then the propagation distance is from 170°W to 110°W, or 6671 km. The third temperature maximum at 170°W occurred on 19 January and at 110°W on 26 February (Table 2), indicating a 38 day travel time. Thus, the average phase speed would be 2.0 ms^{-1}. Using the 140 m temperature maximum at 110°W, the travel time is 22 days and the average phase speed is 3.5 ms^{-1}. The average of these two, 2.75 ms^{-1} is probably a better estimate of the actual phase speed. Similar phase speeds are obtained when the first and second subsurface temperature maxima are used, and when the temperature minima are used.

Baroclinic ocean Kelvin waves travel at speeds between 0.5 - 3 ms^{-1} (Gill, 1982, pp. 437). From previous studies, a typical phase speed for the first baroclinic Kelvin wave is about 2.8 ms^{-1} (Wunsch and Gill, 1976), or about 60° per month (Gill and Rasmusson, 1983). These values are consistent with the calculated average value of 2.75 ms^{-1}.

Thus, the subsurface temperature data from the buoys strongly suggest the presence of several eastward propagating internal Kelvin waves during October 1991 - March 1992. The

task now becomes to relate these observed ocean waves with western Pacific zonal wind forcing.

As I discussed in Chapter I, Kelvin wave forcing is proportional to the square of the wind speed (McPhaden and Hayes, 1991). As discussed in Chapter II, this forcing will be represented by the zonal wind stress component, τ_x . To explore the wind forcing relationship to Kelvin wave generation, τ_x at 0^0 165^0E is cross-correlated with equatorial 150 m or 140 m temperatures at 170^0W - 140^0W, and with equatorial 100 m temperatures at 124^0W - 110^0W.

All data has been linearly detrended prior to the correlation analyses. In these, and subsequent correlations, positive lags mean that the wind stress (or wind) leads the temperature, and negative lags mean that the temperature leads the wind stress (or wind).

Figure 30 shows the cross correlations of observed wind stress and subsurface temperatures. At all longitudes, the largest correlations exist when the western Pacific wind stress leads the equatorial subsurface temperatures, which suggests that atmospheric forcing is driving the ocean temperature fluctuations. Strong positive correlation peaks are found when the temperatures lag behind the wind stress by 10, 18, 27, 37, and 41 days at 170^0W, 155^0W, 140^0W, 124^0W, and 110^0W, respectively. The positive correlations indicate that eastward (westward) wind stresses at 165^0E precede subsurface warming (cooling) at points further east. This suggests that

the warming (cooling) may be forced by west Pacific wind stress events. As suggested above, equatorial Kelvin waves are a likely mechanism for this long distance forcing.

The lag difference between the maximum correlations at 0°170°W and 0°110°W (Fig. 30) is 31 days, indicating an average phase speed of 2.5 ms^{-1}. This value is very close to the theoretical value of 2.8 ms^{-1} discussed by Wunsch and Gill (1976) and to the value of 2.75 ms^{-1} calculated above.

The calculated values represent an average phase speed from 170°W to 110°W, but there may have been wave accelerations, or decelerations along the equatorial waveguide. As suggested in the subsurface temperature data (Figs. 20 and 23) and the correlations (Fig. 30), the internal waves may have accelerated east of 124°W. A possible explanation is that during the 1991-92 El Niño there were anomalously warm SSTs in the eastern equatorial Pacific. These warm surface waters, and the upwelling of cooler water due to the persistent easterly winds, may have created a relatively strong vertical temperature gradient in the eastern Pacific. A stronger vertical temperature gradient would tend to increase the frequency of internal waves (i.e., increase the reduced gravity term) and thus, increase the wave speed.

Using the correlations shown in Figure 30, I have calculated an estimated wave period. The positive and negative correlations in Figure 30 were assumed to represent the downwelling and upwelling wave phases, respectively. I

assumed that the time between the maximum positive correlation and the maximum negative correlation was half a wave period, which lead to an estimated period of 60 - 70 days. This is an average value, since the correlations represent all the suspected Kelvin wave signals in the time series. Note that the FFT analysis (Fig. 24) shows a strong 60 day period in the subsurface temperatures. Applying the estimated 60 - 70 day wave period and the averaged phase speed of 2.75 ms^{-1}, an approximate wavelength of 14,000 - 16,000 km is obtained for the Kelvin waves. These values represent wavelengths of basin-wide scale. Correlations of filtered wind stress and temperatures are included in order to separate intraseasonal influences from higher frequency westerly wind bursts. Intraseasonal 30-60 day oscillations have been suggested to be closely related to westerly wind bursts (Nakazawa, 1988). Correlations for 124°W are not included, because of the lack of data.

Figure 31 shows the correlations after the data were filtered to obtain the intraseasonal (30 - 60 day) oscillations. These 30 - 60 day correlations are similar in overall pattern to the non-filtered correlations (Fig. 30). However, the filtered 30 - 60 day filtered correlations are larger, especially when the subsurface temperatures lead the wind stress.

Figure 32 shows the correlations after 5 - 20 day filtering. The correlations for the higher frequency (5 - 20

day) filtered data show relatively little relation to the non-filtered correlations. Comparisons of Figures 30, 31, and 32 indicate that the non-filtered correlations are reduced by the higher frequency components, especially when temperatures leads the wind stress.

This suggests that the 30 - 60 day intraseasonal wind forcing is responsible for the strong correlations seen in the non-filtered data. Thus, intraseasonal variations in the western Pacific wind stress, and in particular the wind stress associated with tropical cyclones, seem to have been important in forcing subsurface temperature variations throughout the central and eastern equatorial Pacific. These remote responses to the wind seem to have propagated out of the west Pacific in the form of internal equatorial Kelvin waves.

IV. CONCLUSIONS

A. SUMMARY AND DISCUSSION

This study has focused on the response of the upper equatorial Pacific Ocean to anomalous westerly wind forcing during the 1991-92 El Niño. The primary data were mixed layer oceanographic and boundary layer atmospheric fields from the TOGA and EPOCS equatorial moorings. Supporting fields came from the U.S. Navy's operational atmospheric analyses.

From the NOGAPS analyses and buoy observations, the equatorial region can be separated into two wind regimes. From about 156°E to the date line, the zonal winds were predominantly weak westerlies, with numerous strong westerly wind events. These wind events were best developed during the passage of cross-equatorial cyclone pairs (e.g., Axel and Betsy, which produced westerly wind speeds of approximately 12 ms^{-1} in January 1992). In the central equatorial Pacific, around 170°W, a transition region existed where both easterly and westerly winds occurred with almost equal frequency. The eastern Pacific winds were mainly easterly, but strong relaxations of the easterlies occurred throughout the study period. Throughout the equatorial Pacific, the winds also had a strong intraseasonal period of 30 - 60 days, which was mainly the result of the westerly wind events in the western

Pacific and the easterly wind relaxations in the central and eastern Pacific.

The difference in wind regimes affected the local upper ocean response to westerly winds. In the western Pacific, there was an almost immediate cooling in response to an increase in the westerly winds. In some cases the SST cooled by approximately 1°C, which is consistent with previous studies conducted by Chu and Frederick (1990) and Lukas and Lindstrom (1991). For the western Pacific, McPhaden and Hayes (1991) concluded that evaporative cooling was responsible for the majority of observed SST cooling and that entrainment cooling was an order of magnitude smaller. After the initial cooling, there was typically a period of upper ocean warming. Subsurface temperature and zonal ocean current data at 0°, 165°E strongly suggest that this warming was associated with wind-induced eastward advection of warmer water and equatorial downwelling.

Within the central and eastern Pacific, the wind and SST had a different relationship. When the westerlies increased (i.e., when the easterlies relaxed), the SSTs increased within a few days. These positive variations in the wind produced a reduction in the wind stress magnitude and, therefore, a decrease in evaporation, mixing, and upwelling. Thus, westerly wind events in the central and eastern Pacific tended to produce SST warming, in contrast to the cooling associated with westerly wind events in the western Pacific. Thus, the

equatorial SST anomalies observed during the 1991-92 El Niño (Fig. 1) may in part be explained by local westerly wind events.

During the 1991-92 El Niño, the central and eastern equatorial Pacific near-thermocline temperatures experienced large amplitude fluctuations, apparently associated with strong upwelling and downwelling. The largest temperature variations observed were on the order of 10°C and had an intraseasonal period of 30 - 60 days. This intraseasonal period is consistent with the findings of McPhaden and Hayes (1990). From 170°W to 110°W, the phases of the temperature extrema were shifted progressively eastward, which indicated that several eastward propagating internal equatorial Kelvin waves occurred during the study period. Three meter ocean currents at 140°W also suggest the passage of these Kelvin waves. The calculated phase speeds are consistent with the first baroclinic equatorial Kelvin wave dynamics (i.e., 2.0 - 3.5 ms^{-1}).

These internal waves appeared to have been forced by the westerly wind events in the western equatorial Pacific. The remote equatorial ocean response to this western Pacific wind forcing was addressed by cross-correlating the non-filtered and filtered zonal wind stress at 165°E with the subsurface temperatures from 170°W to 110°W. These correlations indicate that the remote forcing of the central and eastern Pacific occurred through the eastward propagation of first baroclinic

Kelvin waves with periods of 60 - 70 days, and basin wide wavelengths (about 15 x 10^3 km).

B. FUTURE WORK

The TOGA and EPOCS ocean and atmospheric data provided valuable insights into equatorial air-sea interactions during the 1991-92 El Niño, but there are many other issues which should be studied further. Some of the topics which can be addressed with present and future data sets are:

(1) Determination of statistical significance of the cross-correlations.

(2) Calculation of buoyancy fluxes from sea surface and air temperature data.

(3) Examination of the subsurface temperature variations from 8°N to 8°S, to possibly determine the latitudinal extent of the equatorial waveguide.

(4) Incorporation of observational data into future modeling studies.

(5) Further study on western Pacific remote forcing of equatorially trapped waves versus propagating atmospheric forcing along entire equatorial Pacific.

LIST OF REFERENCES

Atlantic Oceanographic and Meteorological Laboratory (AOML), Miami. Anonymous OMNET Telemail report of 06 March 1992.

Box, G.E.P., and G.M. Jenkins, 1976: Time Series Analysis, Forecasting and Control, second edition. San Francisco: Holden-Day.

Cane, M.A., 1980: On the dynamics of equatorial currents, with application to the Indian Ocean. *Deep-Sea Res.*, 27, 525-544.

----, and S.E. Zebiak, 1985: A theory for El Niño and southern oscillation. *Science*, 228, 1085-1086.

Chu, P.-S., 1988: Extratropical forcing and the burst of equatorial westerlies in the western Pacific. *J. Meteor. Soc. Japan*, 66, 549-564.

---, and J. Frederick, 1990: Westerly wind bursts and surface heat fluxes in the equatorial western Pacific in May 1982. *J. Meteor. Soc. Japan*, 68, 523-536.

Giese, B.S., and D.E. Harrison, 1991: Eastern equatorial response to three composite westerly wind types. *J. Geophys. Res.*, 96, 3239-3248.

Gill, A.E., 1982: Atmosphere-Ocean Dynamics. Academic Press, San Diego. p.437.

----, and E.M. Rasmusson, 1983: The 1982-83 climate anomaly in the equatorial Pacific. *Nature*, 306, 229-234.

Godfrey, J.S. and E. Lindstrom, 1989: On the heat budget of the equatorial West Pacific surface mixed layer. *J. Geophys. Res.*, 94, 8007-8017.

Goerss, J.S., L.R. Brody, and R.A. Jeffries, 1991: Assimilation of Tropical Cyclone Observations into the Navy Operational Global Atmospheric Prediction System. Preprints, Ninth Conference on Numerical Weather Prediction, October 14-18, 1991, Denver, Colo., Amer. Meteor. Soc., 638-641.

Harrison, D.E., and P.S. Schopf, 1984: Kelvin wave-induced anomalous advection and the onset of surface warming in El Niño. Mon. Wea. Rev., 112, 923-933.

--------, and B.S. Giese, 1991: Episodes of surface westerly winds as observed from islands in the western tropical Pacific. J. Geophys. Res., 96, 3221-3237.

Hogan, T.F., and T.E. Rosmond, 1991: The description of the Navy operational global atmospheric prediction system's spectral forecast model. Mon. Wea. Rev., 119, 1786-1815.

Keen, R.A., 1982: The role of cross-equatorial tropical cyclone pairs in the southern oscillation. Mon. Wea. Rev., 110, 1405- 1416.

Kousky, V.E., 1991a: Climate Diagnostics Bulletin (October). Climate Analysis Center, U.S. Department of Commerce, Washington, D.C., No.91/10.

------, 1991b: Climate Diagnostics Bulletin (November). Climate Analysis Center, U.S. Department of Commerce, Washington, D.C., No.91/11.

------, 1991c: Climate Diagnostics Bulletin (December). Climate Analysis Center, U.S. Department of Commerce, Washington, D.C., No.91/12.

------, 1992a: Climate Diagnostics Bulletin (January). Climate Analysis Center, U.S. Department of Commerce, Washington, D.C., No.92/1.

------, 1992b: Climate Diagnostics Bulletin (February). Climate Analysis Center, U.S. Department of Commerce, Washington, D.C., No.92/2.

------, 1992c: Climate Diagnostics Bulletin (March). Climate Analysis Center, U.S. Department of Commerce, Washington, D.C., No.92/3.

Lau, K.-M., Li Peng, C.H. Sui, and T. Nakazawa, 1989: Dynamics of supercloud clusters, westerly wind bursts, 30-60 day oscillations and ENSO: an unified view. J. Meteor. Soc. Japan, 67, 205-219.

Lukas, R., S.P. Hayes, and K. Wyrtki, 1984: Equatorial sea level response during the 1982-83 El Niño. J. Geophys. Res., C6, 10, 425-430.

-----, 1988: On the role of western Pacific air-sea interaction in the El Niño / Southern Oscillation Phenomenon, Proceedings of the U.S. TOGA Western Pacific Air-sea Interaction Workshop, edited by R. Lukas and P. Webster, pp. 43-69, *UCAR Tech. Rep.*, US-TOGA-8, Univ. Corp. for Atmos. Res., Boulder, Colo.

-----, 1989: Observations of air-sea interactions in the western Pacific warm pool during WEPOCS, in Proceedings of the Western Pacific International Meeting and Workshop on TOGA-COARE, edited by J. Picant,R Lukas,T. Delcruix, pp. 599- 610, ORSTOM, Noumea, New Caledonia.

-----, and E. Lindstrom, 1991: The mixed layer of the western Pacific ocean. *J. Geophys. Rev.*, **69**, 3343-3357.

Madden, R.A., and P. Julian, 1972: Description of global scale circulation cells in the tropics with a 40-50 day period. *J. Atmos. Sci.*, **29**, 1109-1123.

McCreary, J.P., 1976: Eastern tropical ocean response to changing wind systems with application to El Niño. *J. Phys. Oceanogr.*, **6**,634-645.

McPhaden, M.J., and S.P. Hayes, 1990: Moored velocity, temperature and wind measurements in the equatorial Pacific ocean: A review of scientific results, 1985-1990, in the Proceedings of the International TOGA Scientific Conference, ,16-20 July 1990, (WMO/TD-No.379) pp. 59-69.Honolulu, Hawaii, U.S.A.

--------, and S.P. Hayes, 1991: On the variability of winds, sea surface temperature, and surface layer heat content in the western equatorial Pacific. *J. Geophys. Rev.*, **96**, 3331-3342.

Murakami, T., and W.L. Surathipala, 1989: Westerly bursts during the 1982/83 ENSO. *J. Clim.*, 2, 71-85.

Nakazawa, T., 1988: Tropical super-clusters under intra-seasonal variation. Japan-U.S. Workshop on the ENSO Phenomena, University of Tokyo, Meteorology Rep. #88-1, Dept. of Meteorology, Geophysical Institute, 76-78.

Nitta, T., 1989: Development of a twin cyclone and westerly bursts during the initial phase of the 1986-87 El Niño. *J. Meteor. Soc. Japan*, **67**, 677-681.

Philander, S.G.H., 1981: The response of equatorial oceans to a relaxation of trade winds. *J. Phys. Oceanogr.*, **11**, 176-189.

Ramage, C.S., 1985: El Niño variability and tropical cyclones. *Trop. Ocean-Atmos. Newsl.*, **30**, 3-5.

Santos, A., D. Burris, W. Gillman, and B. Guarino 1992: The theoretical relationship between air temperature, water surface temperature,and wind speed and direction. OA 3140 student report. U.S. Naval Postgraduate School, Monterey.

Webster, P.J., and R. Lukas, 1992: TOGA COARE: The coupled Ocean Atmosphere Response Experiment. *Bull. Amer. Meteor. Soc.*, 73, 1377-1416.

Wunsch, C., and A.E. Gill, 1976: Observations of equatorially trapped waves in Pacific sea level variations. *Deep-Sea Res.* 23, 371-390.

Wyrtki, K., 1975: El Niño - the dynamic response of the equatorial Pacific ocean to atmospheric forcing. *J. Phys. Oceanogr.*,15, 572-584.

TABLE 1. PERIODS COVERED BY ATLAS AND EPOCS BUOY DATA. THE U AND V WIND COMPONENTS, SEA SURFACE TEMPERATURE (SST), AND OCEAN TEMPERATURES AT 100 AND 150 M ARE LISTED BELOW FOR EACH BUOY LOCATION. TIME PERIOD: OCT 91 - MAR 92. AVERAGING WAS PERFORMED TO REPLACE MISSING DATA.

	OCT	NOV	DEC	JAN	FEB	MAR
ATLAS 2N156E						
U-wind	------	------	------	------		
V-wind	------	------	------	------		
SST	------	------	------	------		------
T100m	------	------	------	------		------
T150m	------	------	------	------		------
ATLAS 2S156E						
U-wind	------	------	------	------	------	------
V-wind	------	------	------	------	------	------
SST	------	------	------	------	------	------
T100m	------	------	------	------	------	------
T150m	------	------	------	------	------	------
	OCT	NOV	DEC	JAN	FEB	MAR
ATLAS 2N165E						
U-wind	------	------	-		----	------
V-wind	------	------	-		----	------
SST	------	------	------	------	------	------
T100m	------	------	------	------	------	------
T150m	------	------	------	------	------	------
EPOCS 00165E						
U-wind	------	------	------	-	-----	-
V-wind	------	------	------	-	-----	-
SST	------	------	------	-	-----	-
U-Current	------	------	------	-	-----	-
ATLAS 2S165E						
U-wind	------	------	------	------	------	------
V-wind	------	------	------	------	------	------
SST	------	------	------	------	------	------
T100m	------	------	------	------	------	------
T150m	------	------	------	------	------	------

TABLE 1 (CONTINUED).

	OCT	NOV	DEC	JAN	FEB	MAR
ATLAS 00169W						
U-wind	------	------	------			
V-wind	------	------	------			
SST	------	------	------			
T100m	------	------	------			
T150m	------	------	------			
ATLAS 00170W						
U-wind				------	------	----
V-wind				------	------	----
SST				------	------	------
T100m				------	------	------
T150m				------	------	------

	OCT	NOV	DEC	JAN	FEB	MAR
ATLAS 00155W						
U-wind	------	------	------	------	------	------
V-wind	------	------	------	------	------	------
SST	------	------	------	------	------	------
T100m	------	------	------	------	------	------
T140m	------	------	------	------	------	------

	OCT	NOV	DEC	JAN	FEB	MAR
ATLAS 2N140W						
U-wind	------	------	------	------	------	------
V-wind	------	------	------	------	------	------
SST	------	------	------	------	------	------
T100m	------	------	------	------	------	------
T140m	------	------	------	------	------	------
EPOCS 00140W						
U-wind	------	------	------	------	------	------
V-wind	------	------	------	------	------	------
SST	------	------	------	------	------	------
U-current	------	------	------	------	------	

TABLE 1 (CONTINUED).

	OCT	NOV	DEC	JAN	FEB	MAR
ATLAS 2S140W						
U-wind	-----		------	------	------	------
V-wind	-----		------	------	------	------
SST	----		------	------	------	------
T100m	----		------	------	------	-----
T140m	----		------	------	------	------
	OCT	NOV	DEC	JAN	FEB	MAR
ATLAS 00124W						
U-wind	------	------	------	----		--
V-wind	------	------	------	----		--
SST			-----	------	------	------
T100m			-----	------	------	------
T140m			-----	------	------	------
	OCT	NOV	DEC	JAN	FEB	MAR
ATLAS 2N110W						
U-wind		------	------	------	------	------
V-wind		------	------	------	------	------
SST		------	------	------	------	------
T100m		------	------	------	------	------
T140m		------	------	------	------	------
EPOCS 00110W						
U-wind	------	------	------	------	------	------
V-wind	------	------	------	------	------	------
SST	------	------	------	------	------	------
U-current	------	------	-			
ATLAS 2S110W						
U-wind	------	------	------	- --		---
V-wind	------	------	------	--		---
SST	------	------	------	------	-	---
T100m	------	------	------	------	-	---
T140m	------	------	------	------	-	---

TABLE 2. OCEAN TEMPERATURE MAXIMA FROM ATLAS BUOY DATA USED TO ESTIMATE KELVIN WAVE PHASE SPEEDS.

0^0 170^0W (150m)					
1)	17 October	27.4°C			
2)	24 November	29.0°C			
3)	19 January	29.1°C			
0^0 155^0W (140m)					
1)	17 October	26.7°C			
2)	08 December	29.3°C			
3)	30 January	29.5°C			
0^0 140^0W (140m)					
1)	14 October	25.9°C	(Possible max.)		
2)	15 December	26.8°C			
3)	01 February	27.6°C			
0^0 124^0W (140m)					
1)	missing data				
2)	20 December	24.5°C			
3)	10 February	26.0°C			
0^0 110^0W (140m)			0^0 110^0W (100m)		
1)	28 October	16.0°C	09 November	22.1°C	
2)	03 January	15.8°C	02 January	23.3°C	
3)	12 February	17.2°C	26 February	25.8°C	

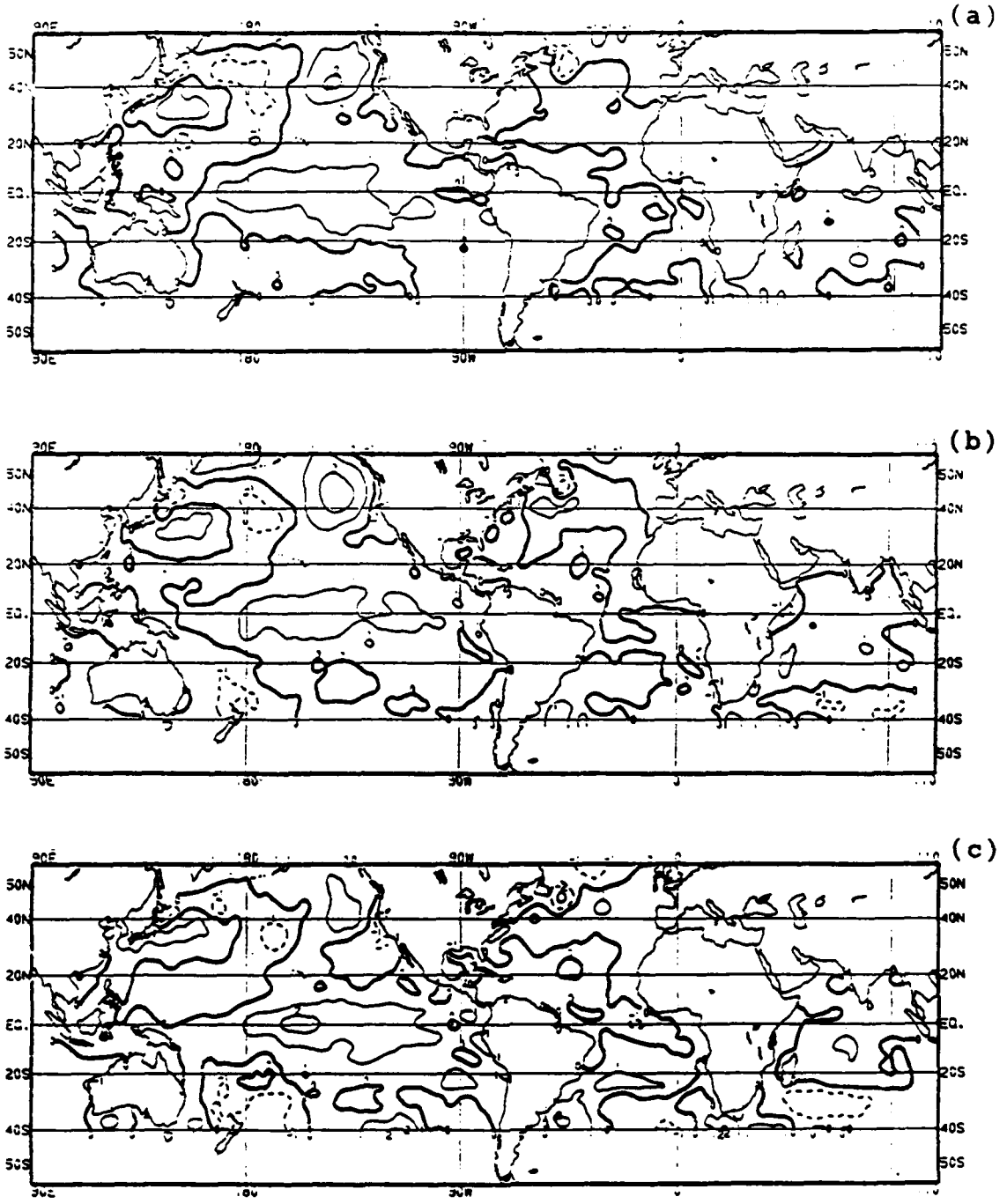

Fig. 1. Sea surface temperature (SST) anomalies for a) OCT 1991 b) NOV 1991 c) DEC 1991 d) JAN 1992 e) FEB 1992 and f) MAR 1992. Anomaly contour is 1°C with negative anomalies dashed. (from Kousky, 1991a - 1992c)

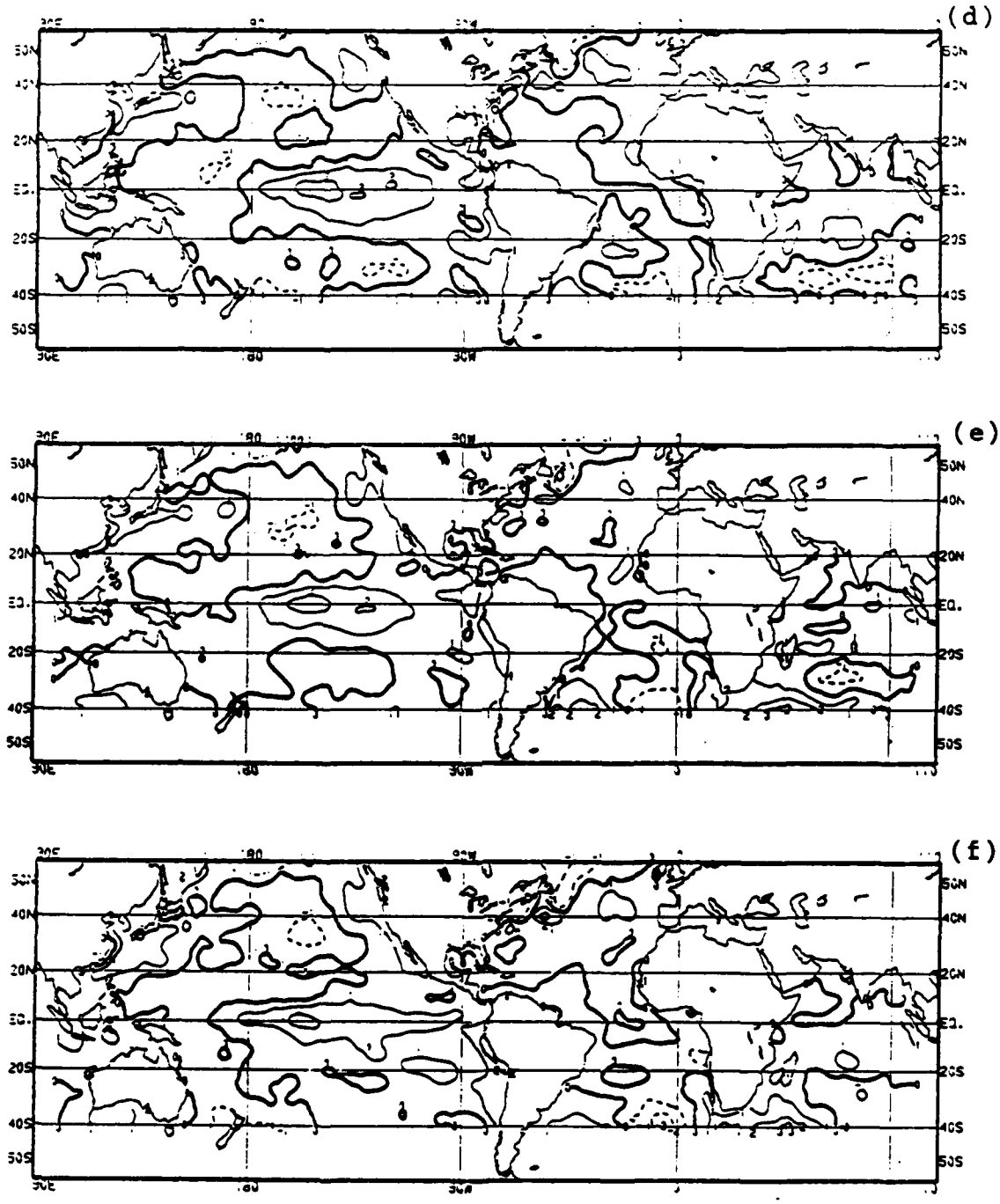

Fig. 1 (Continued).

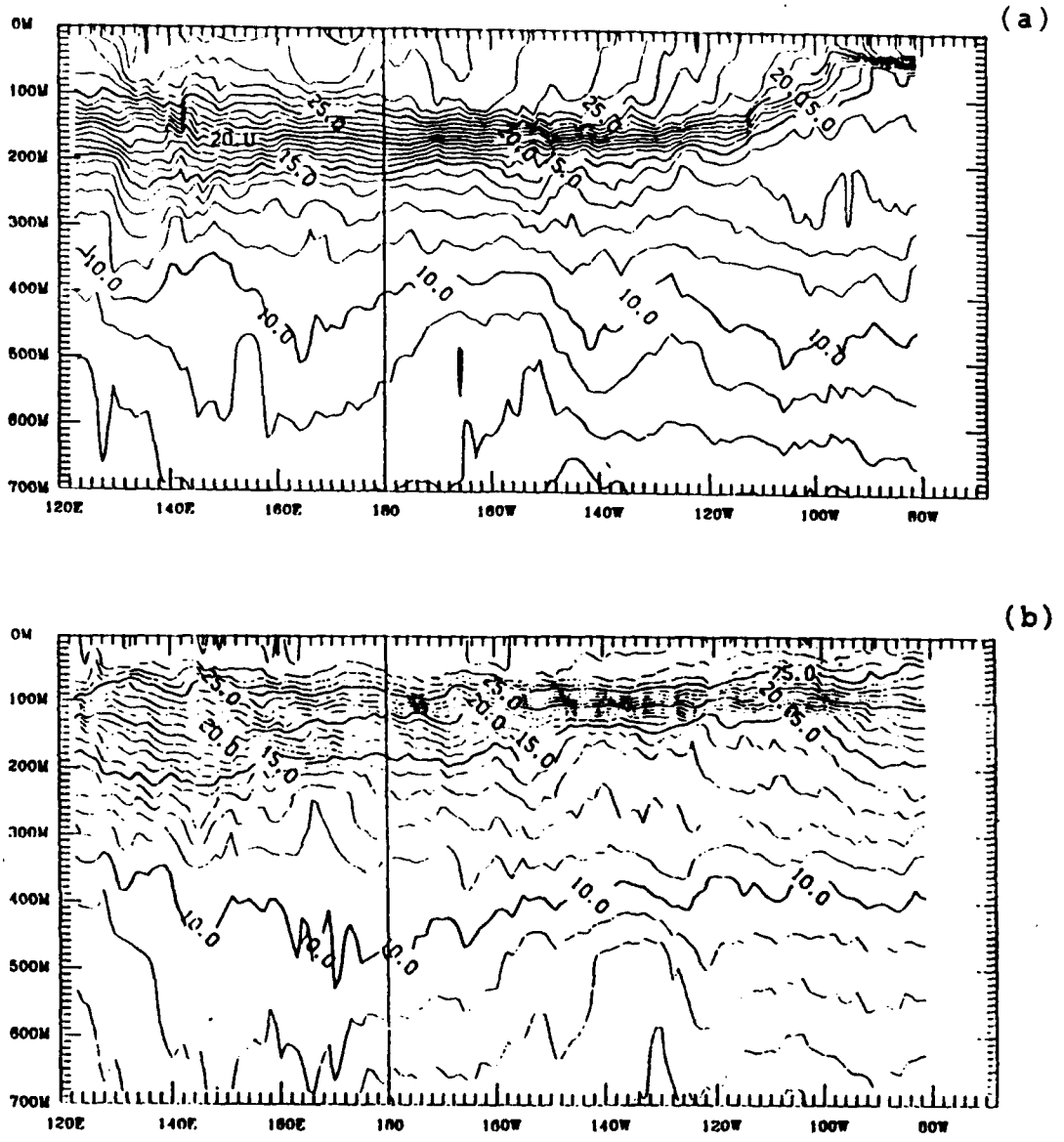

Fig. 2. Equatorial depth-longitude section of ocean temperature for a) OCT 1991 and b) MAR 1992. (from Kousky, 1991a and 1992c)

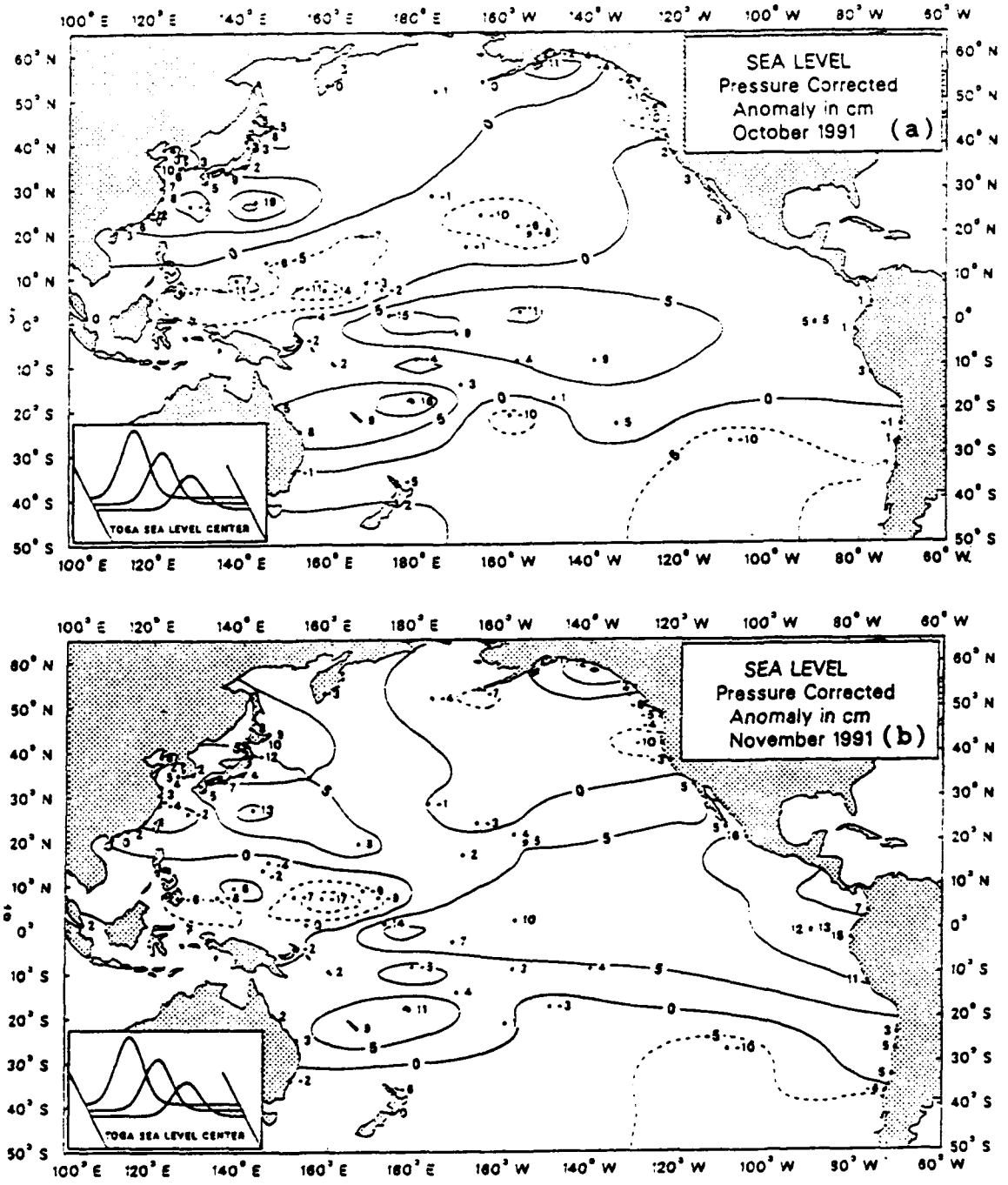

Fig. 3. Sea level anomalies from the 1975-1986 mean and adjusted for atmospheric pressure. a) OCT 1991 b) NOV 1991 c) DEC 1991 d) JAN 1992 e) FEB 1992 f) MAR 1992. (from Kousky, 1991a- 1992c)

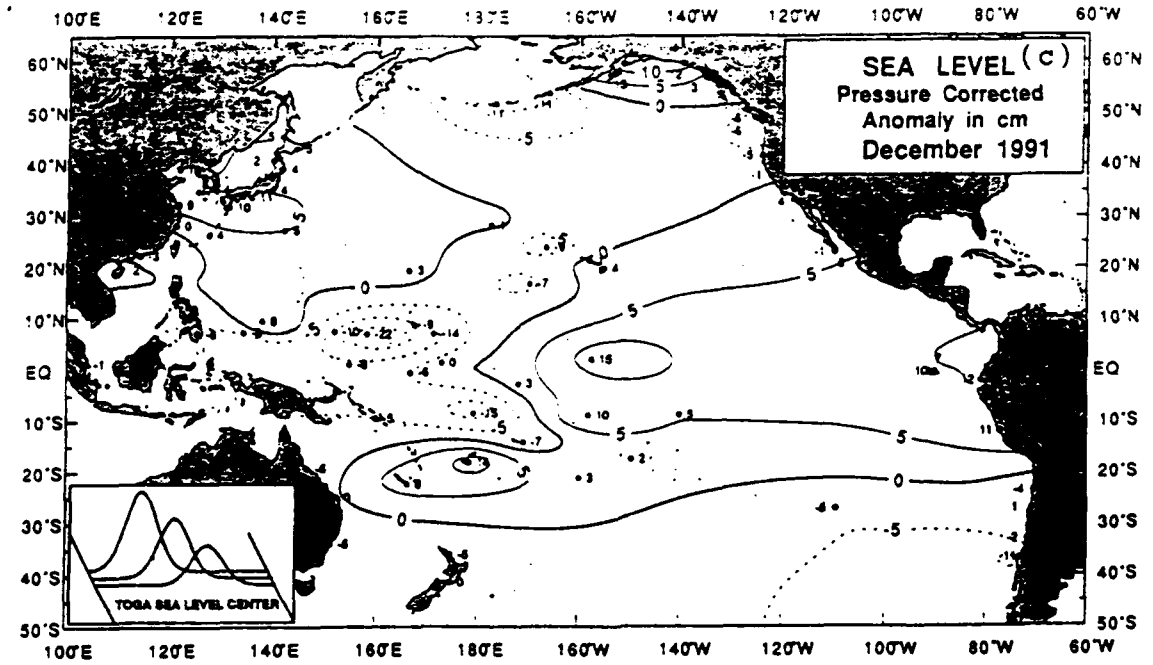

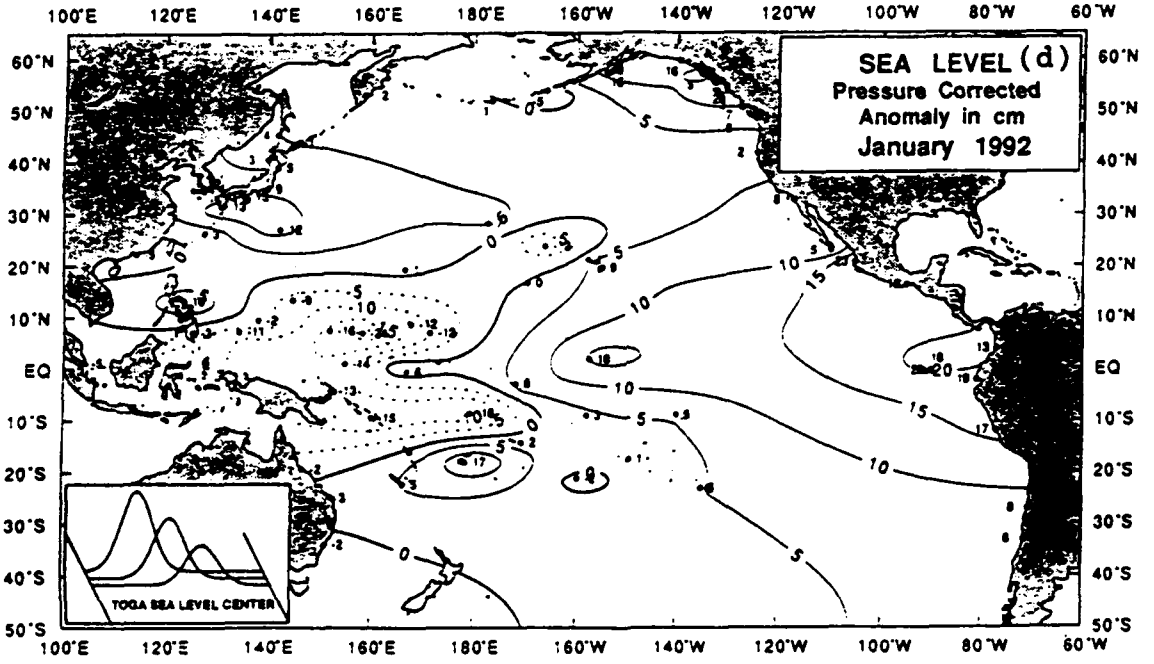

Fig. 3 (Continued).

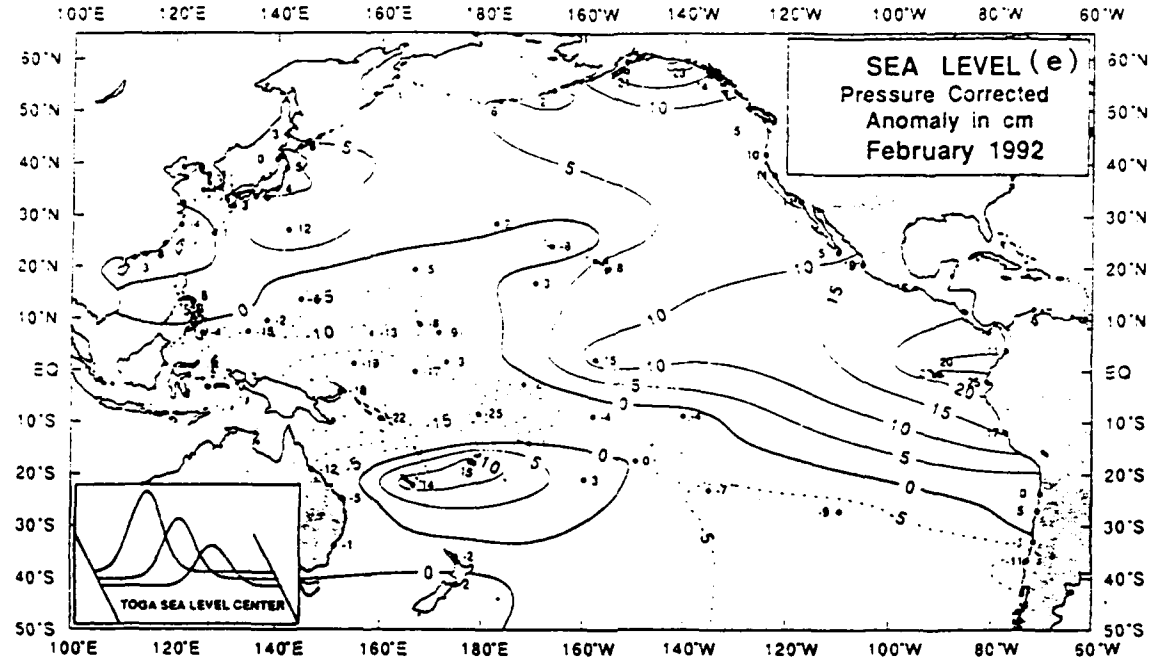

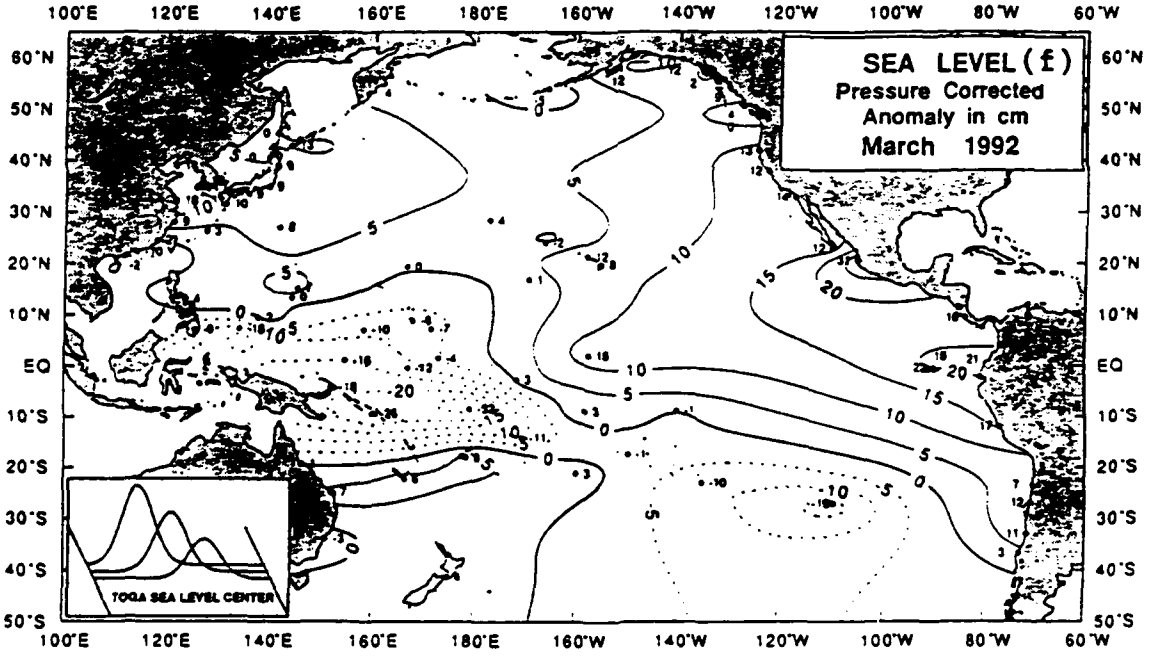

Fig. 3 (Continued).

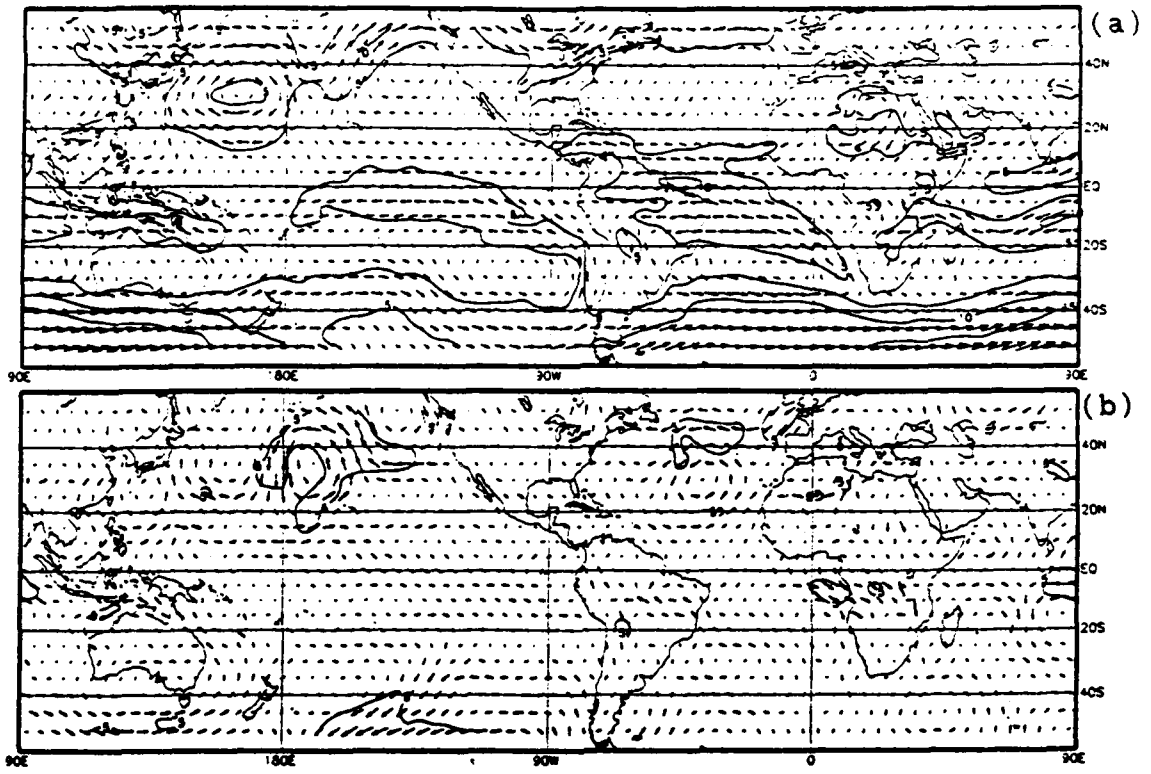

Fig. 4. 850 mb vector winds. Anomalies computed with respect to 1979-1988 monthly means. Contour for isotachs is 10 (5) ms^{-1} for the mean (anomalous) wind for a) OCT 1991 mean b) OCT 1991 anomalous c) NOV 1991 mean d) NOV 1991 anomalous e) DEC 1991 mean f) DEC 1991 anomalous g) JAN 1992 mean h) JAN 1992 anomalous i) FEB 1992 mean j) FEB 1992 anomalous k) MAR 1992 mean l) MAR 1992 anomalous. (from Kousky, 1991a)

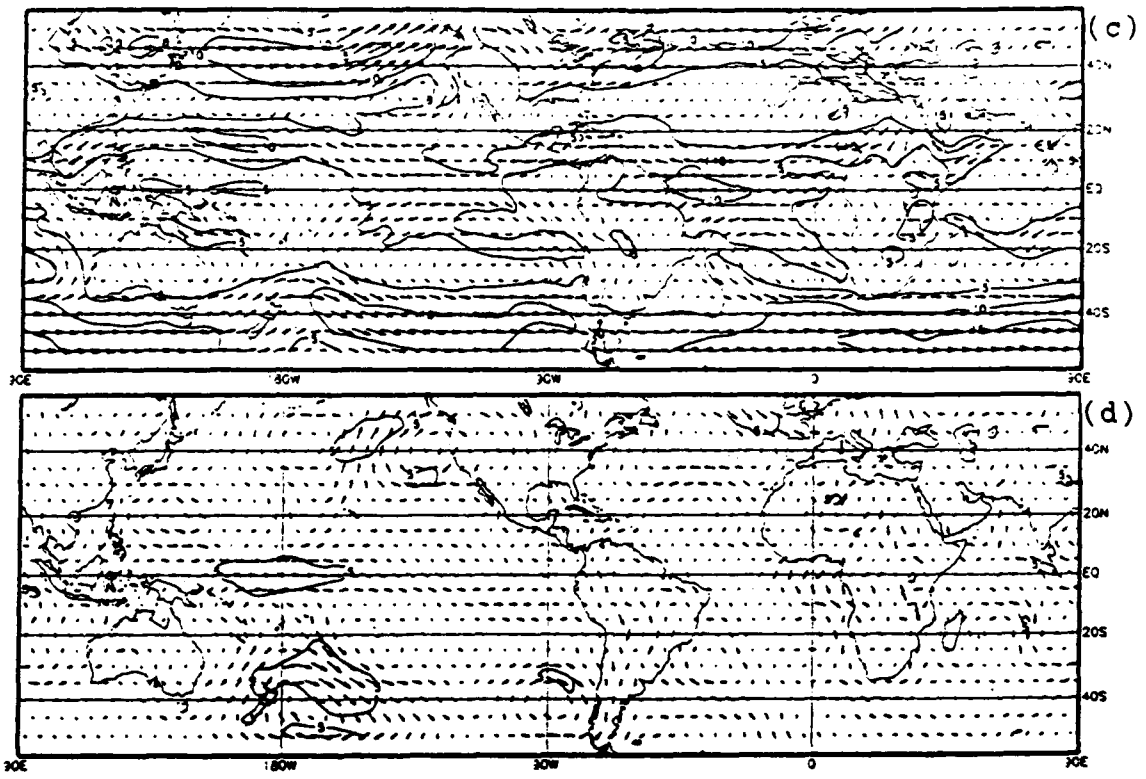

Fig. 4 (Continued).

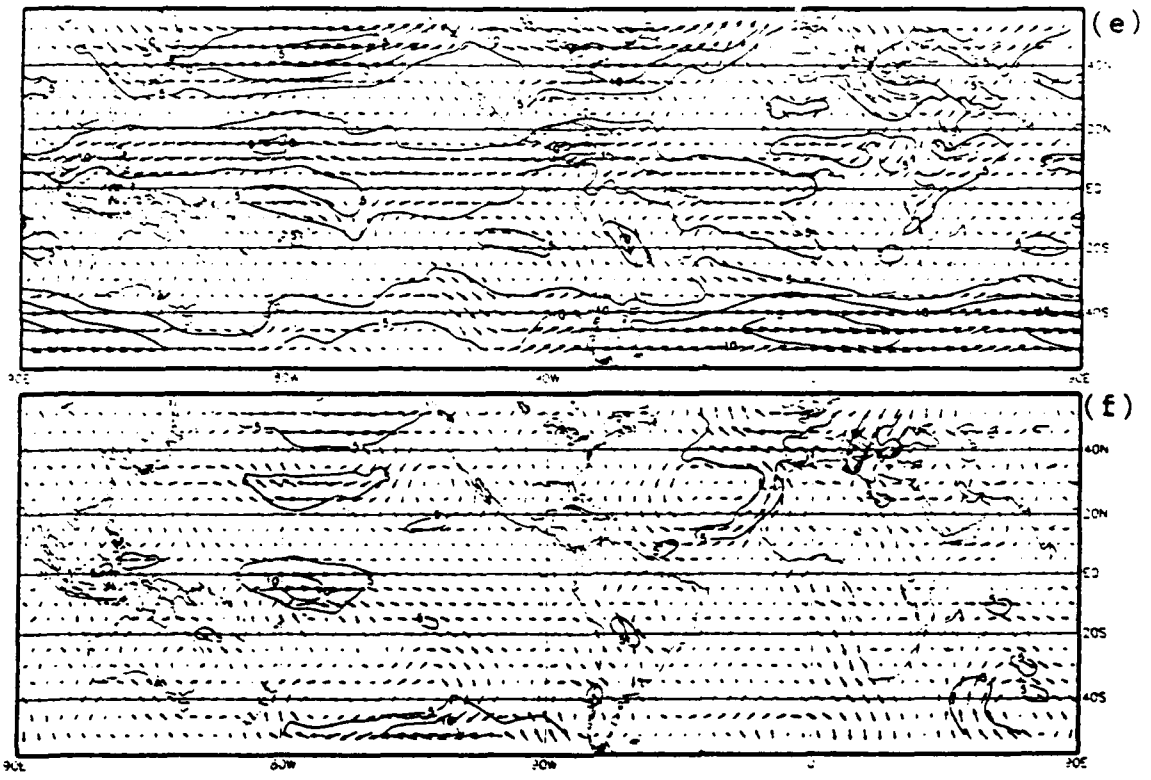

Fig. 4 (Continued).

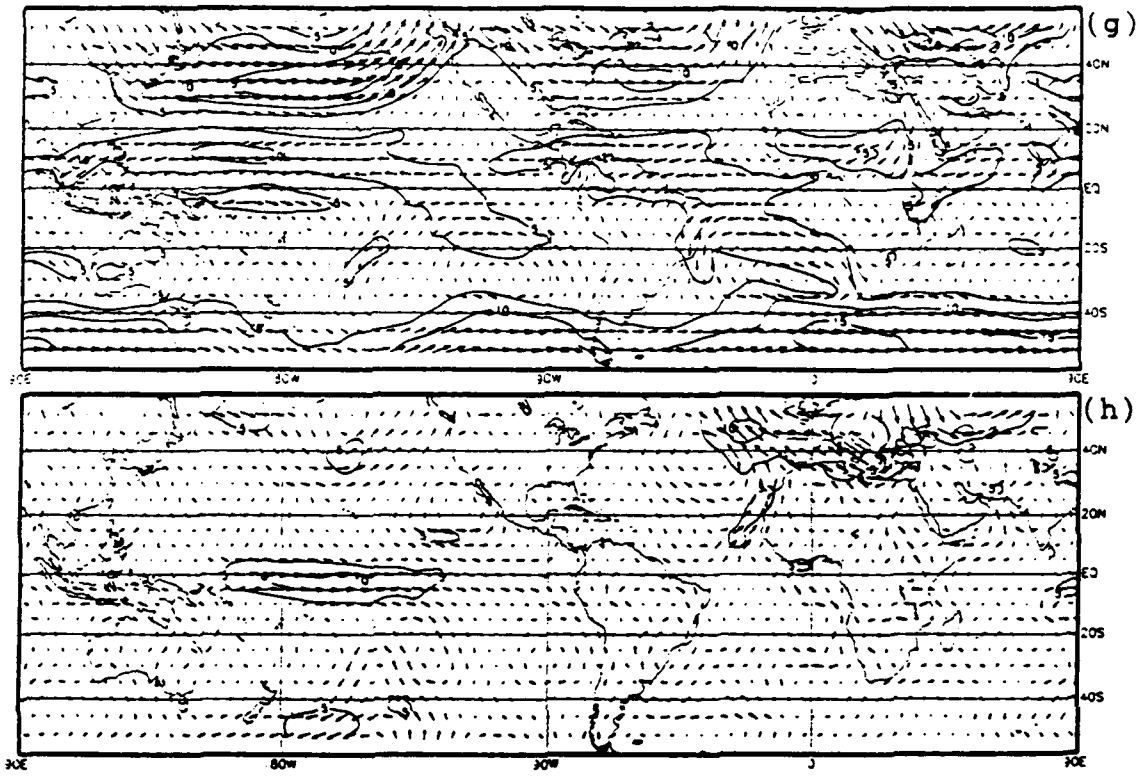

Fig. 4 (Continued).

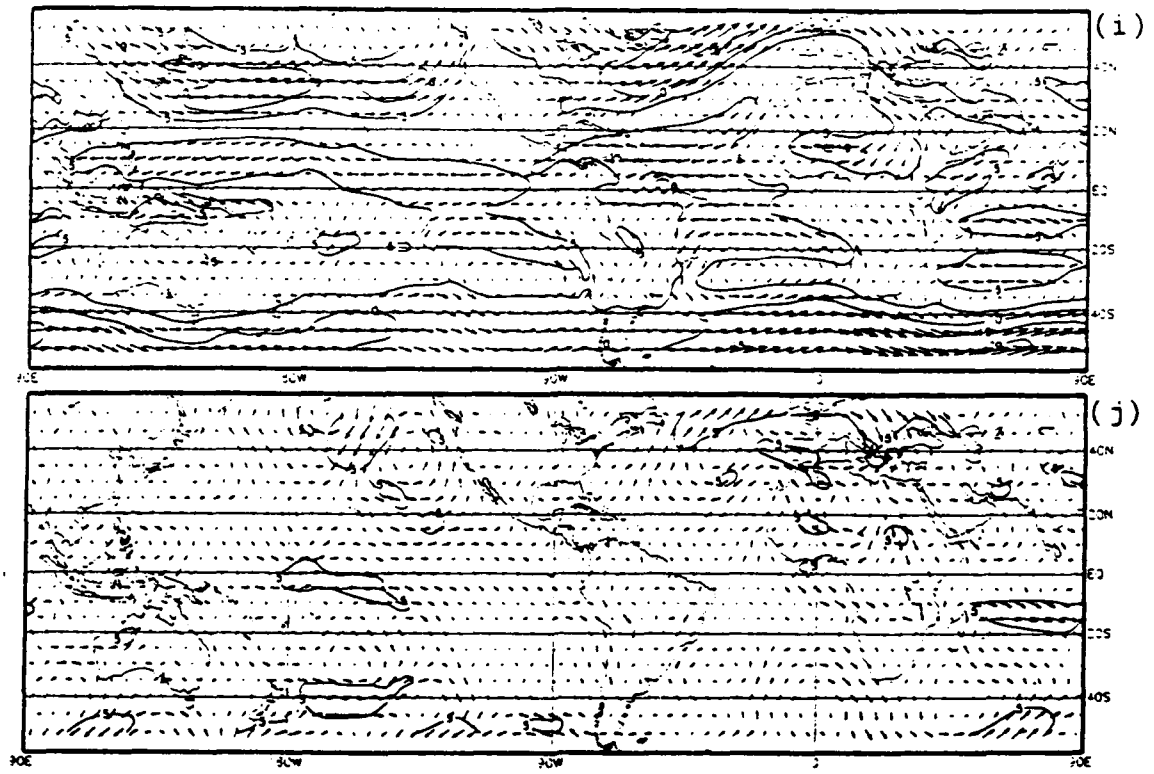

Fig. 4 (Continued).

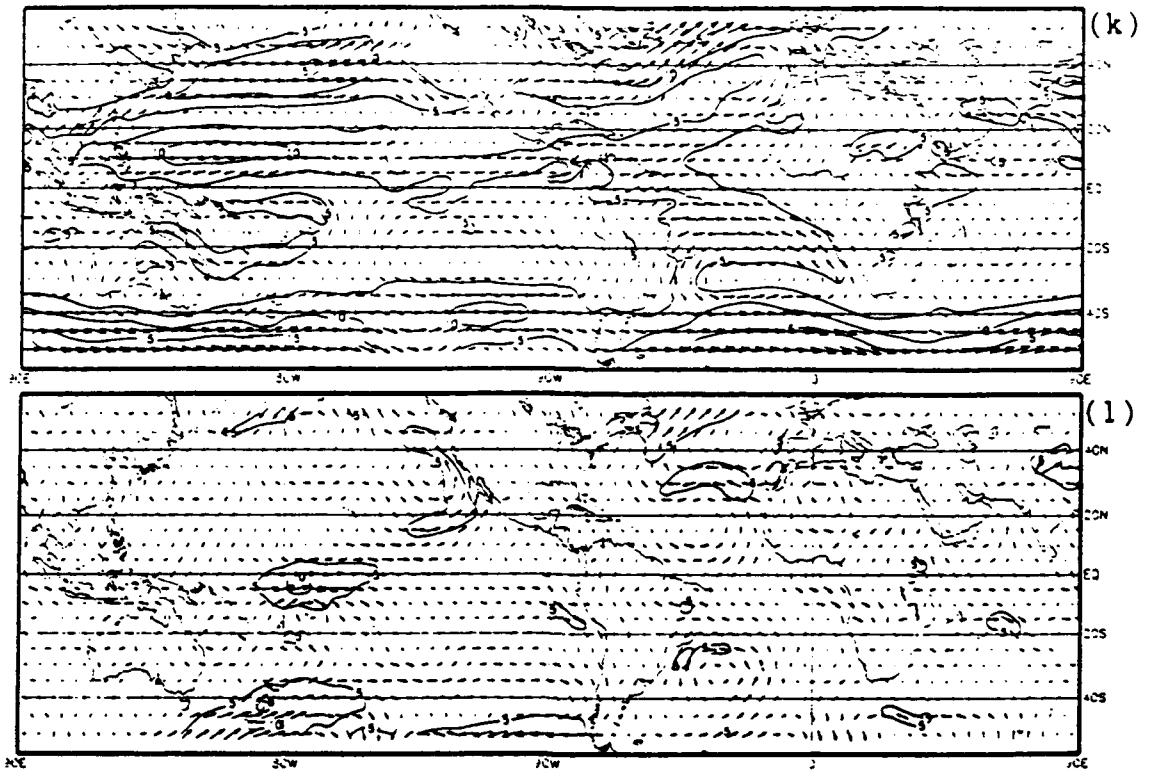

Fig. 4 (Continued).

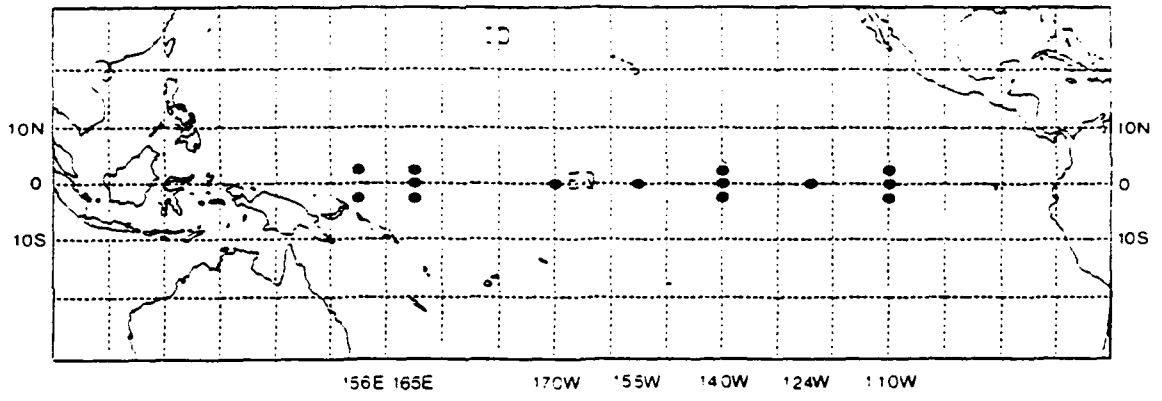

Fig. 5. Locations of utilized ATLAS and EPOCS buoys. The equatorial EPOCS buoys are at 165°E, 140°W, and 110°W.

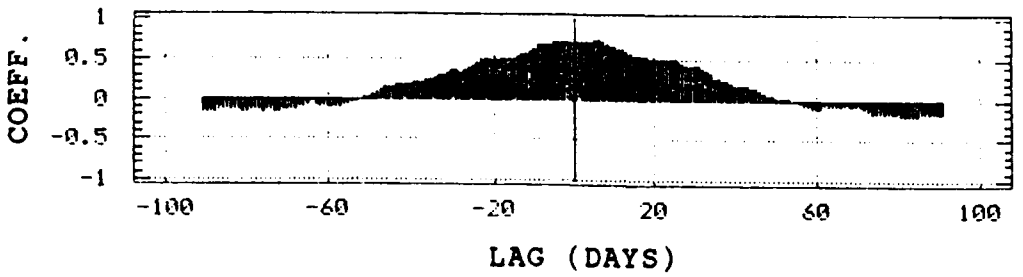

Fig. 6. Estimated cross-correlations of ATLAS 150 m ocean temperatures at 2°N,165°E and 2S°,165°E. Lags are in days. Positive lags are 2°N leading 2°S while negative lags are 2°S leading 2°N.

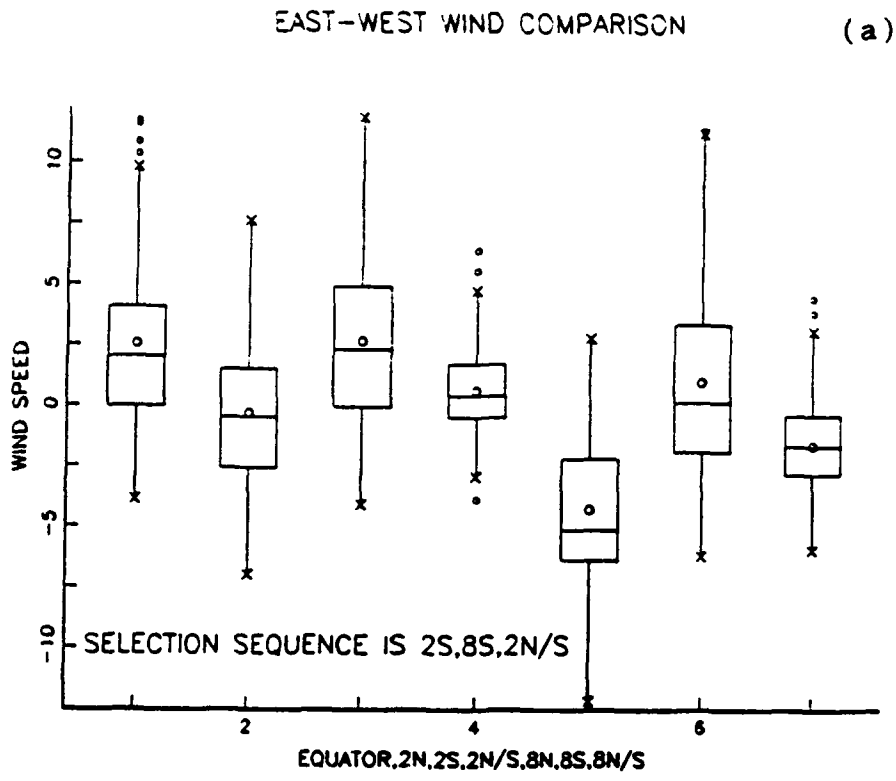

Fig. 7. Box and Whisker comparison of EPOCS and ATLAS a) zonal winds b) SSTs. (from Santos, et. al.,1992)

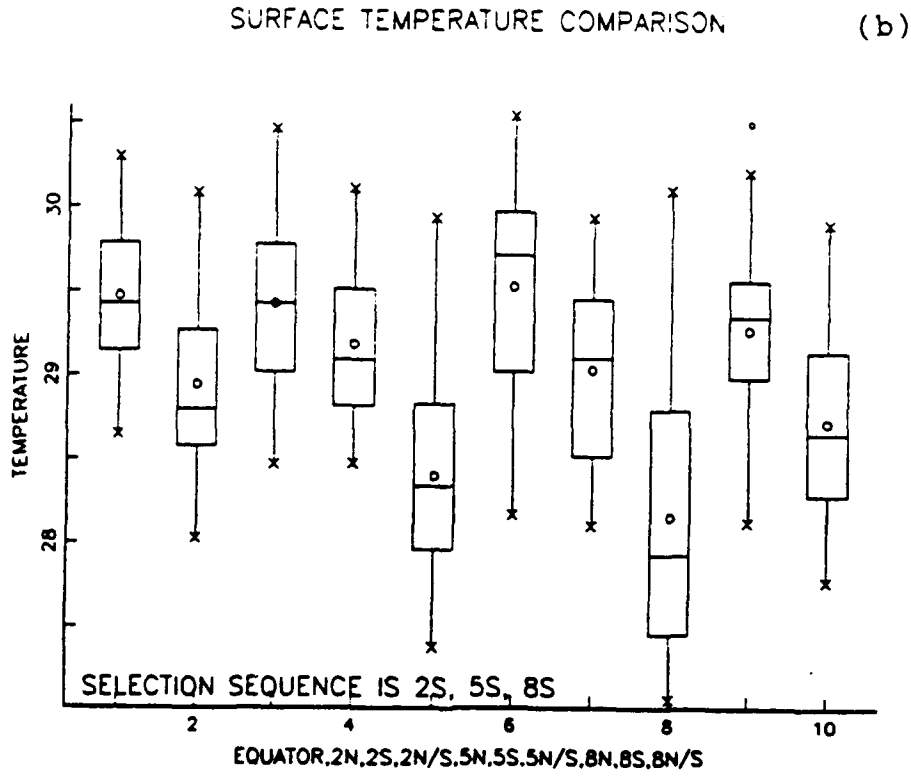

Fig. 7 (Continued).

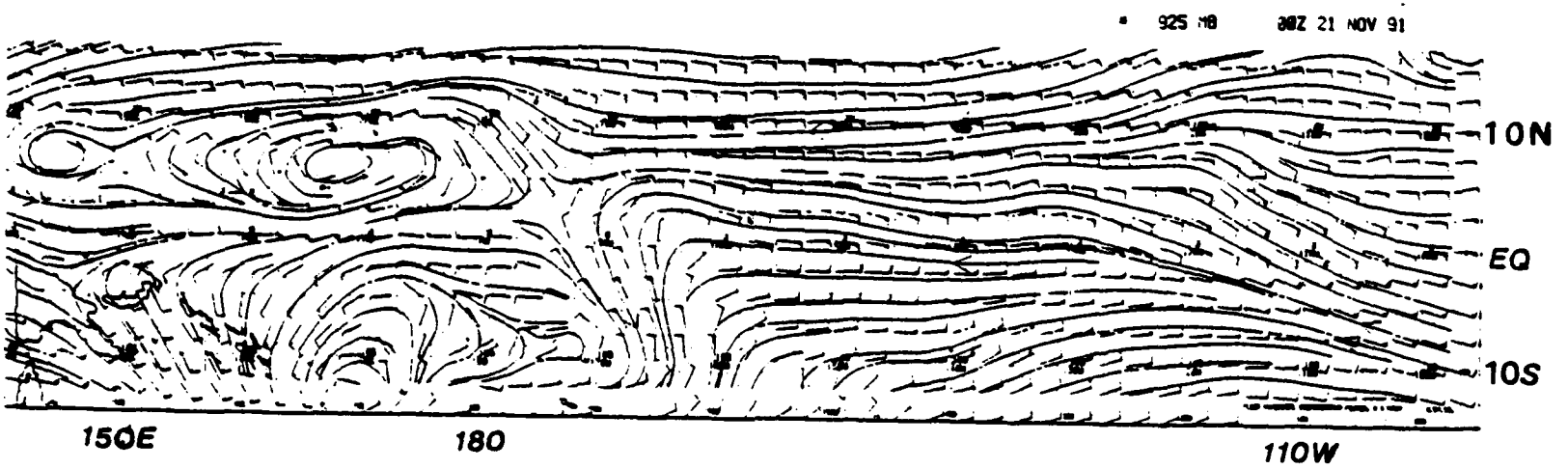

Fig. 8. NOGAPS 925 mb surface wind fields for 21 November 1991. Tropical cyclones Yuri (in the northern hemisphere) and Wilda (in the southern hemisphere) in the western Pacific produced westerly wind events. Note that the eastern Pacific is dominated by easterly winds.

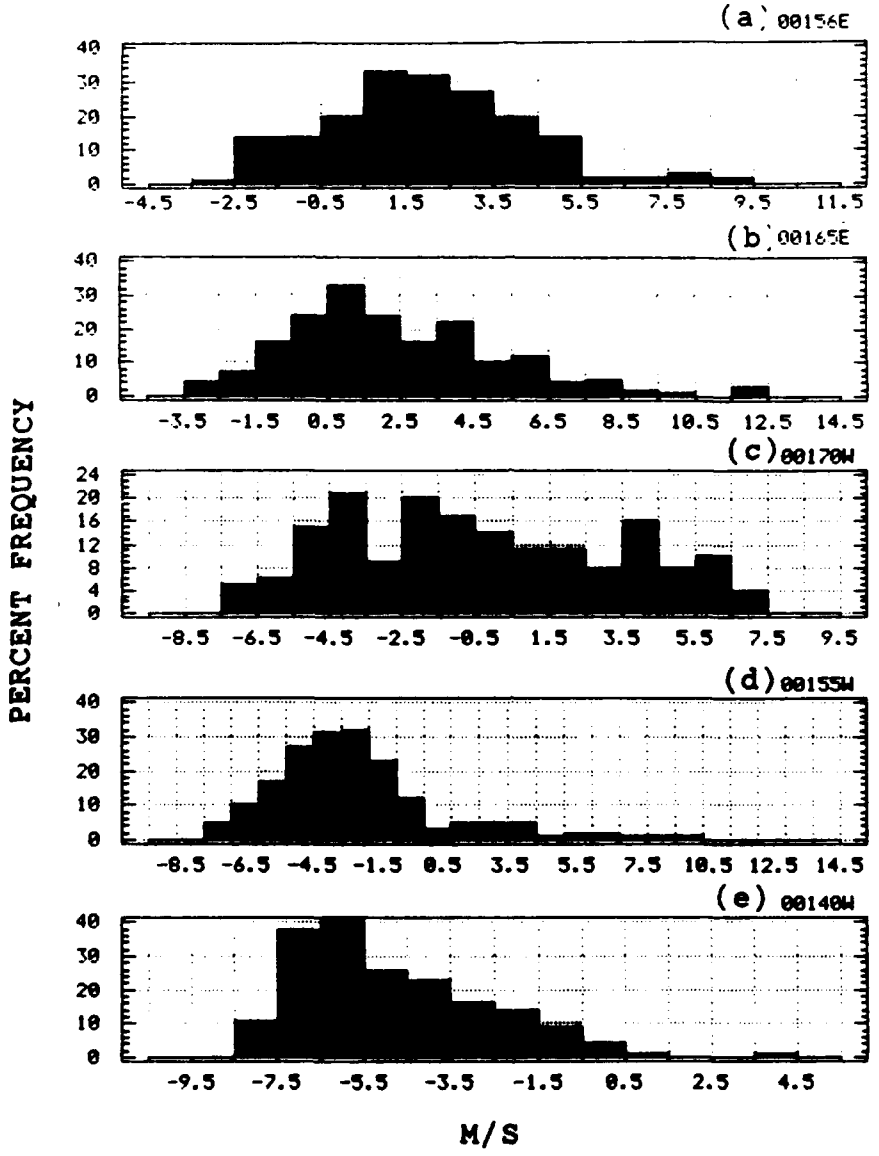

Fig. 9. Discrete frequency histograms of the zonal winds, a) averaged $0^{0}156^{0}E$ b) weighted averaged ATLAS and EPOCS $0^{0}165^{0}E$ c) $0^{0}170^{0}W$ d) $0^{0}155^{0}W$ e) averaged $0^{0}140^{0}W$ f) $0^{0}124^{0}W$ and g) averaged $0^{0}110^{0}W$.

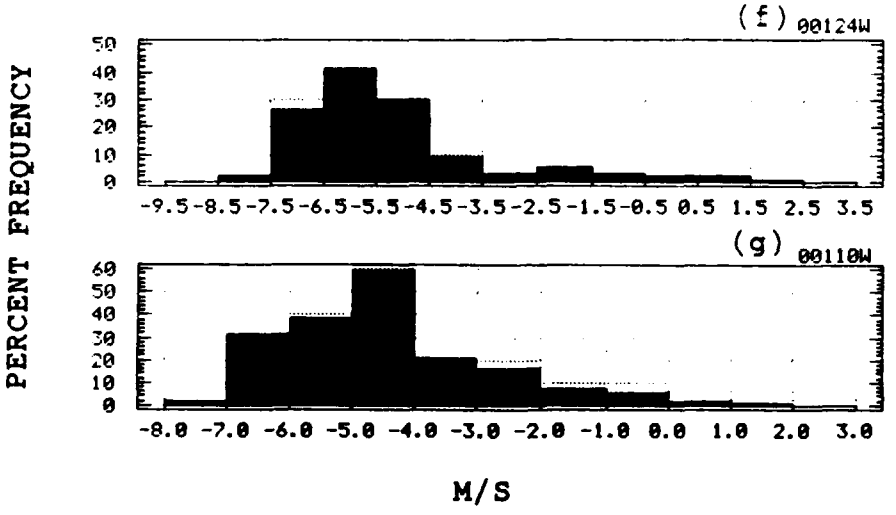

Fig. 9 (Continued).

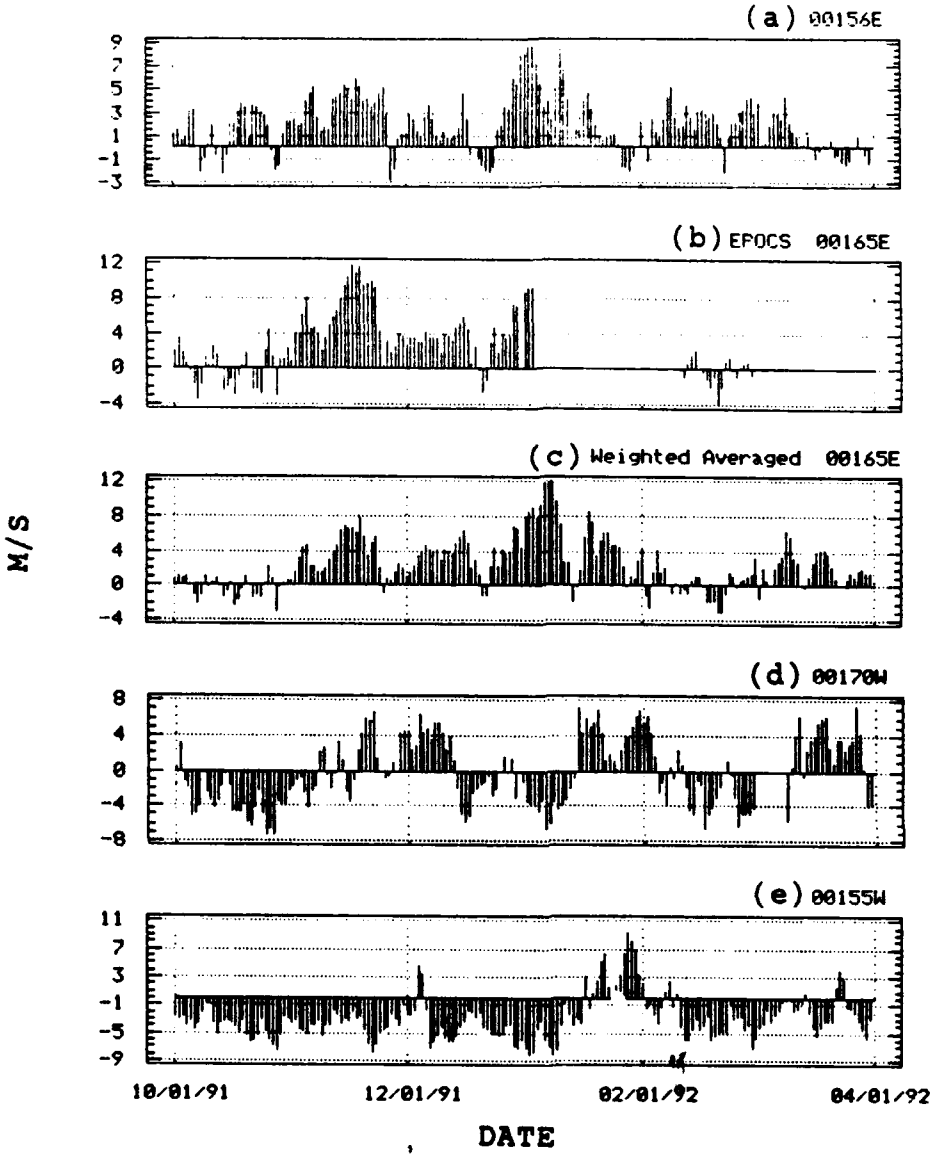

Fig. 10. Time series of the zonal wind from 01 October 1991 - 31 March 1992 for a) averaged $0^{\circ}156^{\circ}E$ b) EPOCS $0^{\circ}165^{\circ}E$ c) weighted averaged ATLAS and EPOCS $0^{\circ}165^{\circ}E$ d) $0^{\circ}170^{\circ}W$ e) $0^{\circ}155^{\circ}W$ f) averaged $0^{\circ}140^{\circ}W$ g) $0^{\circ}124^{\circ}W$ and h) averaged $0^{\circ}110^{\circ}W$.

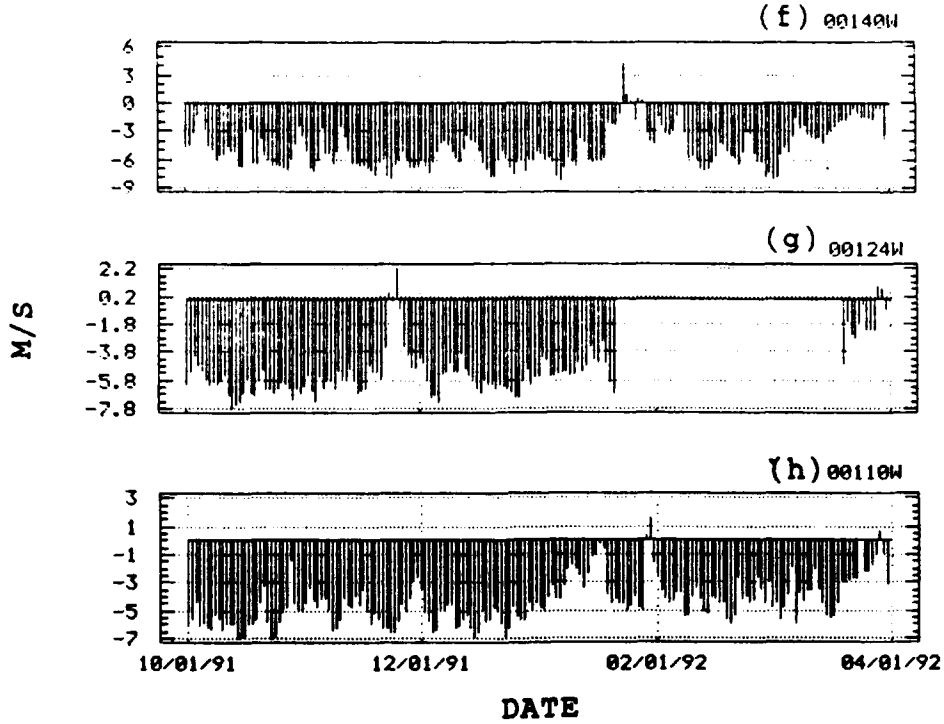

Fig. 10 (Continued).

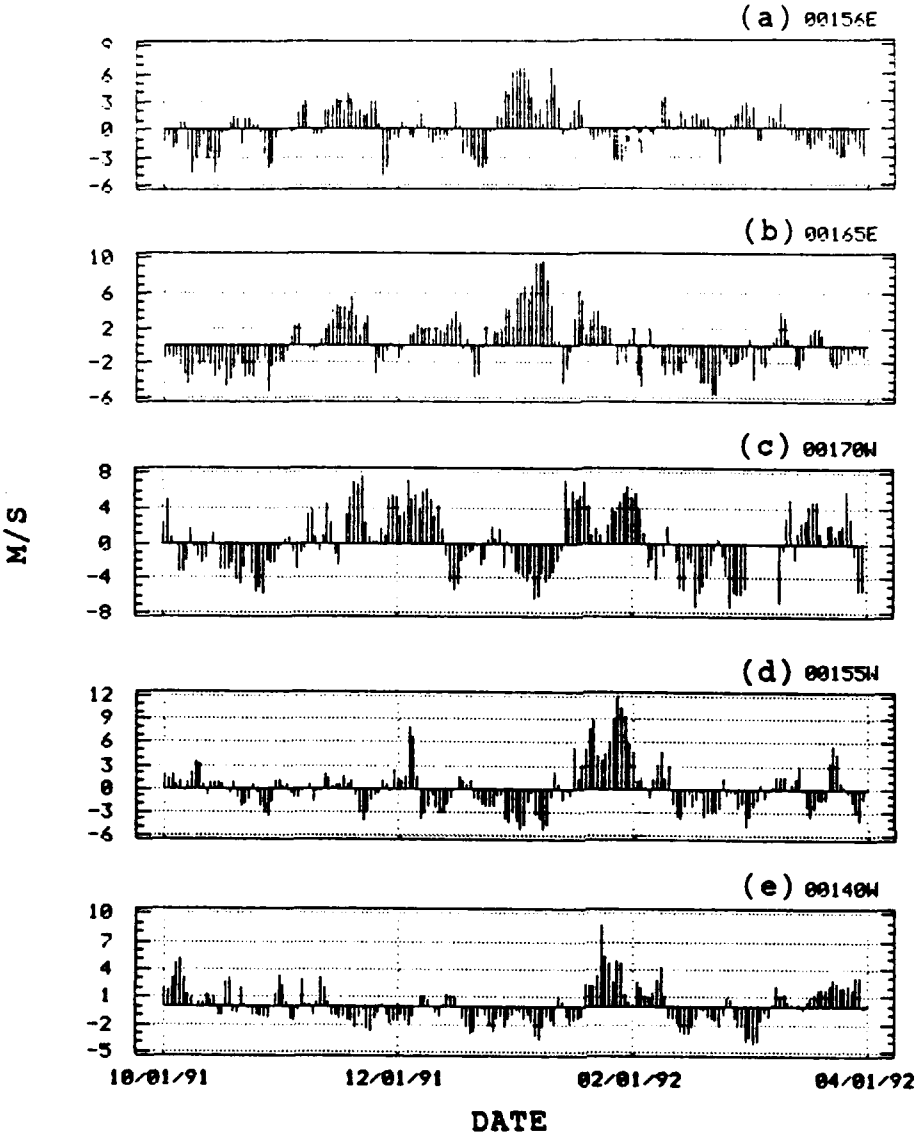

Fig. 11. Time series of the linearly detrended zonal winds from 01 October 1991 - 31 March 1992 for a) averaged 0^0156^0E b) weighted averaged ATLAS and EPOCS 0^0165^0E c) 0^0170^0W d) 0^0155^0W e) averaged 0^0140^0W f) 0^0124^0W and g) averaged 0^0110^0W.

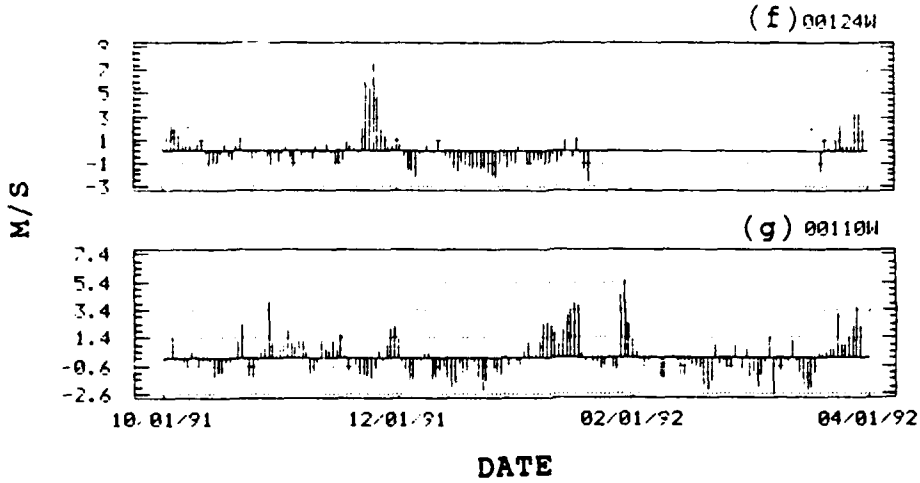

Fig. 11 (Continued).

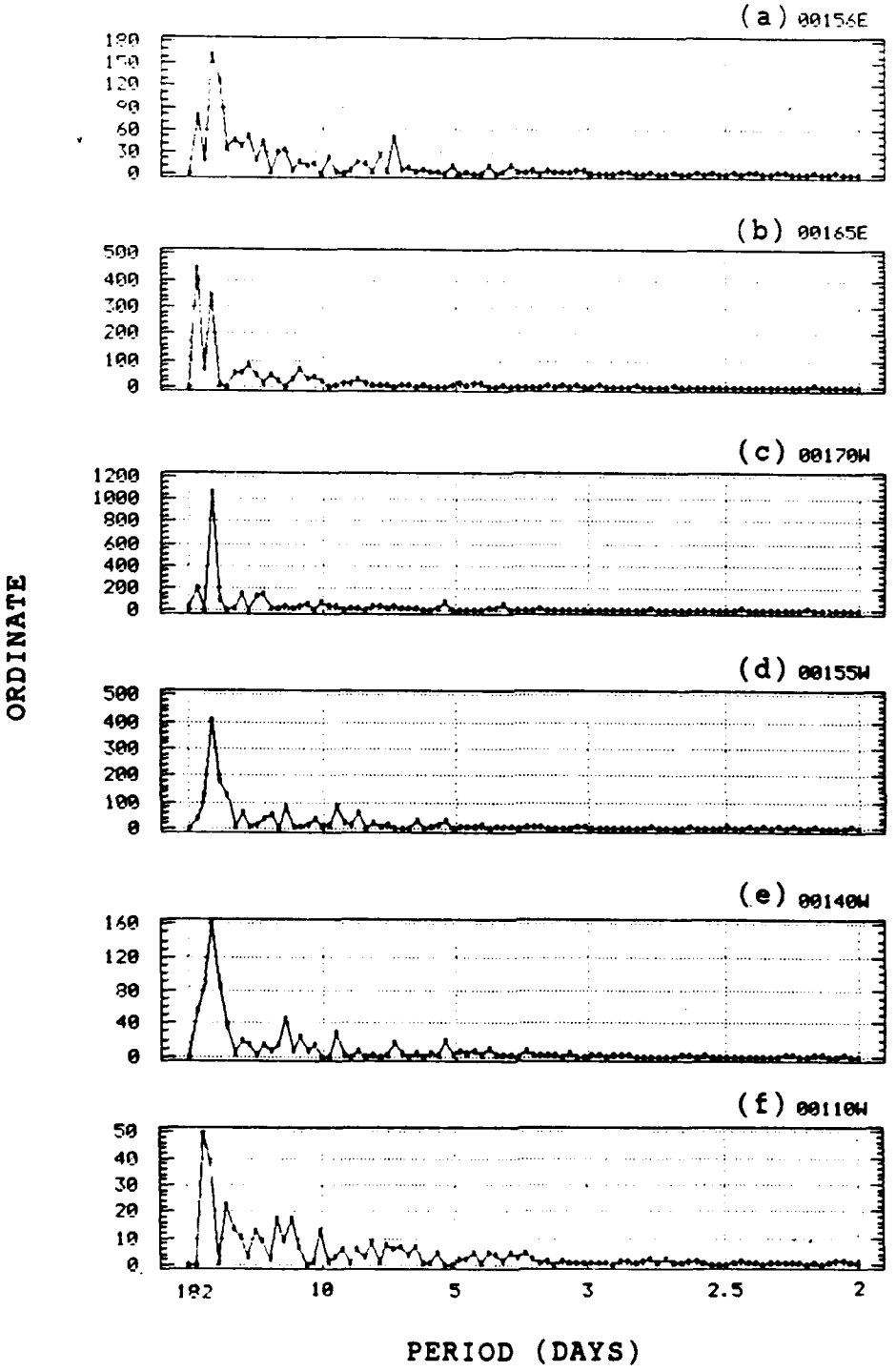

Fig. 12. Periodograms of zonal wind component for a) averaged 0^0156^0E b) weighted averaged ATLAS and EPOCS 0^0165^0E c) 0^0170^0W d) 0^0155^0W e) averaged 0^0140^0W f) averaged 0^0110^0W. Sampling interval is one day.

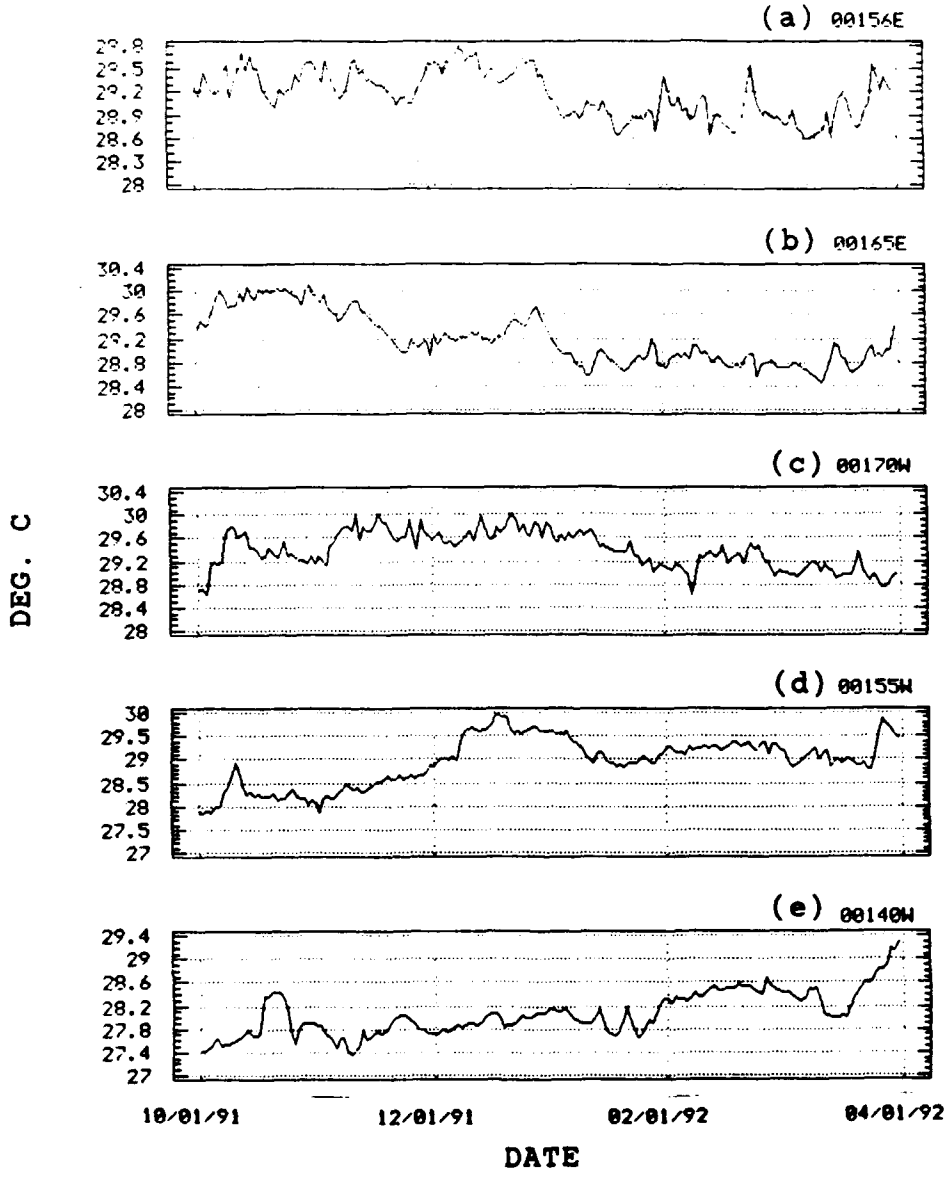

Fig. 13. Time series of SST from 01 October 1991 - 31 March 1992 for a) averaged $0^{\circ}156^{\circ}E$ b) averaged $0^{\circ}165^{\circ}E$ c) $0^{0}170^{0}W$ d) $0^{0}155^{0}W$ e) averaged $0^{\circ}140^{0}W$ f) $0^{\circ}124^{\circ}W$ and g) averaged $0^{\circ}110^{0}W$.

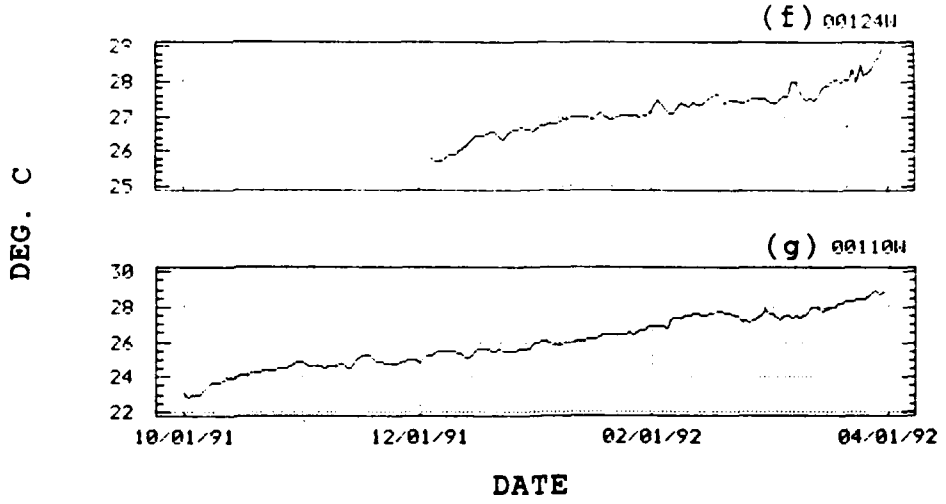

Fig. 13 (Continued).

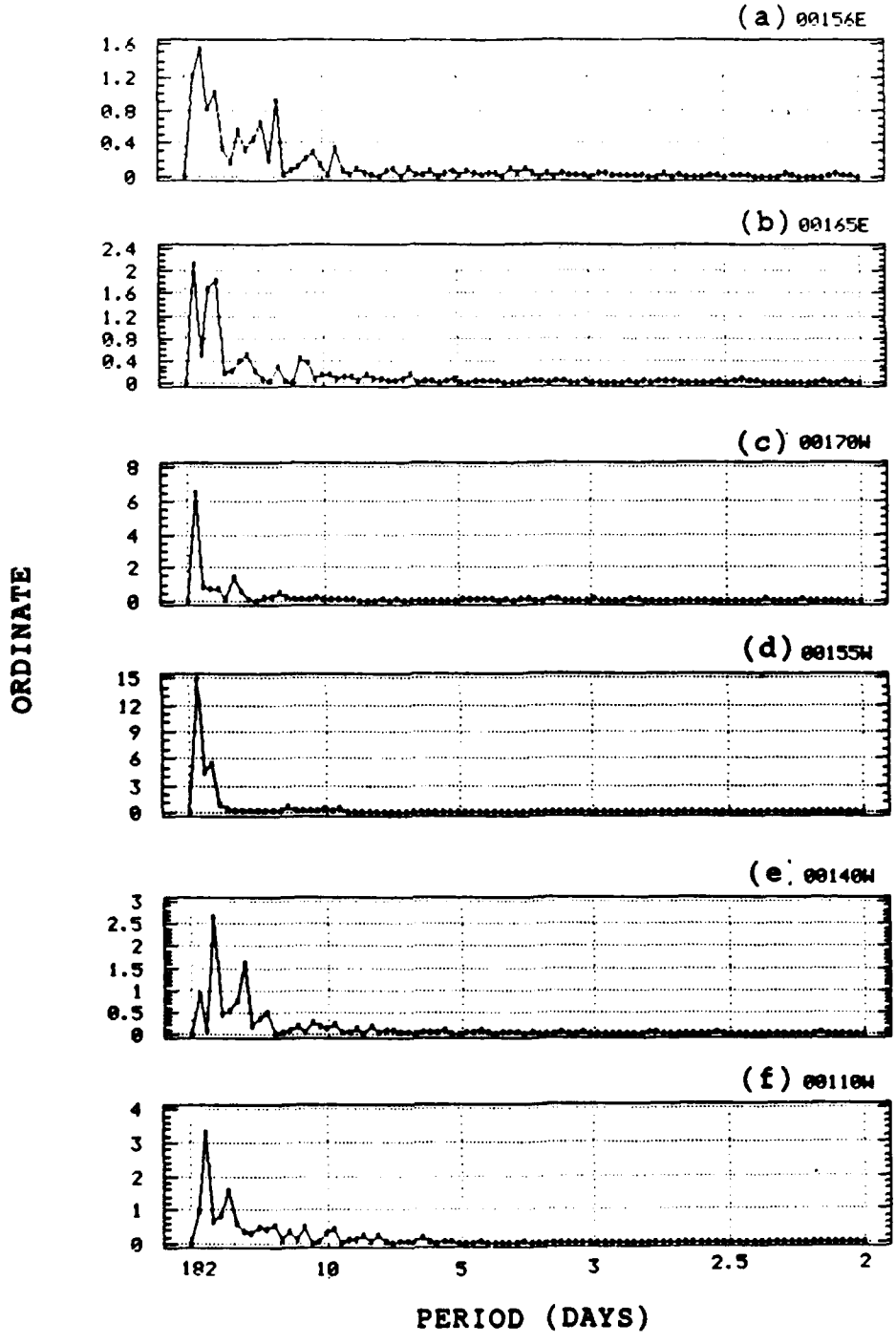

Fig. 14. Periodograms of SST from 01 October 1991 - 31 March 1992 for a) averaged 0^0156^0E b) averaged 0^0165^0E c) 0^0170^0W d) 0^0155^0W e) averaged 0^0140^0W f) averaged 0^0110^0W. Sampling interval is one day.

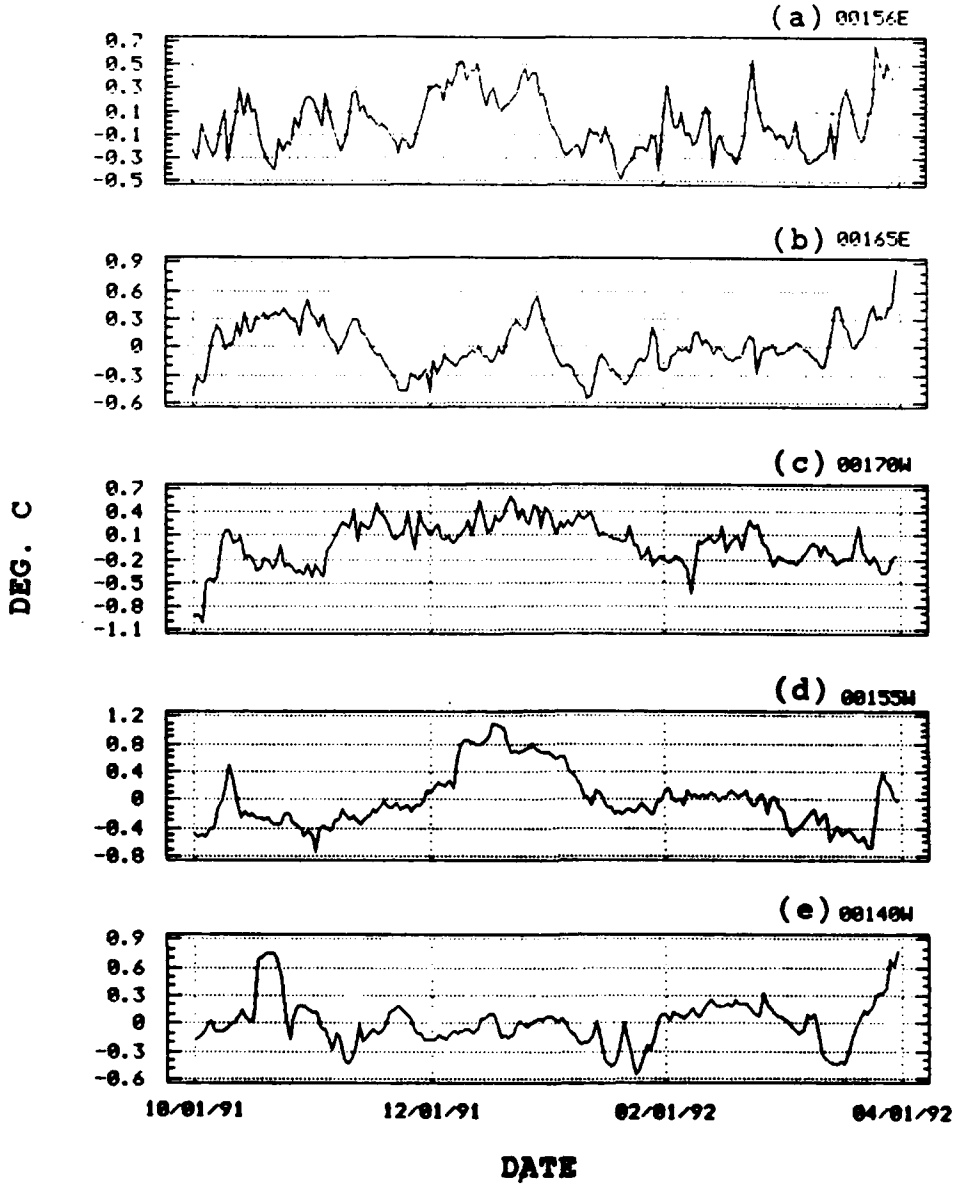

Fig. 15. Time series of linearly detrended SST for 01 October - 31 March 1992 for a) averaged 0^0156^0E b) averaged 0^0165^0E c) 0^0170^0W d) 0^0155^0W e) averaged 0^0140^0W f) 0^0124^0W and g) averaged 0^0110^0W.

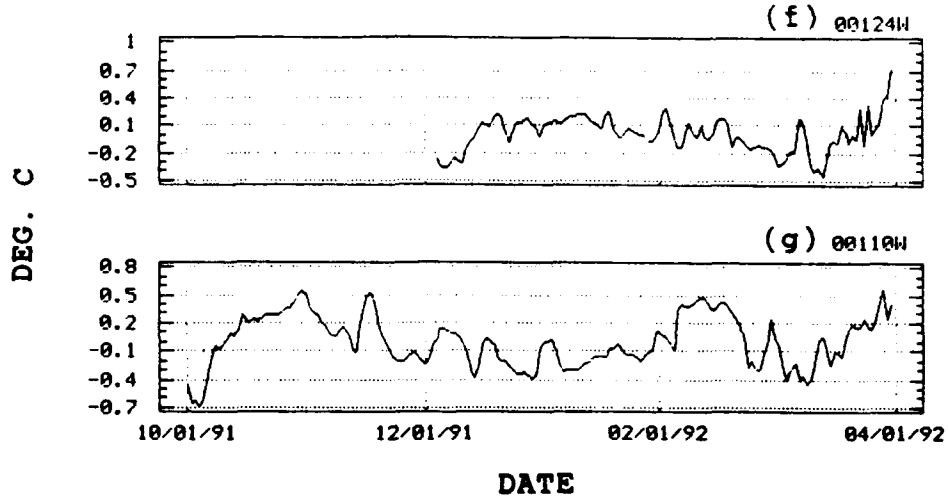

Fig. 15 (Continued).

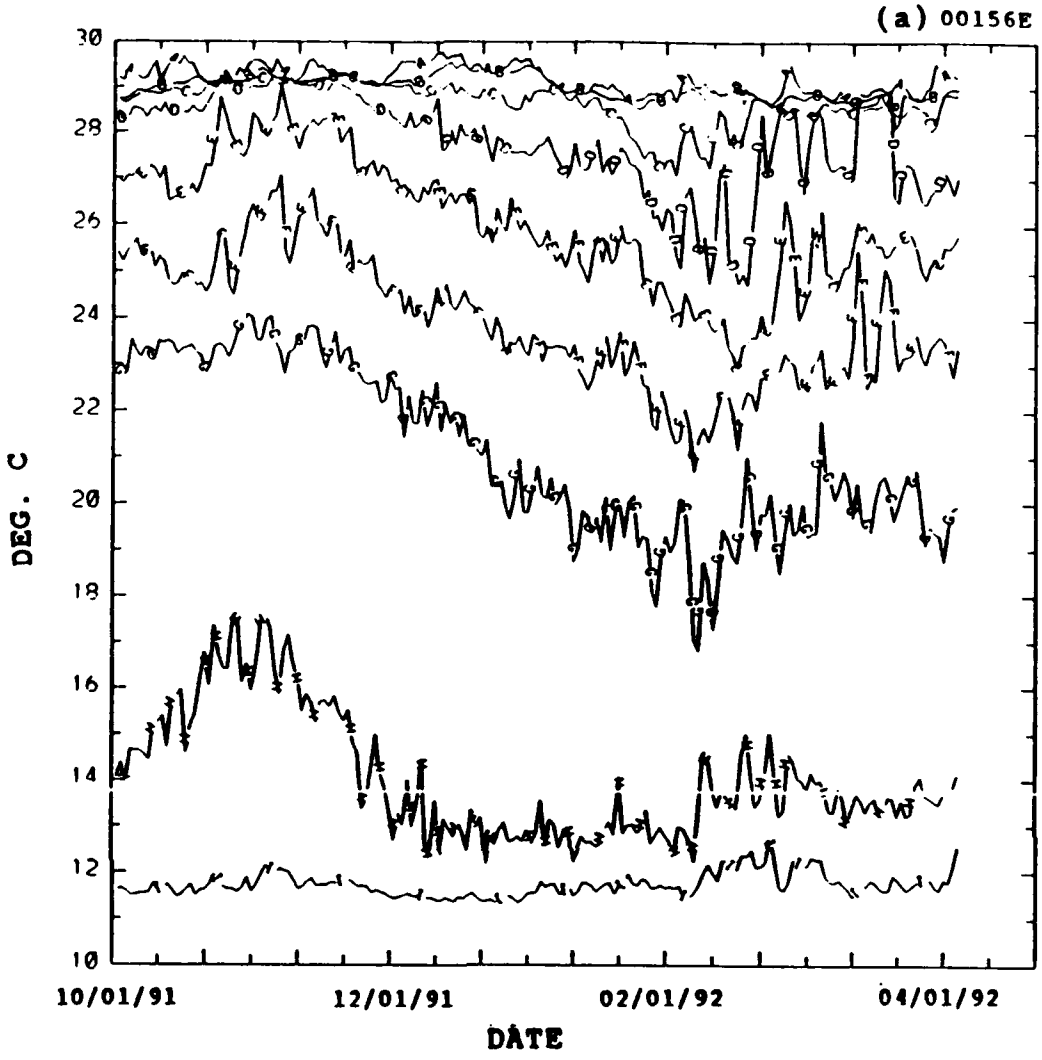

Fig. 16. Time series of ATLAS ocean temperatures for 01 October 1991 - 31 March 1992 for a) 0°156°E b) 0°165°E c) 0°170°W d) 0°155°W e) 0°140°W f) 0°124°W g) 0°110°W. Corresponding depths for figures a, b, and c are: A = 3m, B= 25m, C = 50m, D = 75m, E = 100m, F = 125m, G = 150m, H = 200m, I = 250m. Depths for figures d-g are: A = 3m, B = 20m, C = 40m, D = 60m, E = 80m, F = 100m, G = 120m, H = 140 m, I = 180m.

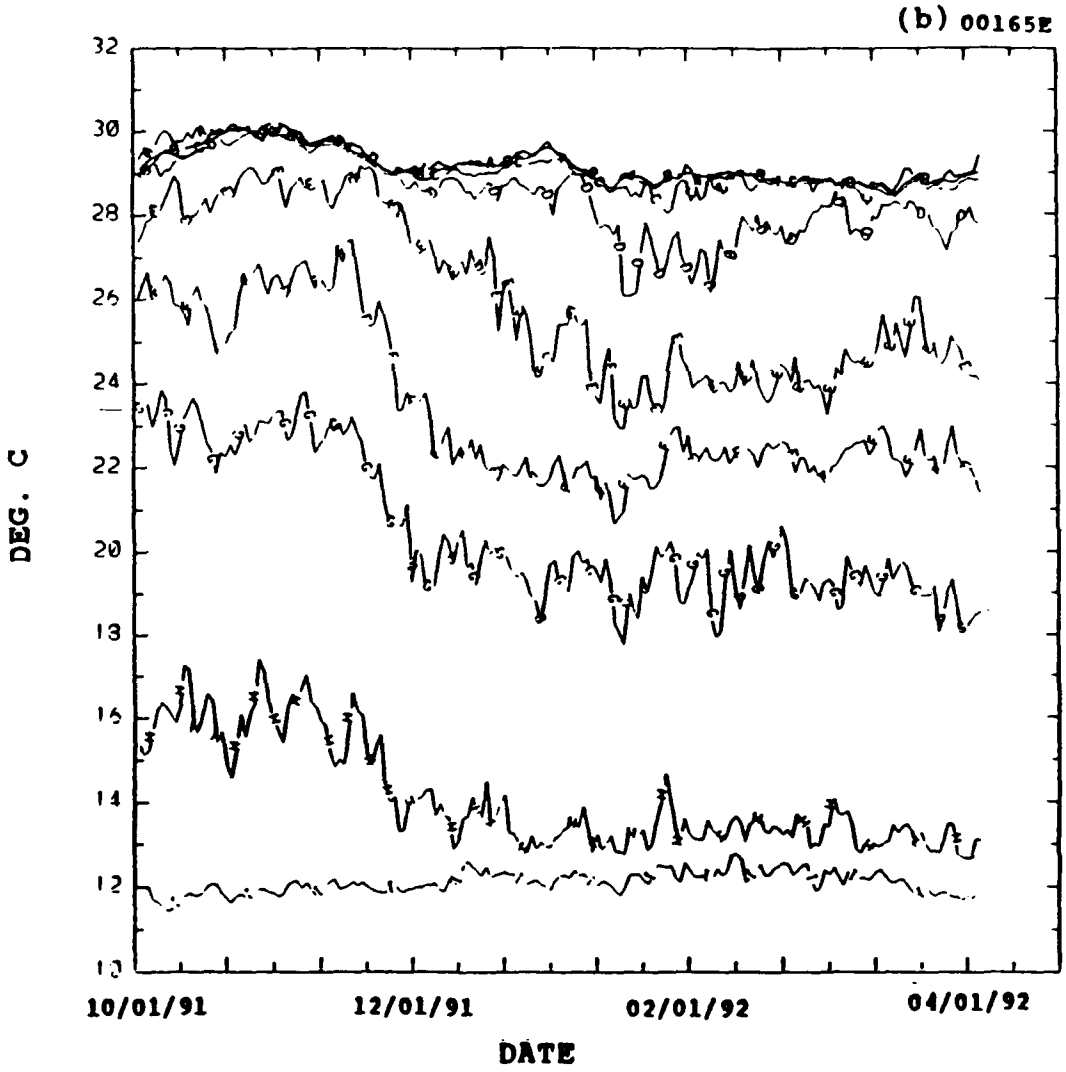

Fig. 16 (Continued).

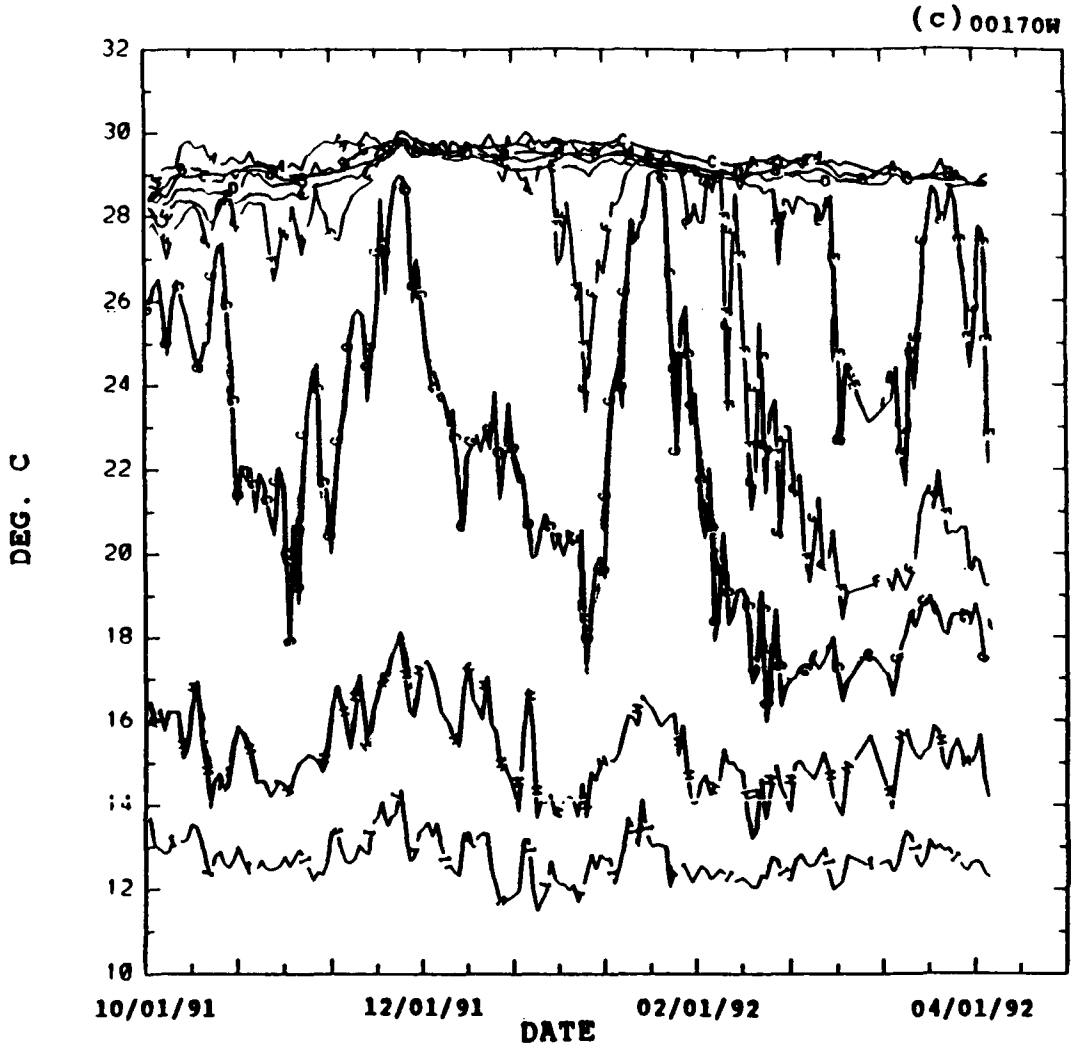

Fig. 16 (Continued).

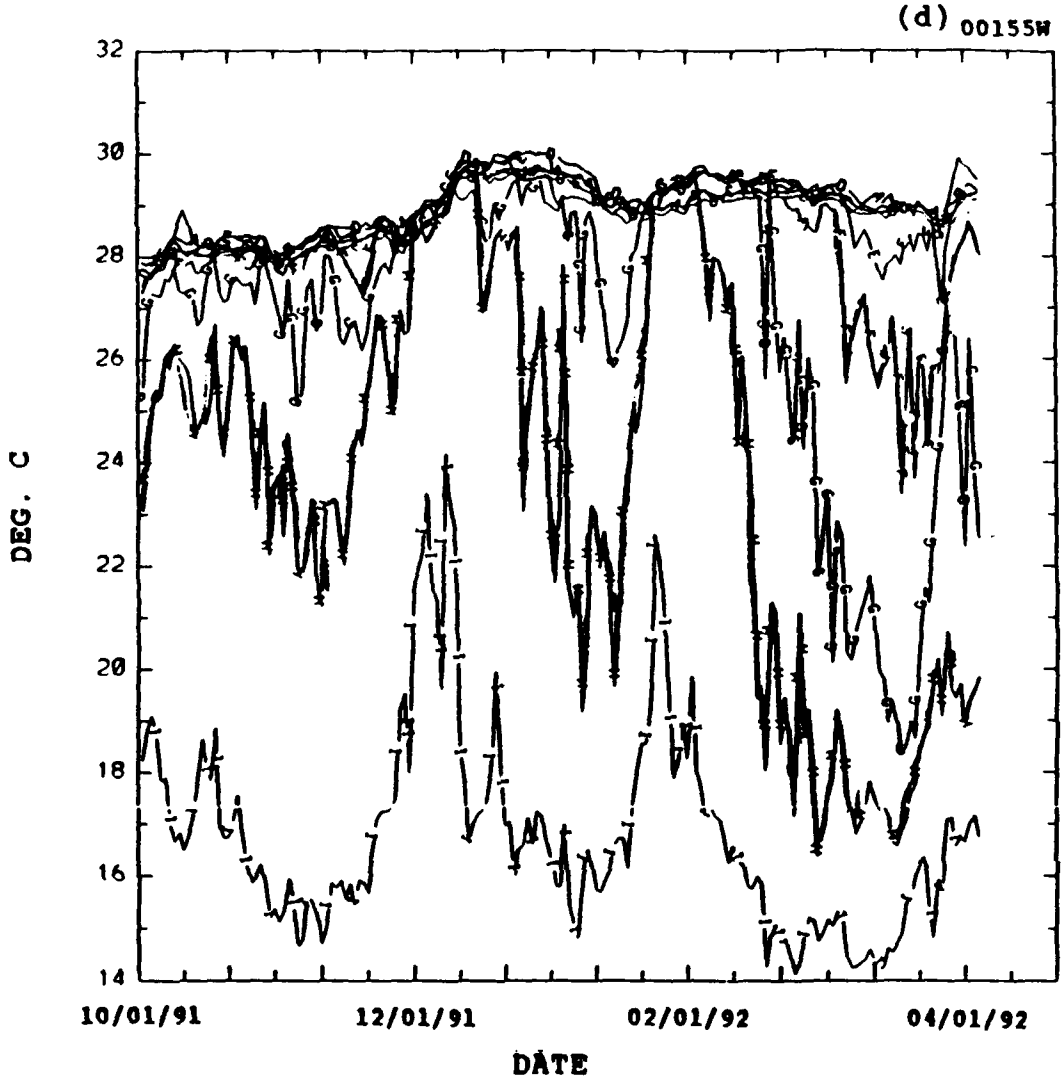

Fig. 16 (Continued).

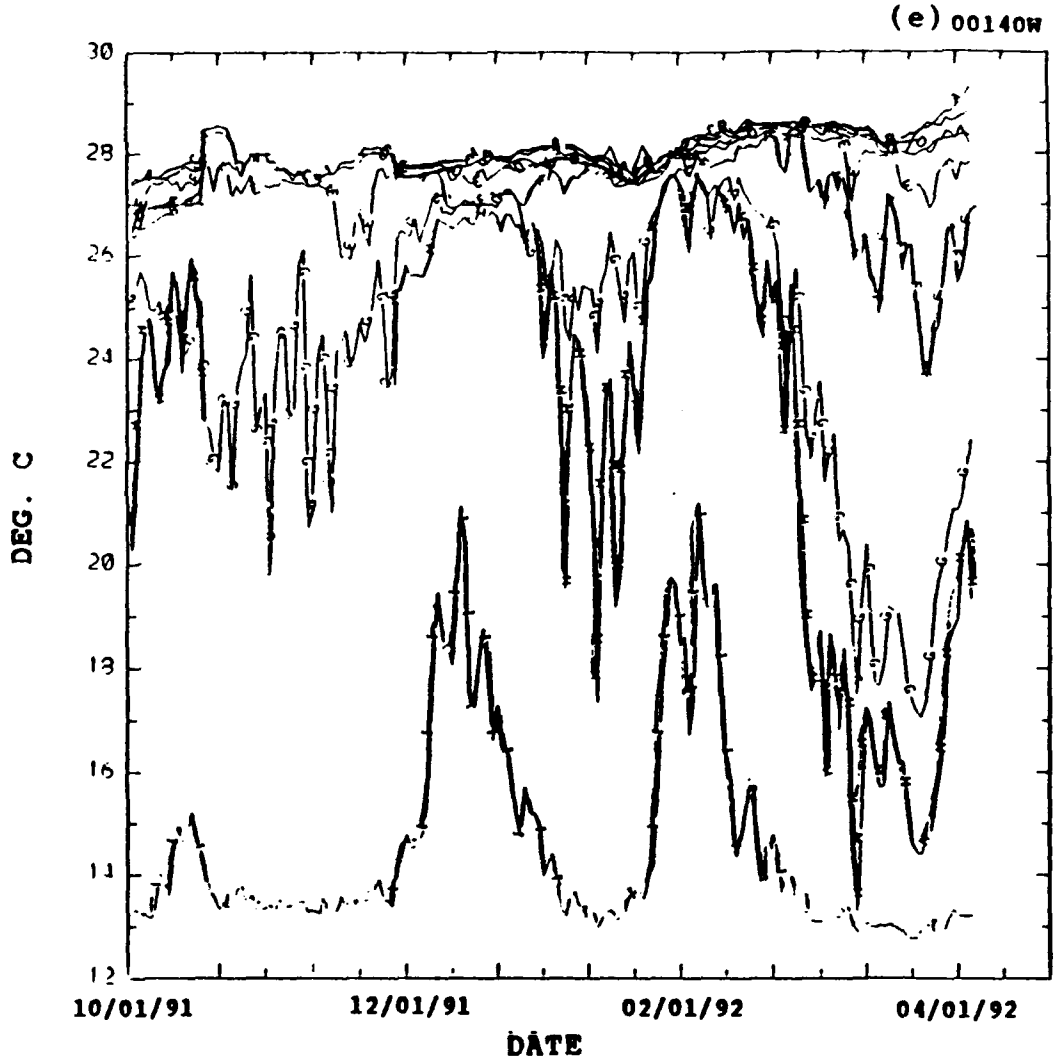

Fig. 16 (Continued).

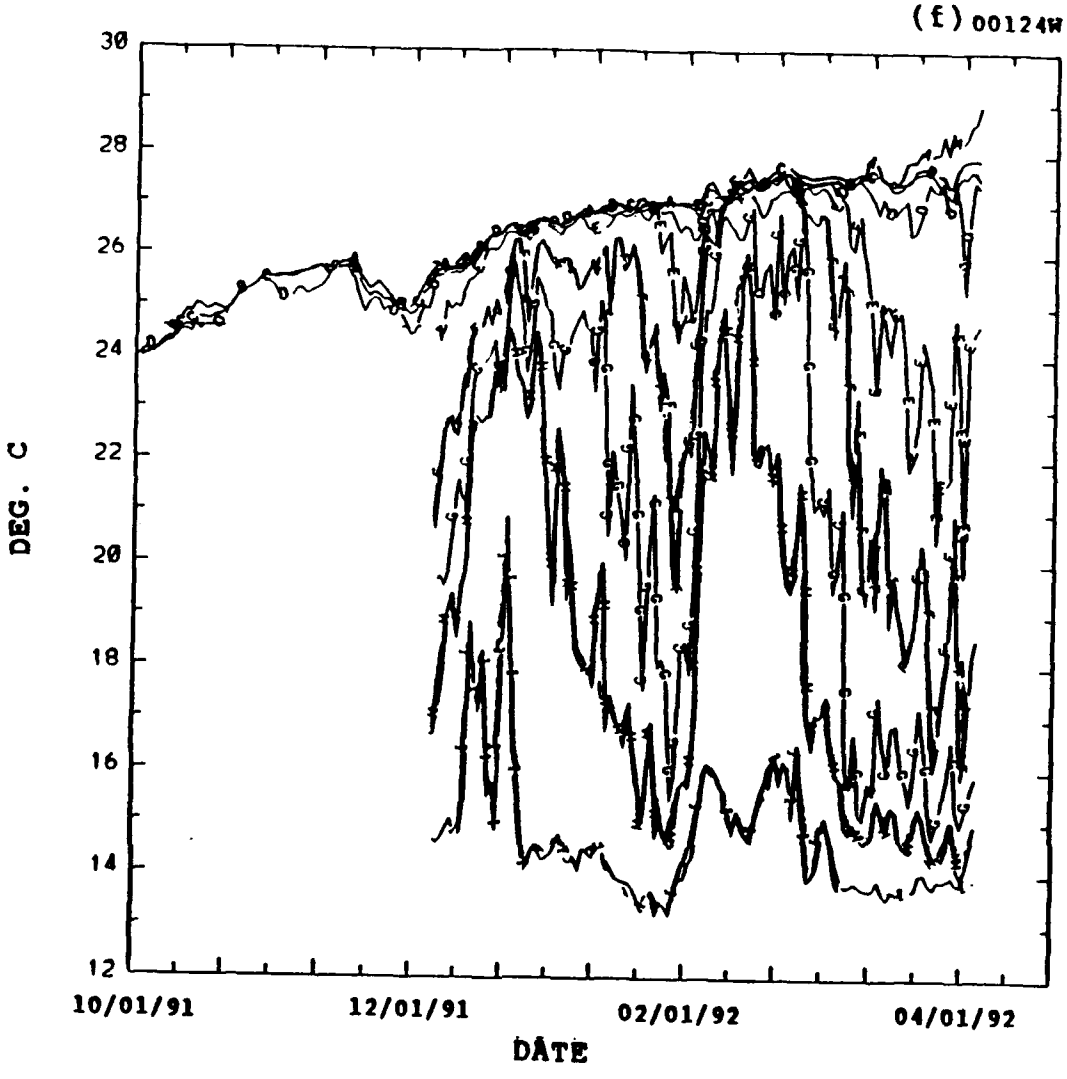

Fig. 16 (Continued).

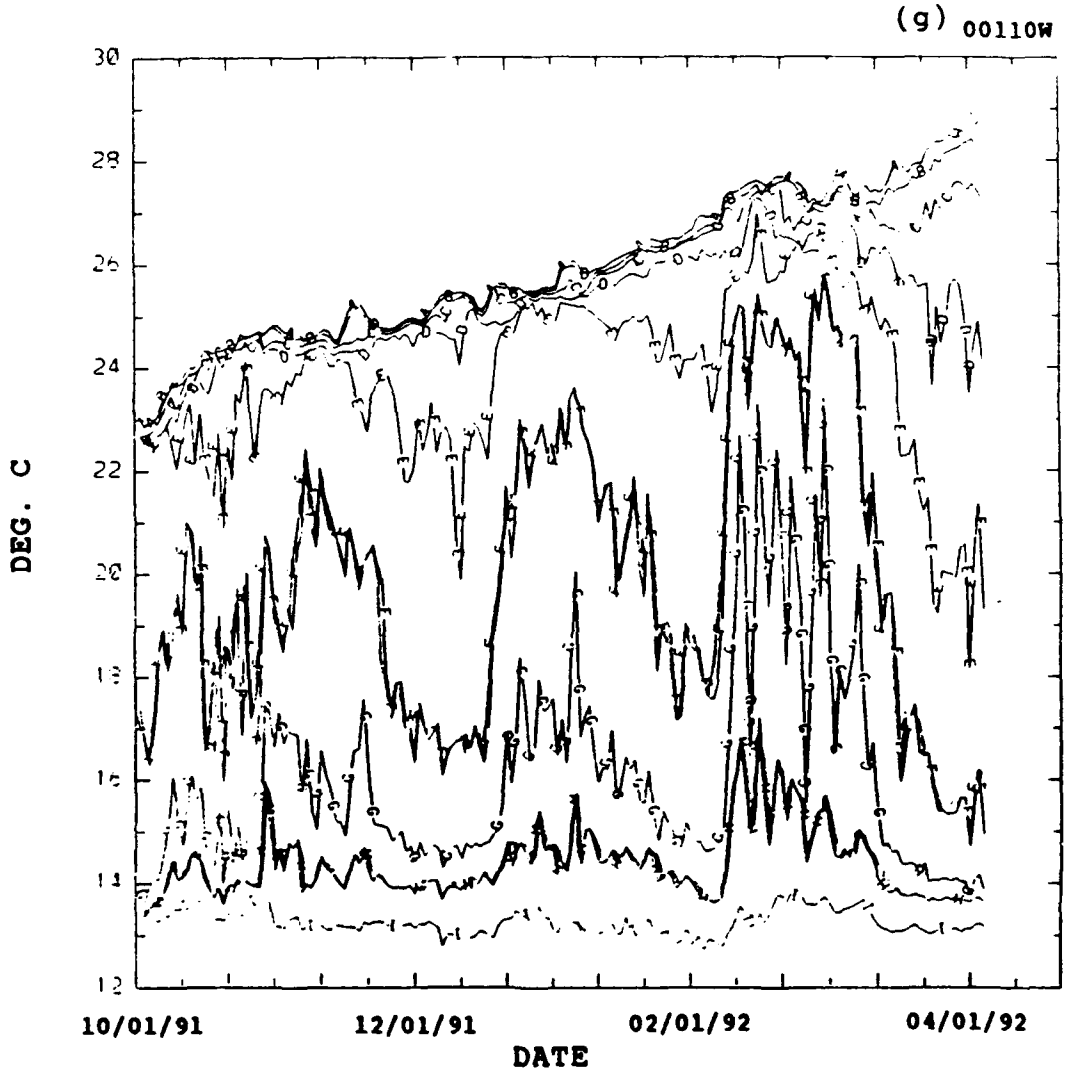

Fig. 16 (Continued).

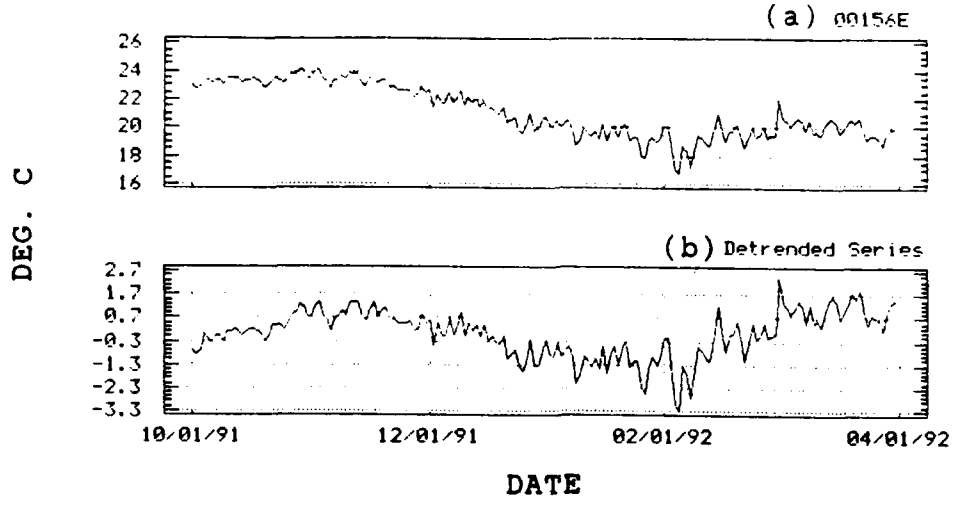

Fig. 17. Time series of ATLAS 150 m ocean temperatures from 01 October 1991 - 31 March 1992 for 0°156°E. a) observed and b) linearly detrended.

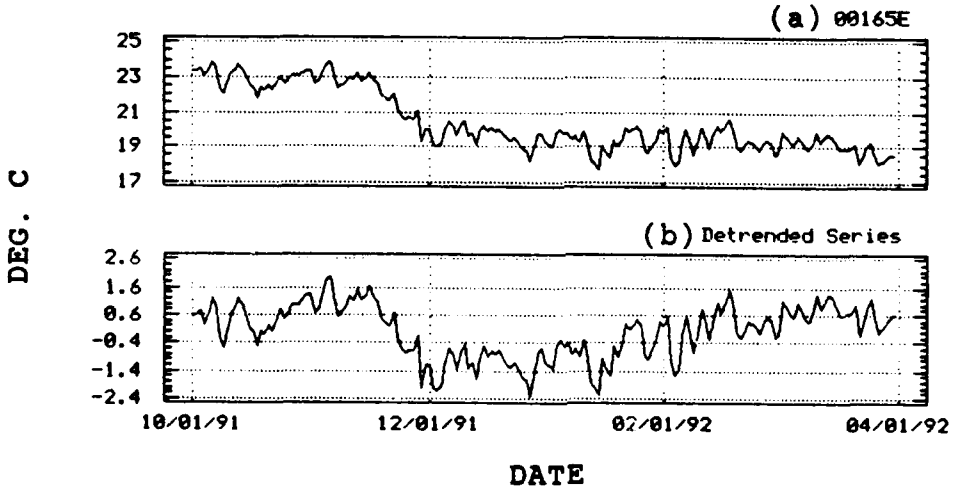

Fig. 18. Same as Fig. 17, except for 0°165°E.

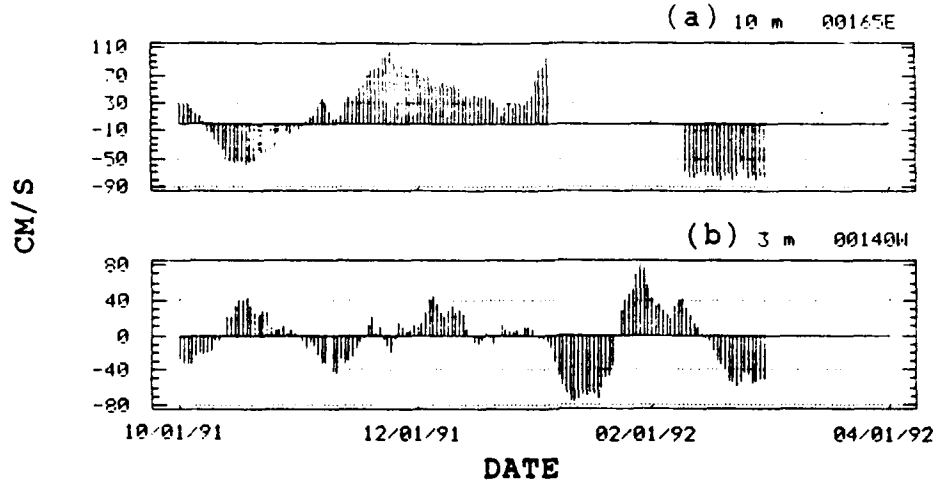

Fig. 19. Time series of the EPOCS zonal ocean current from 01 October 1991 - 31 March 1992. a) 10 m zonal current at 0^0165^0E b) 3 m zonal current at 0^0140^0W.

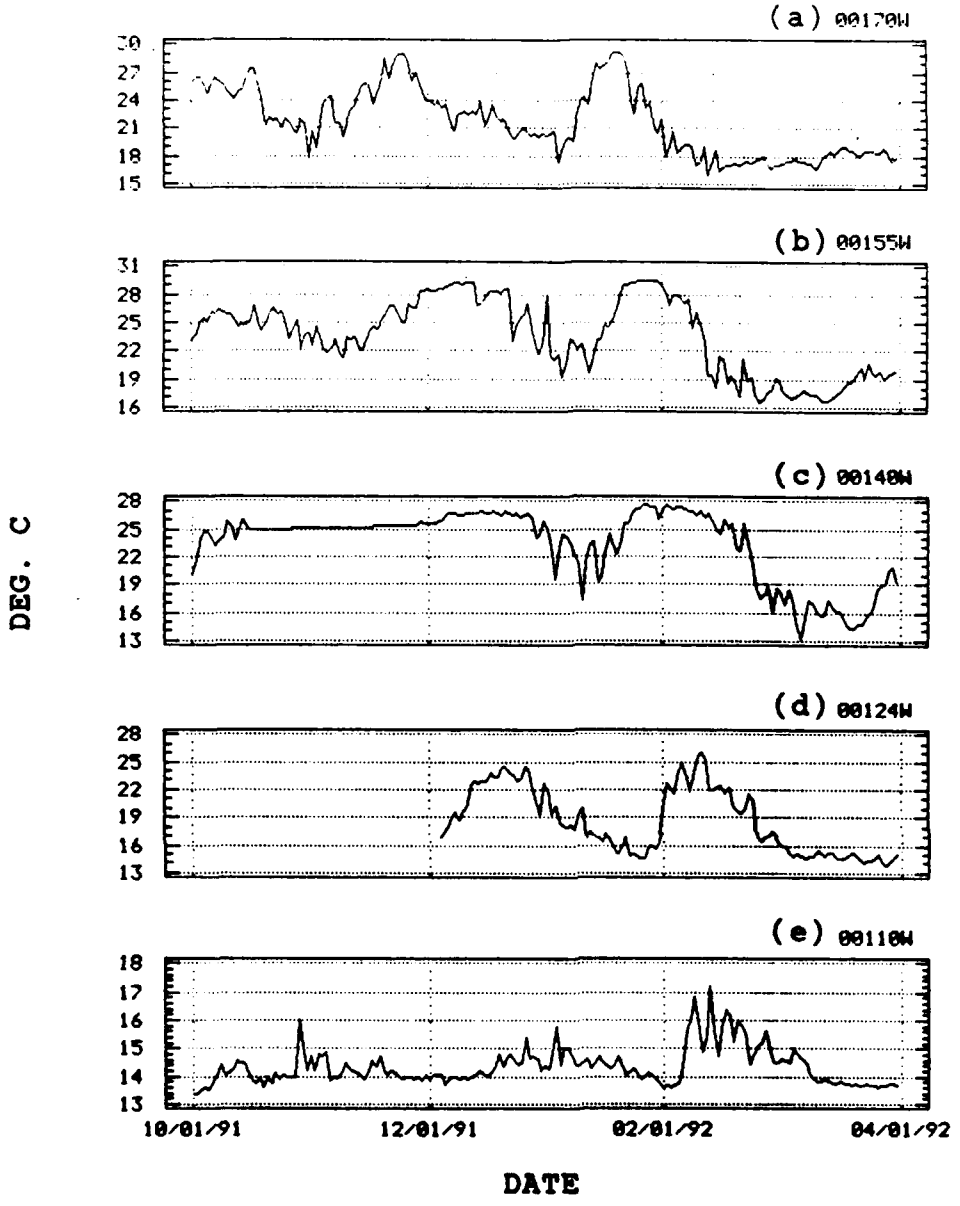

Fig. 20. Time series of ATLAS 150 and 140 m ocean temperatures from 01 October 1991 - 31 March 1992 at a) 0^0170^0W b) 0^0155^0W c) averaged 0^0140^0W d) 0^0124^0W e) averaged 0^0110^0W.

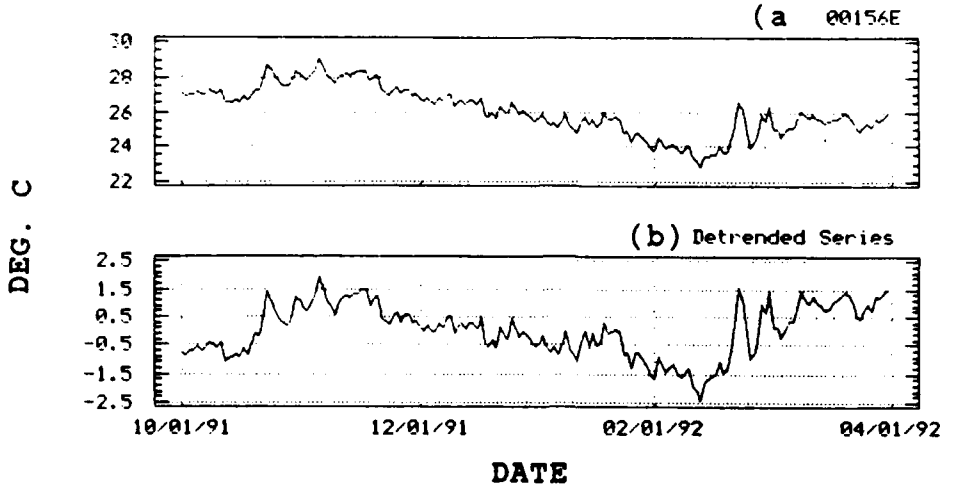

Fig. 21. Time series of ALTAS 100 m ocean temperatures for 01 October 1991 - 31 March 1992 at 0^0156^0E for a) observed and b) linearly detrended.

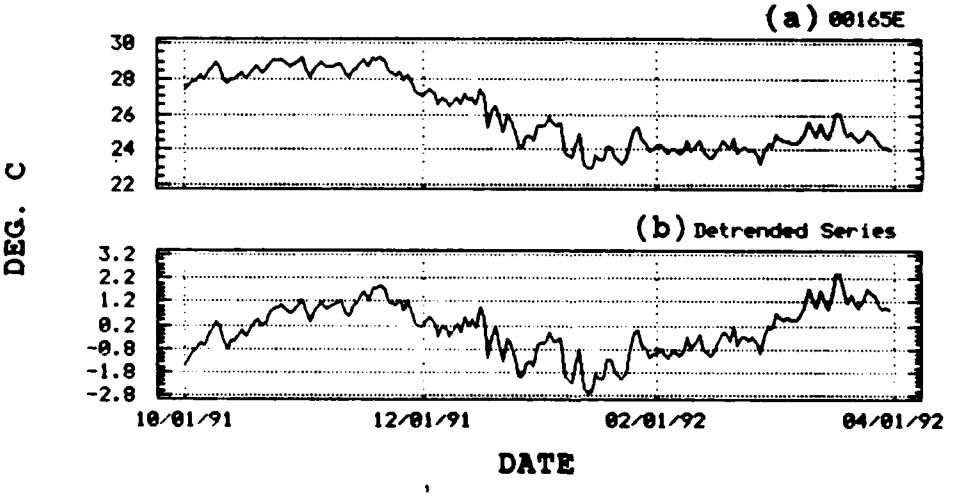

Fig. 22. Same as Fig. 21, except for 0^0165^0E.

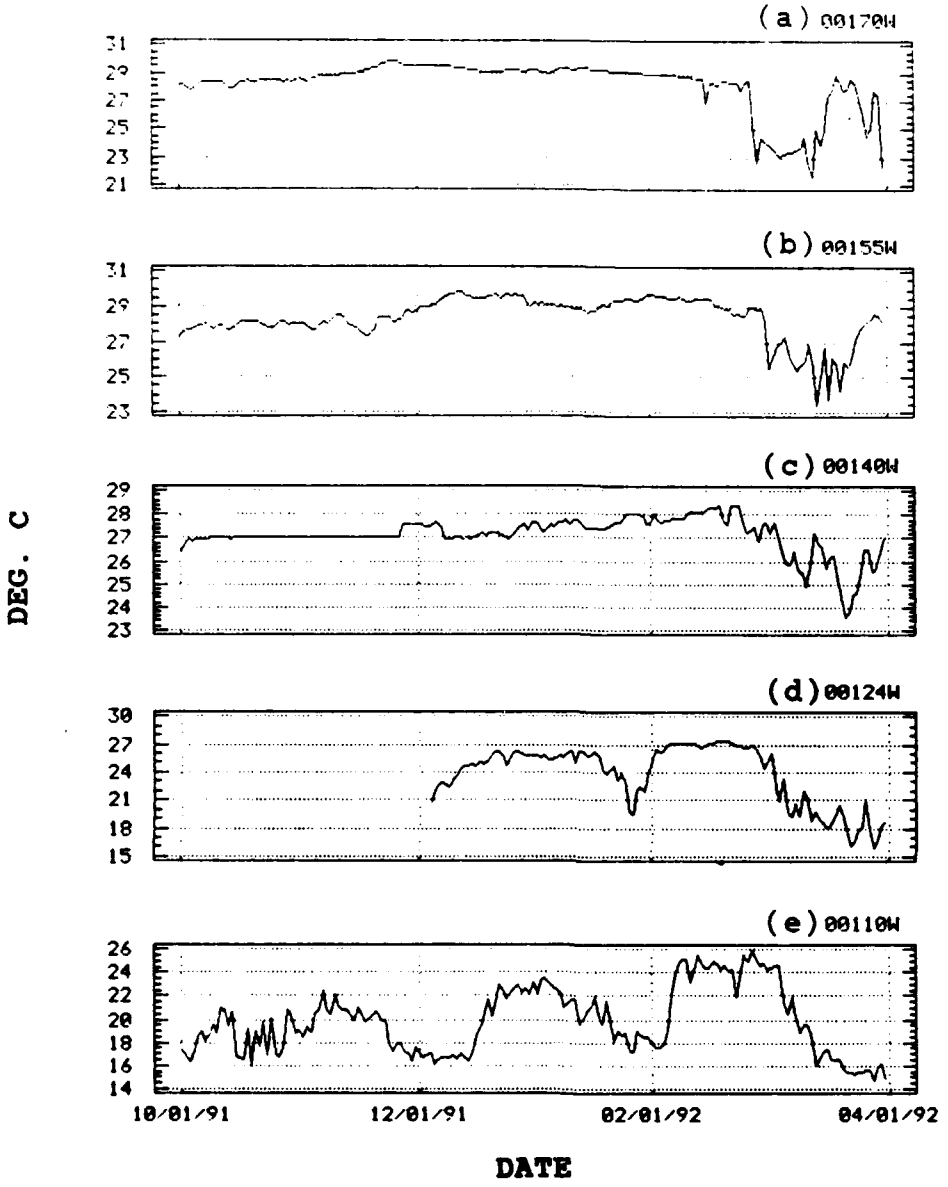

Fig. 23. Same as Fig. 20, except for 100 m temperatures.

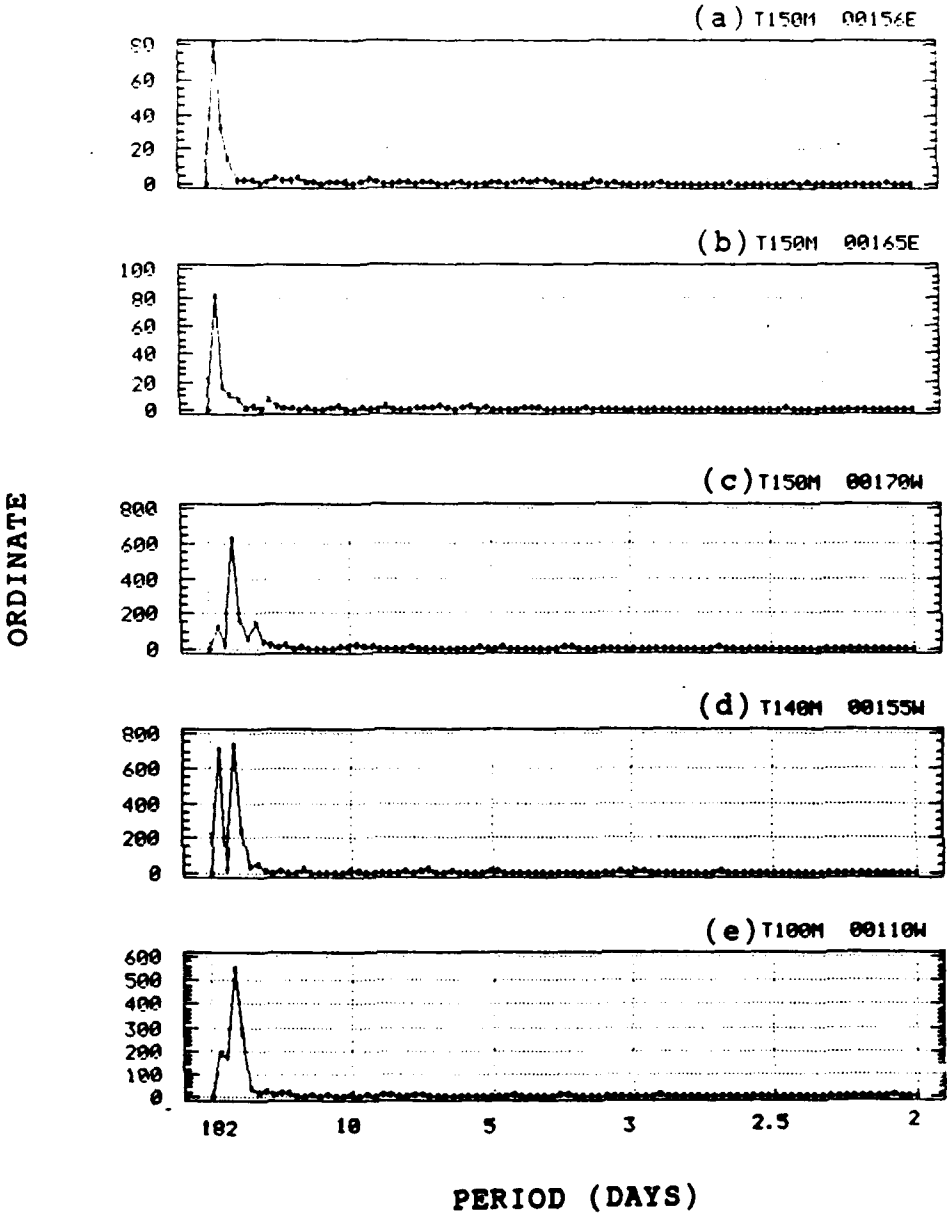

Fig. 24. Periodograms of ATLAS subsurface temperatures for a) averaged $0^{0}156^{0}E$ b) averaged $0^{0}165^{0}E$ c) $0^{0}170^{0}W$ d) $0^{0}155^{0}W$ e) averaged $0^{0}110^{0}W$. Sampling interval is one day.

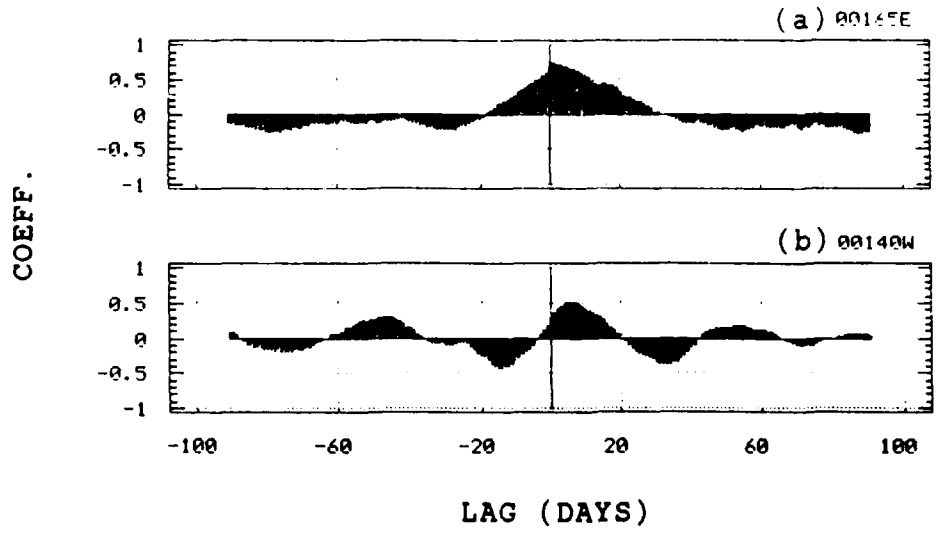

Fig. 25. Estimated cross-correlations between EPOCS zonal wind and EPOCS zonal ocean current for a) 0^0165^0E and b) 0^0140^0W. Positive lags indicate the zonal wind leads the zonal current while negative lags indicate the zonal current leads the zonal wind. Lags are in days.

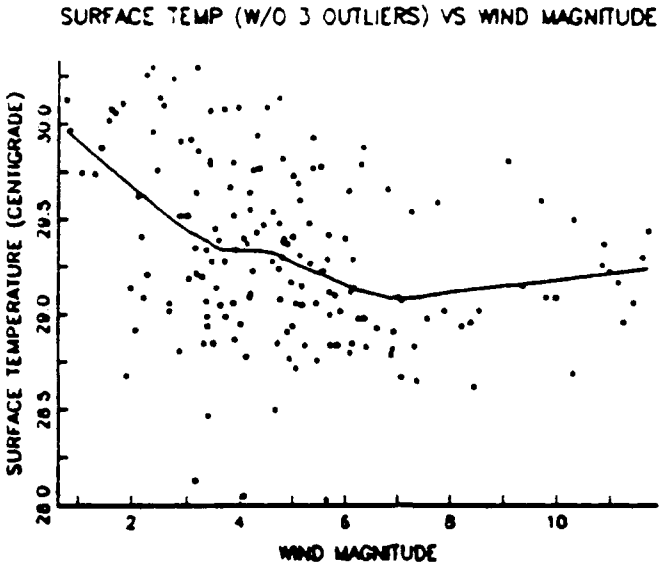

Fig. 26. Scatter plot and non-linear regression for wind magitude and SST at 0^0165^0E. (from Santos et.al.,1992)

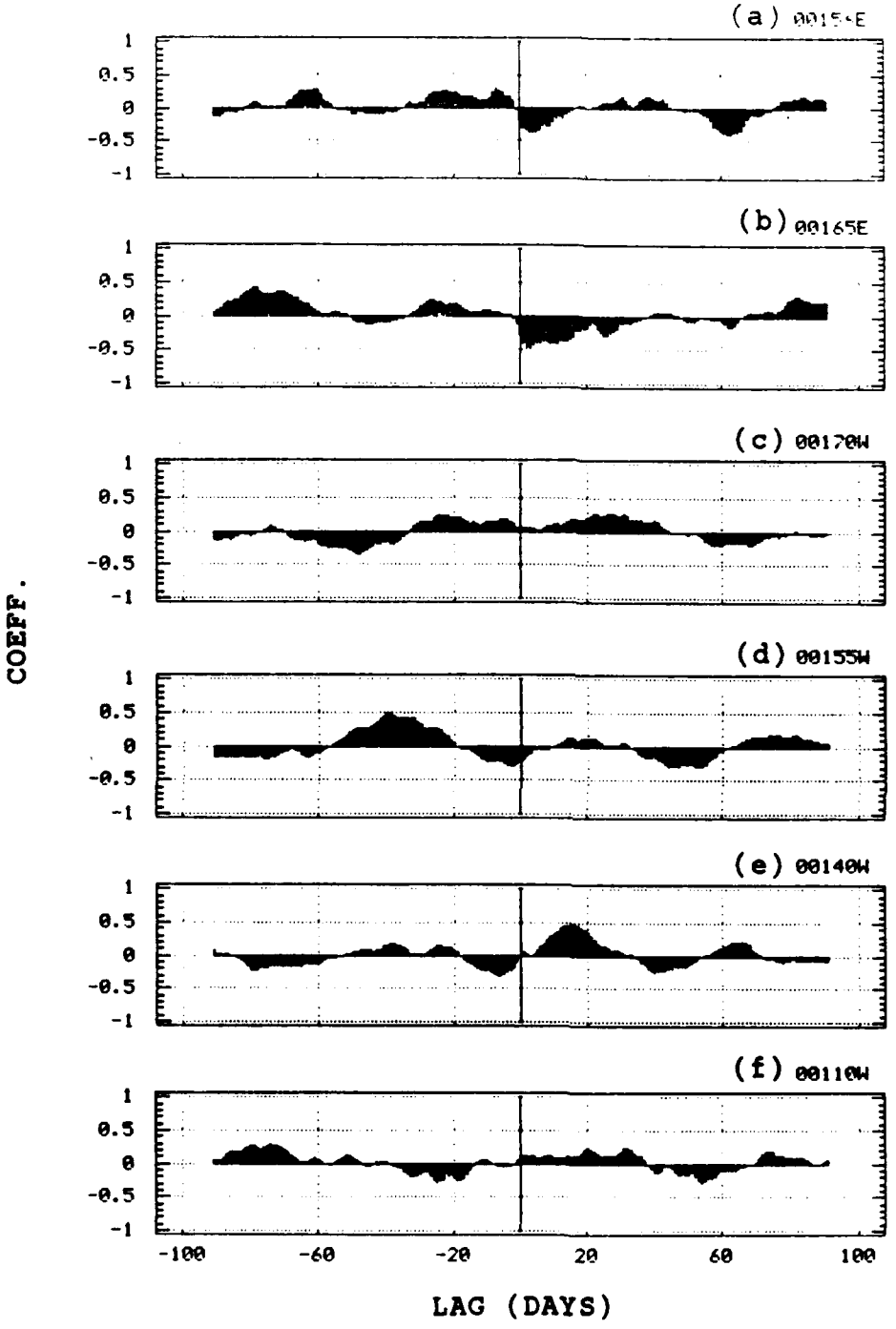

Fig. 27. Estimated cross-correlations of the local zonal wind and SST for a) averaged 0°156°E b) averaged 0°165°E c) 0°170°W d) 0°155°W e) averaged 0°140°W f) averaged 0°110°W. Positive lags indicate the zonal wind leads the SST and negative lags indicate the SST leads the zonal winds. Lags are in days.

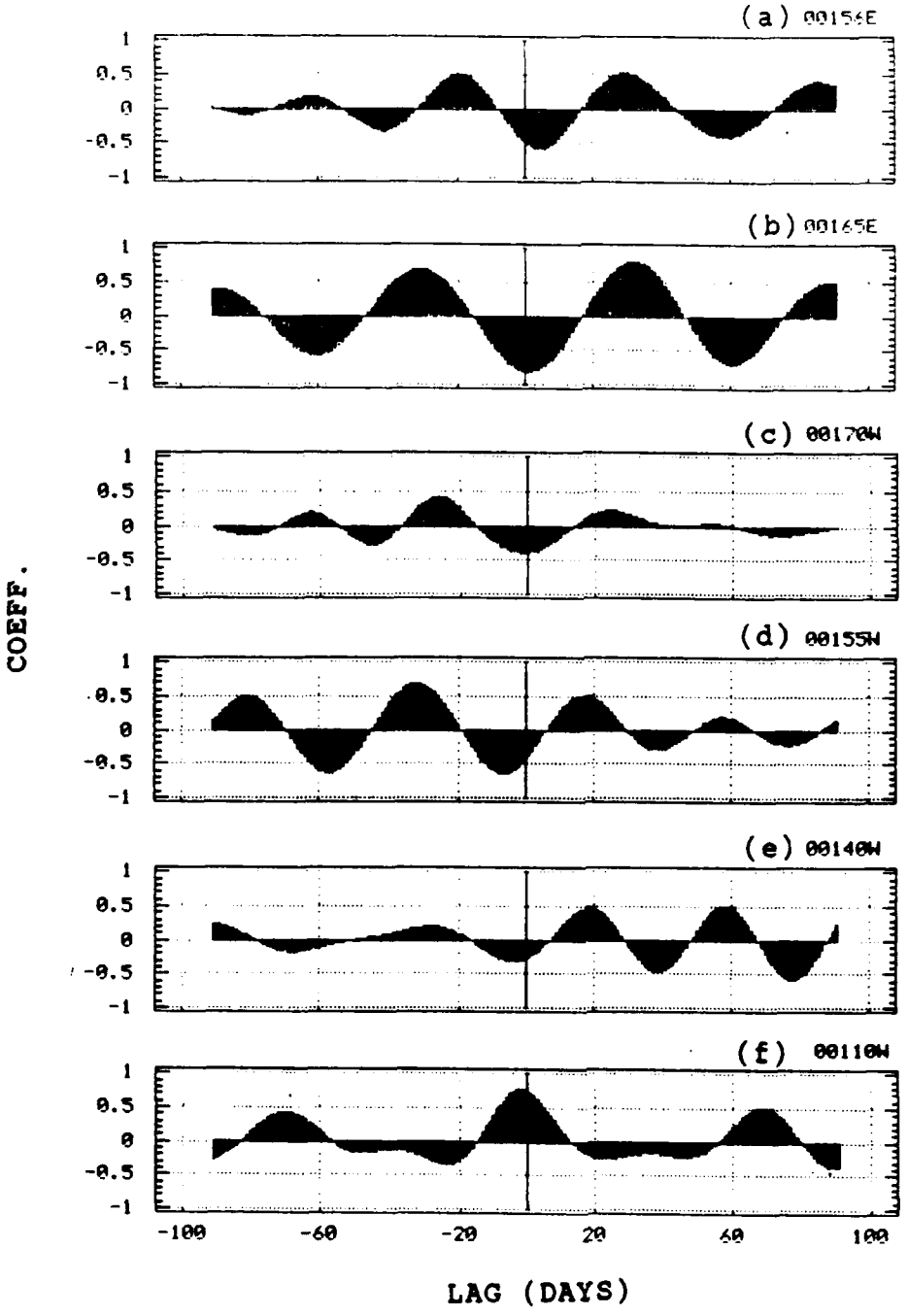

Fig. 28. Same as Fig. 27, except for 30 - 60 day filtered data.

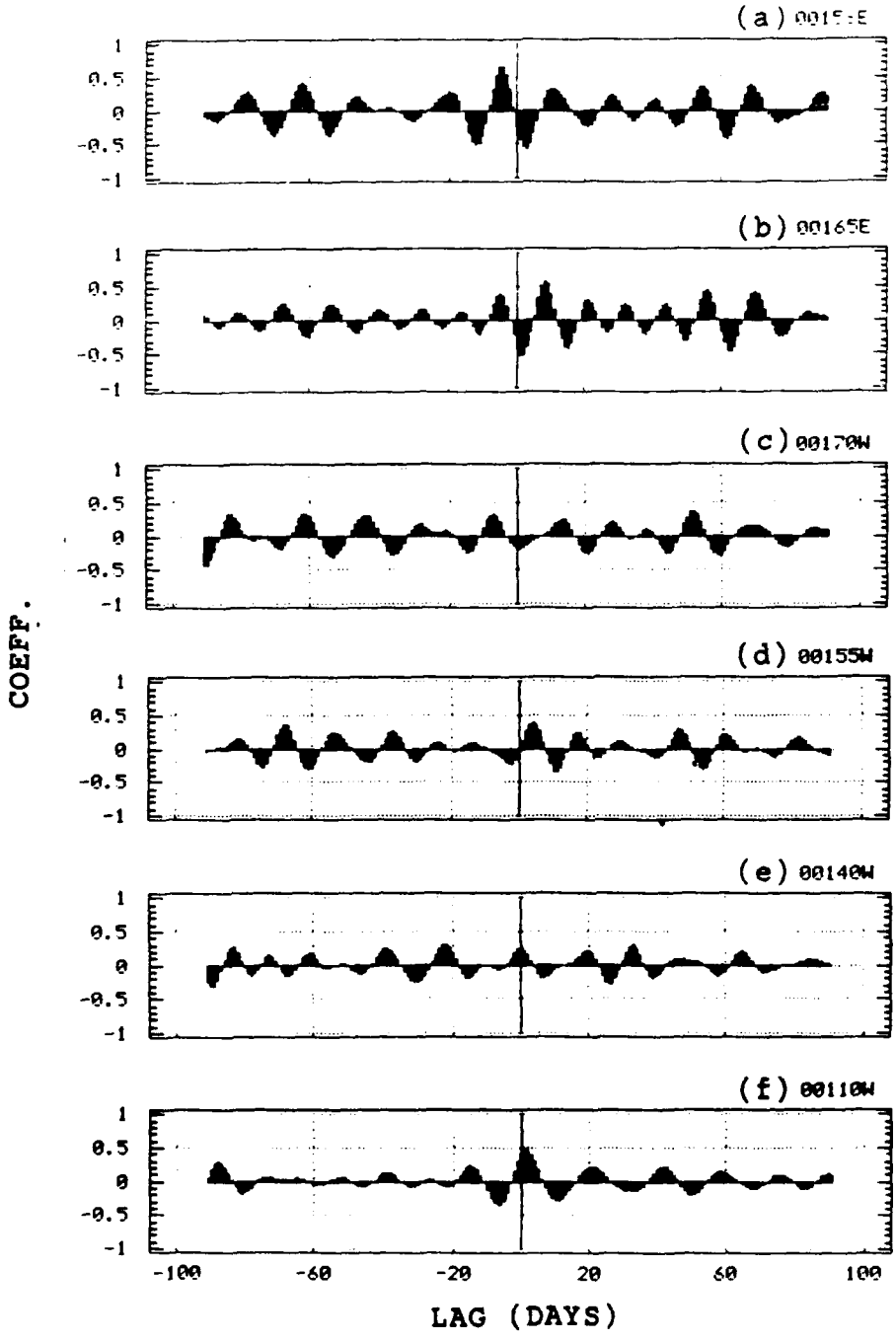

Fig. 29. Same as Fig. 27, except for 5 - 20 day filtered data.

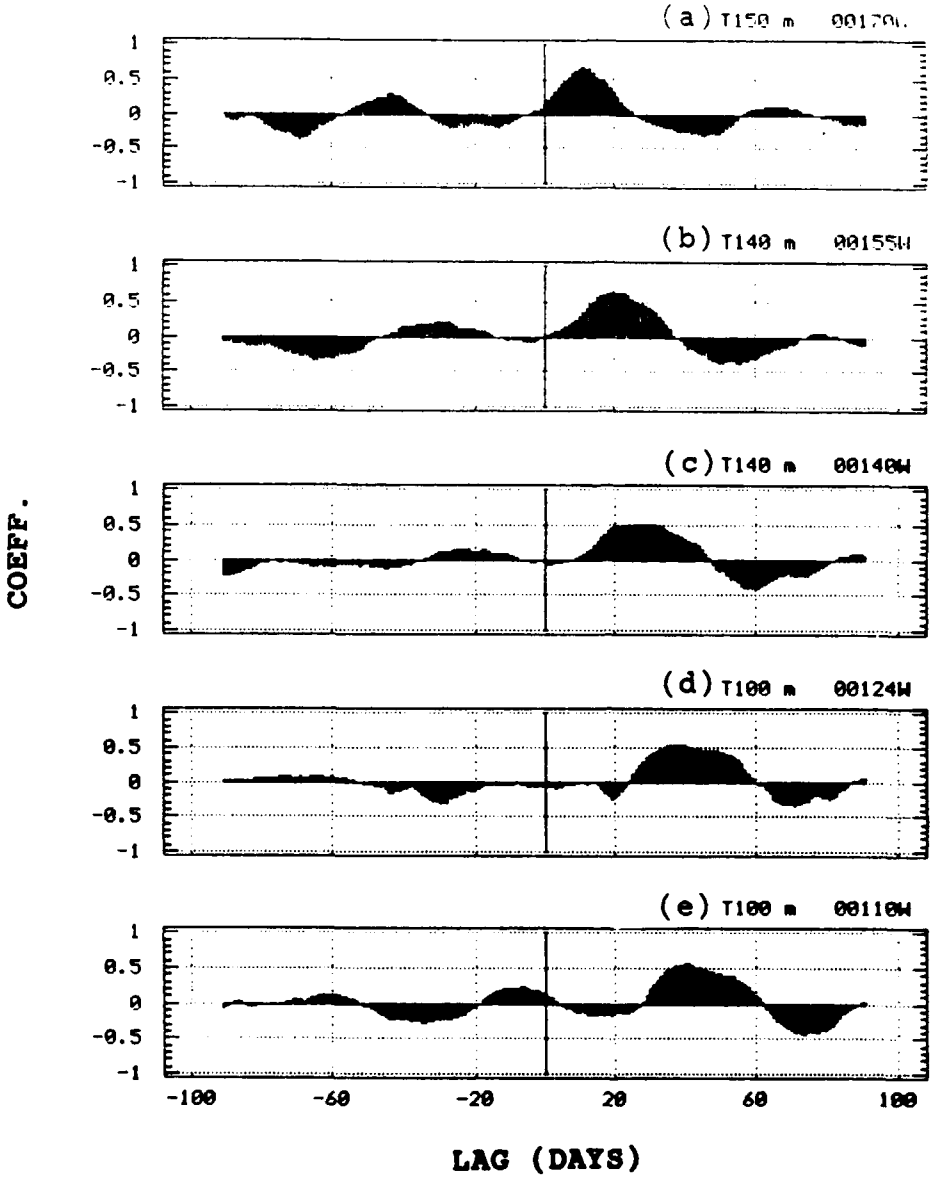

Fig. 30. Estimated cross-correlations between the zonal wind stress at 0°165°E and ATLAS subsurface temperatures for a) 0°170°W b) 0°155°W c) averaged 0°140°W d) 0°124°W and e) averaged 0°110°W. At positive lags the wind stress leads the temperature while at negative lags the temperature leads the wind stress. Lags are in days.

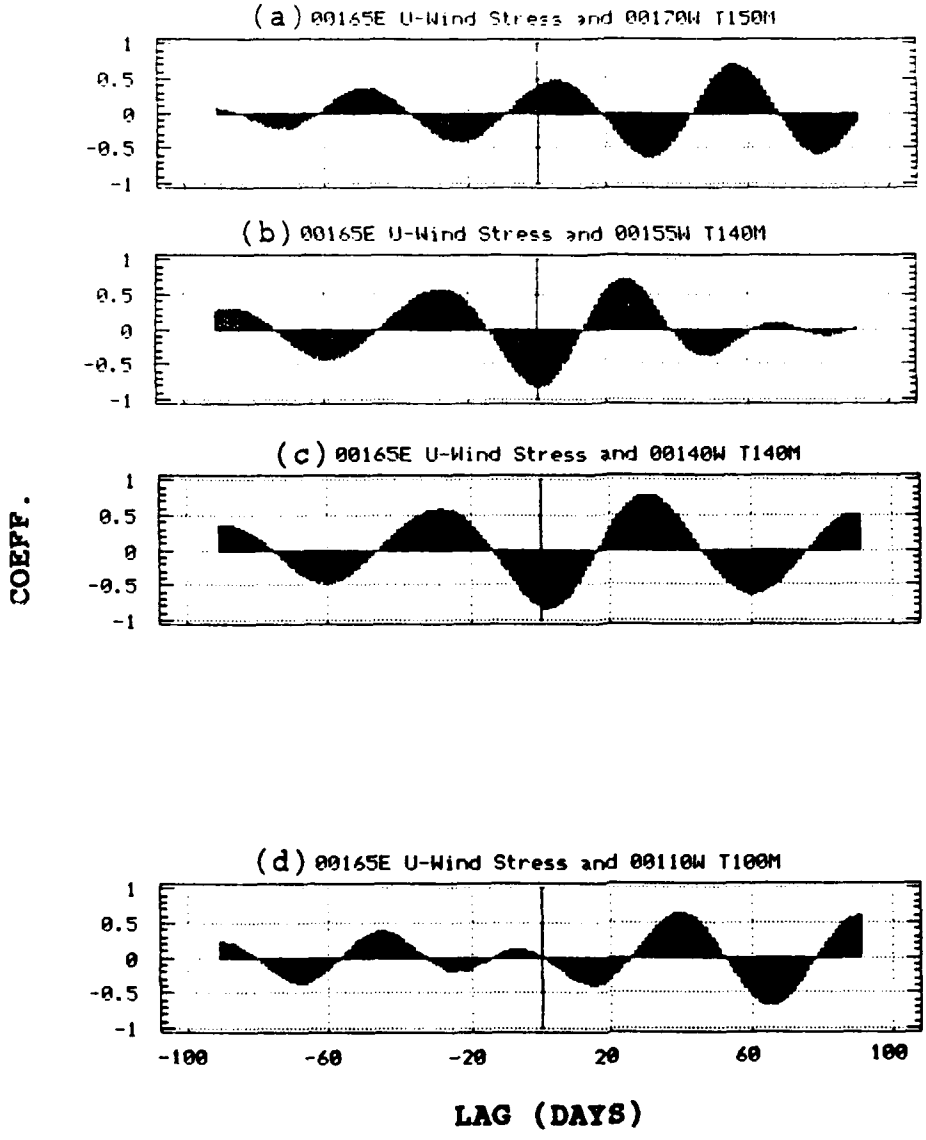

Fig. 31. Same as Fig. 30, except for 30 - 60 day filtered data. 0°124°W not included for lack of data.

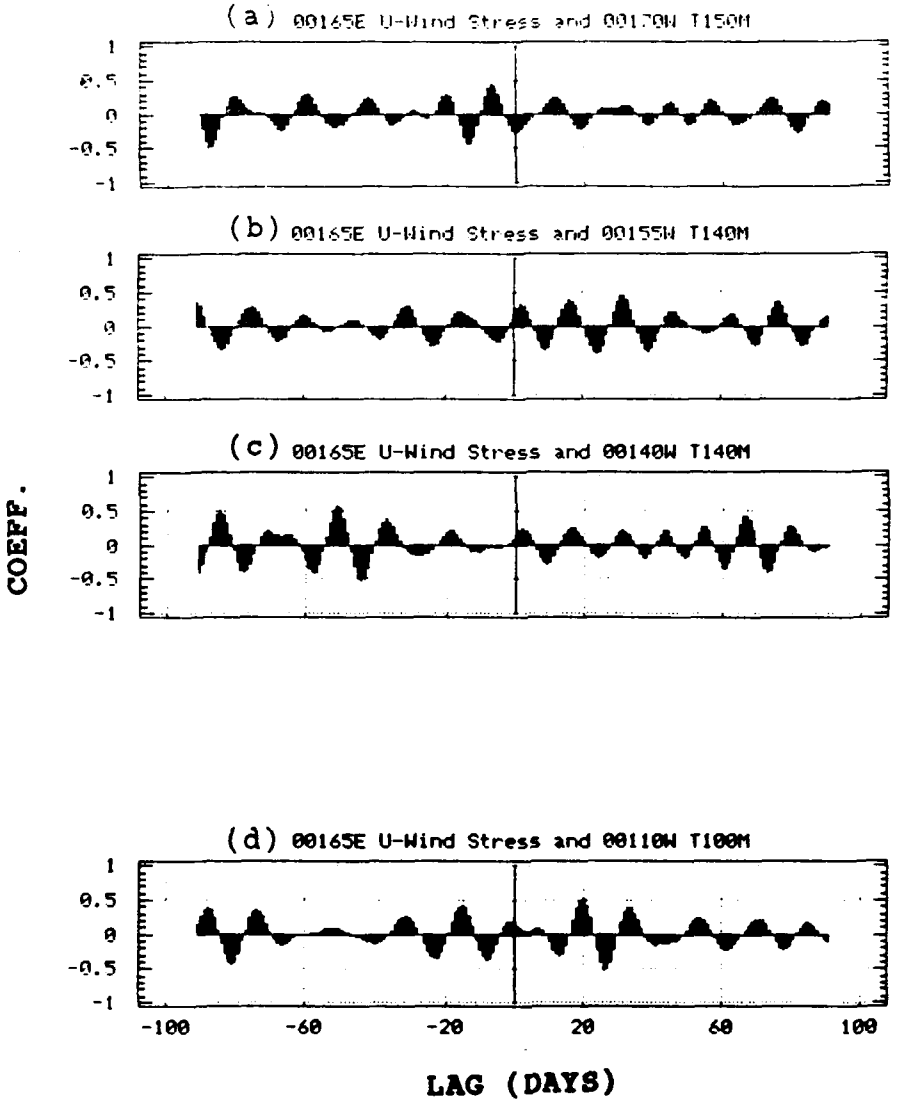

Fig. 32. Same as Fig. 30, except for 5 - 20 day filtered data. 0°124°W not included for lack of data.

INITIAL DISTRIBUTION LIST

1.	Defense Technical Information Center Cameron Station Alexandria, VA 22304-6145	2
2.	Library, Code 52 Naval Postgraduate School Monterey, CA 93943-5000	2
3.	Chairman (Code OC/Co) Department of Oceanography Naval Postgraduate School Monterey, CA 93943-5000	1
4.	Chairman (Code MR/Hy) Department of Meteorology Naval Postgraduate School Monterey, CA 93943-5000	1
5.	James T. Murphree (Code MR/Me) Department of Meteorology Naval Postgraduate School Monterey, CA 93943-5000	1
6.	Peter C. Chu Department of Oceanography Naval Postgraduate School Monterey, CA 93943-5000	1
7.	LT Grant A. Cooper, USN PSC 819 Box 31 FPO AE 09645-3200	1
8.	Pat Phoebus Naval Oceanographic and Atmospheric Research Laboratory Monterey, CA 93943-5006	1